PHYSICAL REVIEW B **90**, 035149 (2014)

Charge-density-wave order with momentum $(2Q,0)$ and $(0,2Q)$ within the spin-fermion model: Continuous and discrete symmetry breaking, preemptive composite order, and relation to pseudogap in hole-doped cuprates

Yuxuan Wang and Andrey Chubukov
Department of Physics, University of Wisconsin, Madison, Wisconsin 53706, USA
(Received 29 June 2014; published 31 July 2014)

We analyze charge order in hole-doped cuprates within the the spin-fermion model. We show that a magnetically mediated interaction, which is known to give rise to d-wave superconductivity and charge order with momentum along zone diagonal, also gives rise to charge order with momenta $Q_x = (2Q,0)$ and $Q_y = (0,2Q)$ consistent with the experiments. We show that an instability towards $\Delta_k^Q = \langle c^\dagger_{\mathbf{k}+\mathbf{Q}} c_{\mathbf{k}-\mathbf{Q}}\rangle$ with $\mathbf{Q} = Q_x$ or Q_y is a threshold phenomenon, but the dimensionless spin-fermion coupling is above the threshold, if the magnetic correlation length ξ exceeds a certain critical value. At a critical ξ, the onset temperature for the charge order terminates at a quantum-critical point distant from the magnetic one. We argue that the charge order with Q_x or Q_y changes sign under $\mathbf{k} \to \mathbf{k} + (\pi,\pi)$, but $|\Delta_k^Q| \neq |\Delta^Q_{k+(\pi,\pi)}|$. In real space, such an order has both bond and site components; the bond one is larger. We further argue that Δ_k^Q and Δ^Q_{-k} are not equivalent, and their symmetric and antisymmetric combinations describe, in real space, incommensurate density modulations and incommensurate bond current, respectively. We derive the Ginzburg-Landau functional for four-component $U(1)$ order parameters $\Delta^Q_{\pm k}$ with $\mathbf{Q} = Q_x$ or Q_y and analyze it first in mean-field theory and then beyond mean field. Within mean field we find two types of charge-density-wave (CDW) states, I and II, depending on system parameters. In state I, density and current modulations emerge with the same $\mathbf{Q} = Q_x$ or Q_y, breaking Z_2 lattice rotational symmetry, and differ in phase by $\pm\pi/2$. The selection of $\pi/2$ or $-\pi/2$ additionally breaks Z_2 time-reversal symmetry, such that the total order parameter manifold is $U(1) \times Z_2 \times Z_2$. In state II, density and current modulations emerge with different $\mathbf{Q}$ and the order parameter manifold is $U(1) \times U(1) \times Z_2$, where in the two realizations of state II, Z_2 corresponds to either lattice rotational or time-reversal symmetry breaking. We extend the analysis beyond mean field and argue that discrete symmetries get broken before long-range charge order sets in. For state I, which, we argue, is related to hole-doped cuprates, we show that, upon lowering the temperature, the system first breaks Z_2 lattice rotational symmetry ($C_4 \to C_2$) at $T = T_n$ and develops a nematic order, then breaks Z_2 time-reversal symmetry at $T_t < T_n$ and locks the relative phase between density and current fluctuations, and finally breaks $U(1)$ symmetry of a common phase of even and odd components of Δ_k^Q at $T = T_{\rm CDW} < T_t < T_n$ and develops a true charge order. We argue that at a mean field, $T_{\rm CDW}$ is smaller than superconducting $T_{\rm SC}$, but preemptive composite order lifts $T_{\rm CDW}$ and reduces $T_{\rm SC}$ such that at large ξ charge order develops prior to superconductivity. We obtain the full phase diagram and present quantitative comparison of our results with ARPES data for hole-doped cuprates.

DOI: 10.1103/PhysRevB.90.035149 PACS number(s): 74.20.−z, 71.10.Li

I. INTRODUCTION

Intensive experimental studies of hole-doped cuprates over the last few years have provided strong indications that the pseudogap region is a state (or even a set of states) with broken symmetry. First, x-ray and neutron scattering data on $La_{1.875}Ba_{0.125}CuO_4$ strongly indicate [1,2] that lattice rotational symmetry is broken from C_4 down to C_2 below a certain temperature $T^*(x)$. Evidence for rotational symmetry breaking has been also found in neutron scattering data on YBCO [3] and in STM data on $Bi_2Sr_2CaCu_2O_{8+\delta}$, at energies comparable to T^* [4,5]. Second, measurements of the Kerr angle at optical frequencies detected a polar Kerr effect [6], and polarized elastic neutron scattering measurements detected an intra-unit-cell magnetic order [7,8]. The onset temperatures for the Kerr effect and for intracell magnetic order are not equal, but roughly follow the same doping dependence as $T^*(x)$. The most natural interpretation of these two measurements would be that time-reversal symmetry is broken, although the absence of a sign change of a Kerr signal under the change of the direction of the applied magnetic field raises a possibility that the Kerr effect may be a reciprocal phenomenon, associated with the breaking of mirror symmetries. Recent optical experiments in the terahertz regime have found [9] a nonzero linear birefringence, which was also interpreted as the result of the breaking of mirror symmetries *and* of C_4 lattice rotational symmetry. The temperature dependence of the onset of a linear birefringence in YBCO closely follows the one for Kerr signal.

Third, x-ray measurements on YBCO [10,11], $Bi_2Sr_{2-x}La_xCuO_{6+\delta}$ [12], and $Bi_2Sr_2CaCu_2O_{8+\delta}$ [13] detected a static incommensurate charge-density-wave (CDW) order with momenta $\mathbf{Q}_x = (2Q,0)$ and/or $\mathbf{Q}_y = (0,2Q)$, and $2Q$ was determined to be equal to the distance between neighboring hot spots, points where the Fermi surface (FS) intersects with the magnetic Brillouin zone boundary [12,13]. The observed order is not long ranged, but this well may be due to pinning by impurities [14,15]. Earlier NMR measurements [16,17] and more recent sound velocity measurements [18] in a magnetic field H found a true CDW order at $H \geqslant 20$ T. Quantum oscillation measurements [19] and measurements of Hall and Seebeck coefficients [20]

were interpreted as feedback effects from the CDW order on fermions. The onset temperature $T_{\rm CDW}(x)$ of the CDW order was found to be smaller than $T^*(x)$ but follows a similar doping dependence. Fourth, ARPES measurements deep under the superconducting dome have found [21–23] a change of system behavior at a certain doping, and were interpreted as evidence for the existence of a quantum-critical point (QCP) at $x = x_{\rm cr}$, at which a new order emerges. It is tempting to associate this emerging order with CDW.

These and other experimental data [24,25] pose a challenge to the theory. System behavior in the metallic region outside the pseudogap can be reasonably well described within a theoretical framework that fermions interact by exchanging quanta of collective excitations. One proposal along these lines [26] is that these excitations are charge fluctuations enhanced by phonons (a similar set of ideas has been recently displayed for Fe pnictides [27]). An incommensurate CDW order with $\mathbf{Q}$ along x or y directions in the momentum space is a natural part of this scenario, and studies of a true and fluctuating CDW order within a microscopic Hubbard-Holstein model and using a more general reasoning of frustrated phase separation mechanism did indeed find [28] a CDW QCP at around optimal doping, identified the pseudogap temperature with the onset of CDW order [29], and obtained a number of features in Raman scattering [30], STM [31], and ARPES [32], consistent with the experimental data in hole-doped cuprates [33]. Furthermore, the residual momentum-dependent repulsive interaction mediated by charge critical fluctuations was argued to give rise to d-wave superconducting instability, although an additional interaction component, for fermions in antinodal regions, had to be included to match the experimental angular variation of the d-wave gap [34]. An alternative proposal is that relevant collective excitations are spin fluctuations, peaked at or near antiferromagnetic momenta (π,π). The corresponding spin-fluctuation approach [35–38] naturally explains d-wave symmetry of the superconducting state and yields a non-Fermi-liquid behavior of fermionic self-energy and optical conductivity [39,40] in a rather wide frequency range, even when magnetic correlation length is only a few lattice spacings. This approach does describe precursors to magnetism [41–43] and accounts reasonably well for the phase diagram of electron-doped cuprates [44], where pseudogap behavior is very likely a crossover behavior due to magnetic precursors [45]. At the same time, until recently, the spin-fluctuation approach was believed to be incapable to describe charge order and symmetry breaking in the pseudogap phase of hole-doped cuprates. Other explanations of charge order/symmetry breaking have been proposed, including loop-current order [46] or d-density-wave (current) order [47,48]. Other widely discussed scenarios of the pseudogap associate pseudogap behavior with precursors to either Mott physics [49–53] or superconductivity [54–56].

The spin-fluctuation scenario was revitalized by Metlitski and Sachdev [57] who found that the spin-mediated interaction is attractive not only in the d-wave superconducting channel but also in the d-wave charge channel, at momenta $\mathbf{Q}_d = 2\mathbf{k}_{\rm hs}$, where $\mathbf{k}_{\rm hs}$ is the momentum of one of the hot spots on a FS and $2\mathbf{k}_{\rm hs} = (\pm 2Q, \pm 2Q)$ are directed along one of the Brillouin zone diagonals. In real space, an instability in a d-wave charge channel implies a charge bond order, for which $\langle c^\dagger(\mathbf{r}+\mathbf{a})c(\mathbf{r})\rangle$ acquires an $\mathbf{r}$-dependent component of different sign for $\mathbf{a}$ along x and y directions, while $\langle c^\dagger(\mathbf{r})c(\mathbf{r})\rangle$ remains unperturbed. The analysis of CDW instability with $\mathbf{Q}_d = 2\mathbf{k}_{\rm hs}$ within the spin-fluctuation approach was extended by Efetov, Meier, and Pépin [58], who argued that the pseudogap behavior may be the consequence of the competition between bond order and superconductivity (SC) (in their scenario, the modulus of the combined SC/CDW "supervector" order parameter emerges at T^* but its direction gets fixed along the SC "axis" only at a smaller $T_{\rm SC}$). The "supervector" scenario is appealing from theory perspective and allows one to explain some experimental data [59,60]. However, it has three discrepancies with the experiments. First, the momenta $2\mathbf{k}_{\rm hs}$ are directed along one of the two Brillouin zone diagonals, while CDW momentum detected by resonant x-ray scattering [12,13] and in STM [4,5] is along horizontal or vertical axis in momentum space [$\mathbf{Q} = \mathbf{Q}_x = (2Q,0)$ or $\mathbf{Q} = \mathbf{Q}_y = (0,2Q)$]. Second, bond-order instability is close to superconducting $T_{\rm SC}$, but is below $T_{\rm sc}$ (Refs. [57,58]), while experiments see the development of charge order above superconducting $T_{\rm sc}$. Third, bond order with momentum $\mathbf{Q}_d = 2\mathbf{k}_{\rm hs}$ does not break time-reversal or mirror symmetries and therefore does not explain Kerr, neutron scattering, and magnetoelectric birefringence experiments [6–9].

In this paper, we present a different scenario for the pseudogap due to spin-fluctuation exchange. We argue that magnetically mediated interaction yields an attraction in the CDW channel for incoming momenta $\mathbf{Q}_x$ and $\mathbf{Q}_y$, and, when magnetic correlation length is large enough, gives rise to a CDW instability at a nonzero temperature $T_{\rm CDW}$. That such critical temperature exists is not guaranteed *a priori*, despite that, as we show below, there are logarithms in the perturbation theory. The reason is that magnetically mediated interaction is dynamical, and the gap equation is an integral equation in frequency. For the latter, the summation of the leading logarithms does not necessarily give rise to an instability [37,61], and one one has to go beyond the leading logarithmic approximation to verify whether or not the interaction exceeds a certain finite threshold. We show that for CDW with $\mathbf{Q} = Q_x$ or Q_y, the interaction is above the threshold, and the linearized gap equation, or, more accurately, the set of coupled equations for $\Delta_k^Q = \langle c^\dagger_{\mathbf{k}+\mathbf{Q}} c_{\mathbf{k}-\mathbf{Q}}\rangle$ and $\Delta^Q_{k+(\pi,\pi)}$, does have a solution at a finite $T = T_{\rm CDW}$. We compute $T_{\rm CDW}$ first in Eliashberg-type calculations and then by treating the effects of thermal bosonic fluctuations beyond Eliashberg theory, and compare $T_{\rm CDW}$ with $T_{\rm SC}$ obtained using the same procedures. In Eliashberg calculation, we show that $T_{\rm CDW}$ and $T_{\rm SC}$ are finite at $\xi = \infty$ at $T_{\rm SC} > T_{\rm CDW}$. With more accurate treatment of thermal fluctuation (equivalently, the contribution from zero bosonic Matsubara frequency), we find that the ratio $T_{\rm SC}/T_{\rm CDW}$ approaches one at infinite ξ, i.e., $T_{\rm SC}$ and $T_{\rm CDW}$ must be quite close at large ξ. We also analyze nonladder diagrams and show that they are small numerically.

The CDW order parameter Δ_k^Q changes sign under momentum shift by (π,π), as the bond order does, but it also has a nonzero onsite (a true CDW) component $\langle c^\dagger(r)c(r)\rangle = f(r)$

because $|\Delta_k^Q| \neq |\Delta^{\mathbf{Q}}_{\mathbf{k}+(\pi,\pi)}|$. This agrees with the structure of the charge order extracted from STM and x-ray data [5,62]. Because the onsite component of $\Delta_{\mathbf{k}}^{\mathbf{Q}}$ is nonzero (albeit small), we will be calling this order a CDW, primarily to distinguish it from a true bond order with diagonal $\mathbf{Q}_d = (2Q, \pm 2Q)$, for which, by symmetry, $\Delta_{\mathbf{k}}^{\mathbf{Q}_d} = -\Delta^{\mathbf{Q}_d}_{\mathbf{k}+(\pi,\pi)}$.

We analyze the structure CDW order in detail, first in mean-field approximation and then by going beyond mean field. Within mean field, we first assume that $\Delta_k^{Q_x}$ and $\Delta_k^{Q_y}$ are even functions in k and discuss the interplay between CDW orders with Q_x and Q_y. The linearized equations for both CDW orders have solution at the same $T = T_{\text{CDW}}$. What happens at a smaller T depends on how the two orders Δ^{Q_x} and Δ^{Q_y} interact with each other. We show that the interaction is repulsive, i.e., the two orders tend to repel each other. If the repulsion is weak, the two orders appear simultaneously and with the same amplitude, and the system develops a checkerboard order. If the repulsion is strong enough, it becomes energetically advantageous for a system to spontaneously break lattice rotational symmetry from C_4 down to C_2 and develop CDW with only Q_x or Q_y. In the real space, such an order has the form of stripes, e.g., $\langle c^\dagger(r)c(r)\rangle \propto \cos(2Qr_y)$ with $\mathbf{Q} = Q_y = (0,2Q)$. To understand which type of CDW order develops, we derive the Ginzburg-Landau action to order $(\Delta_k^Q)^4$ and analyze its form. We find that the repulsion is strong enough such that the system prefers to break C_4 symmetry down to C_2 and develop a stripe order. This is consistent with STM data [5]. A different scenario for CDW order with $\mathbf{Q} = (2Q,0)$ and $(0,2Q)$ has been proposed recently [63], in which CDW is induced by superconducting fluctuations. In that scenario, CDW emerges as a checkerboard order.

We next take a more careful look at the dependence of Δ_k^Q on the center-of-mass momentum k. CDW order with, say, $\mathbf{Q} = Q_y$ can be constructed out of hot fermions with $\mathbf{k} \approx \mathbf{k}_0 = (\pi - Q,0)$ and $-\mathbf{k}_0 = (-\pi + Q,0)$ (pairs 1-2 and 5-6 in Fig. 1). The CDW order parameters $\Delta_{k_0}^Q$ and $\Delta_{-k_0}^Q$ are not identical because $2\mathbf{k}_0$ is not a reciprocal lattice vector. As a result, Δ_k^Q with $\mathbf{k} \approx \mathbf{k}_0$ generally has two components: one is even in k and the other is odd (e.g., $\Delta_k^{Q_y} \propto \cos k_x$ and $\Delta_k^Q \propto \sin k_x$, respectively). In contrast, for charge order with diagonal $\mathbf{Q}_d = 2\mathbf{k}_{\text{hs}}$, only the even in k solution is possible because the center-of-mass momentum is at $\mathbf{k}_0 = (\pi,0)$ or $(0,\pi)$ and $\mathbf{k}_0$ and $-\mathbf{k}_0$ are equivalent points.

We show that the even component $\Delta_{1,k}^{Q_y} = (\Delta_k^{Q_y} + \Delta_{-k}^{Q_y})/2$ represents a variation of site and bond charge densities [a variation of the site density is $\delta\rho(r) \propto \cos 2Qr_y$], while the odd component $\Delta_{2,k}^{Q_y} = (\Delta_k^{Q_y} - \Delta_{-k}^{Q_y})/2$ represents a fermionic current $j_x(r) \propto \sin 2Qr_y$ This current gives rise to a nonzero orbital magnetic field $H_z \propto \cos 2Qr_y$ and, by definition, breaks time-reversal symmetry (TRS). This, however, does not lead to orbital ferromagnetism as $\int H_z dV$ vanishes.

We compute T_{CDW} for even and odd components and show that T_{CDW} for the even component is larger, in agreement with Refs. [64,65], but the one for the odd component is a close second. We derive the Ginzburg-Landau (GL) model for four $U(1)$ CDW fields $\Delta_{1,k}^{Q_x}$, $\Delta_{2,k}^{Q_x}$, $\Delta_{1,k}^{Q_y}$, and $\Delta_{2,k}^{Q_y}$. We

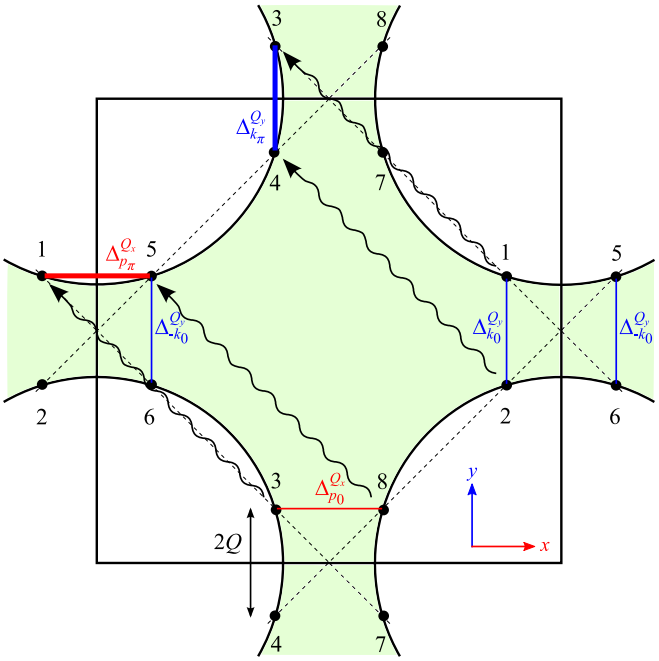

FIG. 1. (Color online) The Fermi surface, Brillouin zone, and magnetic Brillouin zone (dashed line). Hot spots are defined as intersections of the FS with magnetic Brillouin zone. The hot spot pairs 1-2 and 3-4 denote the CDW pairing we consider. They are coupled through the antiferromagnetic exchange interaction peaked at momentum (π,π), as shown by the dashed arrows.

argue that at low T, both density and charge components are generally nonzero, and the system develops a CDW order of one of two types, depending on the interplay between system parameters. We label the corresponding ordered states as states I and II. In the state I, density and current modulations emerge with the same $\mathbf{Q}$ (either Q_x or Q_y) via a continuous second-order transition. Such an order spontaneously breaks C_4 lattice rotational symmetry down to C_2, like in the case when only $\Delta_{1,k}^Q$ was set to be nonzero. The density and the current component with a given Q are both nonzero at low enough T and the phase difference between them is locked at $\pm\pi/2$. The order parameter in this state breaks Z_2 lattice rotational symmetry and $U(1)$ symmetry of the common phase of the two order parameters, and breaks an additional Z_2 symmetry by selecting the relative phase to be either $\pi/2$ or $-\pi/2$. It is natural to associate this additional Z_2 symmetry with time reversal (TR), which is then explicitly broken in state I.

In state II, incommensurate density and current modulations emerge with different $\mathbf{Q}$ via first-order transition. There are two realizations of state II: in the first, all four CDW components are nonzero and have equal magnitudes, while relative phases between $\Delta_{1,k}^{Q_x}$ and $\Delta_{2,k}^{Q_x}$ and between $\Delta_{1,k}^{Q_y}$ and $\Delta_{2,k}^{Q_y}$ are, simultaneously, either $\pi/2$ or $-\pi/2$. This is a C_4-symmetric checkerboard state with order parameter manifold $U(1) \times U(1) \times Z_2$, where Z_2 is associated with TR. In the second realization, only one density and one current components are nonzero, e.g., $\Delta_{1,k}^{Q_x}$ and $\Delta_{2,k}^{Q_y}$. Such

an order breaks C_4 lattice symmetry down to C_2, but does not additionally break TR symmetry because the phases of $\Delta_{1,k}^{Q_x}$ and $\Delta_{2,k}^{Q_y}$ are uncorrelated. The order parameter is again $U(1) \times U(1) \times Z_2$, with Z_2 now associated with lattice rotational symmetry.

We extend the analysis of the Ginzburg-Landau action beyond mean field by applying the Hubbard-Stratonovich transformation to collective variables and analyzing the resulting action within the saddle-point approximation, in close similarity to the analysis of the nematic order in Fe pnictides [66]. We specifically focus on state I, which in mean field emerges via a continuous transition. We show that discrete symmetries get broken before long-range charge order sets in. We show that, upon lowering the temperature, the system first breaks Z_2 lattice rotational symmetry ($C_4 \to C_2$) at $T = T_n$ and develops a nematic order. Below T_n, $\langle |\Delta_{i,\mathbf{k}}^{Q_y}|^2 \rangle$ becomes nonequal to $\langle |\Delta_{i,\mathbf{k}}^{Q_x}|^2 \rangle$ ($i = 1,2$), while $\langle \Delta_{i,\mathbf{k}}^{Q_{x,y}} \rangle = 0$, i.e., density and current modulations do not develop, $\langle \delta\rho(r) \rangle = \langle j_x(r) \rangle = 0$. Such a nematic order has been discussed in a series of recent publications on the cuprates [67] and Fe pnictides [66]. Then, at a smaller $T_t \leqslant T_n$, another composite order parameter $\Upsilon \propto \langle \Delta_1^{Q_y} (\Delta_2^{Q_y})^* \rangle \rangle$ becomes nonzero (for the order with $\mathbf{Q} = Q_y$), while still $\langle \Delta_{i,\mathbf{k}}^{Q_{x,y}} \rangle = 0$. Under time reversal, Υ transforms into $-\Upsilon$, hence this composite order breaks TRS. This order can be understood as the locking of a relative phase ψ of $\Delta_{1,\mathbf{k}}^{Q_y}$ and $\Delta_{2,\mathbf{k}}^{Q_y}$ at $\psi = \pi/2$ or $-\pi/2$ without the locking of the common phase of $\Delta_{1,\mathbf{k}}^{Q_y}$ and $\Delta_{2,\mathbf{k}}^{Q_y}$. The emergence of a preemptive composite order which breaks time-reversal symmetry has been verified in Ref. [68] using a different computational technique. Finally, below $T_{\mathrm{CDW}} < T_t$, the system breaks $U(1)$ symmetry of the common phase and the system develops a true CDW order (a quasi-long-range order in two dimensions). Within our theory, we identify the temperatures T_n and T_t as the experimental pseudogap temperature T^*.

The existence of the preemptive order is the crucial element in our scenario. Without it, CDW instability would be subleading to d-wave superconductivity and to bond order with diagonal $\mathbf{Q}_d = (2Q, \pm 2Q)$ as in the mean-field approximation both have larger onset temperatures than T_{CDW}. However, the superconducting order parameter and order parameter for bond charge order have only one, even in k, component, and for these two there is no preemptive instability which would break time-reversal symmetry. Moreover, neither superconductivity nor bond order break C_4 symmetry. For bond order, this is the consequence of the fact that bond orders with $(2Q,2Q)$ and $(2Q,-2Q)$ only weakly interact with each other because in a fourth-order square diagram for the interaction term some fermions are necessarily far away from the FS. As a result, the two orders appear simultaneously and form a checkerboard-type structure. If the system parameters are such that T_n gets larger than the onset temperature for superconductivity/bond order, the first instability upon lowering of T is into a state with a composite CDW order with $Q_x(Q_y)$. Once composite order forms, it reconstructs fermionic excitations and tends to reduce the onset temperatures for superconductivity/bond order because composite charge order and superconductivity/bond order compete for the FS. At the same time, a composite CDW order increases the susceptibility for the primary CDW fields and hence increases T_{CDW}, much like a spin-nematic order in Fe pnictides increases the Néel temperature of spin-density-wave (SDW) order [66]. An increase of T_{CDW} compared to the onset of superconductivity/bond order becomes even stronger once we include into consideration two-dimensional (2D) fluctuation effects because composite order only breaks discrete Ising symmetry, while near-degenerate d-wave superconductivity and bond order form the weakly anisotropic $O(4)$ model, in which T_{SC} is strongly reduced by fluctuations from the $O(4)$ manifold.

The two transitions at T_n and T_{CDW} have been also found in the scenario [63] that CDW order is due to strong superconducting fluctuations, but in that case CDW order has only an even in k component and there is no intermediate T range where C_4 symmetry and/or TRS are broken.

We next consider doping evolution of T_{CDW} and the interplay between charge order and superconductivity at various dopings. We argue that T_{CDW} decreases when magnetic correlation length ξ decreases and vanishes at some finite ξ, setting up a charge QCP at some distance away from the magnetic instability [see Figs. 17(a) and 17(b)]. A similar doping dependence holds for the onset temperature for bond order with diagonal $\mathbf{Q}$, as we also demonstrate. The ideas about a nonmagnetic QCP at around optical doping have been presented in earlier publications [46,69,70], and in our theory we found such QCP in microscopic calculations. The onset temperatures of nematic and TRS-breaking composite orders follow the same doping dependence as T_{CDW}. Within the saddle-point Hubbard-Stratonovich theory, T_n and T_t merge with T_{CDW} at some small T below which the system undergoes a single first-order CDW transition [71]. Whether this holds beyond the saddle-point approximation remains to be seen, but in any case near the critical ξ, T_{SC} is higher than both T_{CDW} and T_n, and at larger dopings (smaller ξ) only superconducting order develops. The precise location of the CDW QCP will likely by affected by superconductivity, as it generally happens when one order develops under the umbrella of another [72–74].

We assume that charge QCP exists and combine the doping dependencies of T_{SC}, T_{CDW}, T_n, and T_t into the full phase diagram, which we show in Fig. 17(c). We conjecture that the reduction of T_{SC} in the underdoped regime is primarily the result of a direct competition between superconductivity and composite CDW order, while a reduction due to fluctuations between superconductivity and bond order [58] plays a secondary role. We emphasize that in our model, superconductivity and CDW order are produced by the same underlying spin-fluctuation exchange interaction, and in this respect they are, in the terminology of Refs. [75,76], intertwined rather than competing orders. The situation is again similar to the one for underdoped pnictides where superconductivity and SDW orders are also intertwined orders as they originate from the same four-fermion pair-hopping interaction [73,74].

We compare our theoretical phase diagram with the one for hole-doped cuprates and present quantitative comparison of our theory with ARPES data, including Fermi arcs in the

normal state [77] and the doping evolution of the spectral function at low T, when the systems moves from a pure superconducting state into a state where superconductivity and charge order coexist. We argue that the agreement with the data is quite good, but to describe the evolution of the ARPES dispersion along the cuts closer to zone diagonals one needs to go beyond what we did so far and solve for the CDW order parameter Δ_k^Q for k rather far away from the midpoint between hot spots.

The structure of the paper is the following. In the next section, we consider the model. In Sec. III, we analyze the onset of CDW order with momentum $Q_x = (2Q,0)$ and $Q_y = (0,2Q)$ at near-infinite magnetic correlation length, when spin-fluctuation-mediated interaction is the strongest and fermionic self-energy is large and cannot be neglected. We present our solution of the ladder set of equations for the CDW order parameter first to logarithmical accuracy and then beyond the logarithmical approximation. We show that the CDW problem belongs to a class of threshold problems, however, the value of the coupling in our case is above the threshold. We compute $T_{\rm CDW}$ first in Eliashberg-type calculations and then by treating the effects of thermal bosonic fluctuations beyond Eliashberg theory, and compare $T_{\rm CDW}$ with $T_{\rm SC}$ obtained using the same procedures. We also analyze nonladder diagrams and present a nonlinear equation for the CDW order parameter. In Sec. IV, we expand near the ladder solution, show that the solution corresponds to the minimum of the effective action within the CDW subset, and discuss the interplay between CDW and superconducting and bond-order instabilities. In Sec. V, we discuss the structure of the CDW solution within the mean-field approximation. We first approximate CDW order parameters $\Delta_k^Q = \langle c^\dagger_{\mathbf{k}+\mathbf{Q}} c_{\mathbf{k}-\mathbf{Q}}\rangle$ by Δ^{Q_x} and Δ^{Q_y} in hot regions and analyze the interplay between CDW orders with Q_x and Q_y. We show that CDW order breaks lattice rotational C_4 symmetry down to C_2 and develops in the form of stripes. We then show that CDW order Δ_k^Q actually has two components, one is even under $\mathbf{k} \to -\mathbf{k}$ and the other is odd ($\Delta_{1,k}^Q$ and $\Delta_{2,k}^Q$, respectively). Both are $U(1)$ fields, and the odd component changes sign under time reversal. We derive the GL functional for four coupled CDW order parameters $\Delta_{1,k}^{Q_x}$, $\Delta_{2,k}^{Q_x}$, $\Delta_{1,k}^{Q_y}$, and $\Delta_{2,k}^{Q_y}$ and argue that either state I or state II is realized at low T, depending on the interplay between the two input parameters. We show that in state I, CDW order still breaks C_4 lattice symmetry down to C_2, and, in addition, the phases of $\Delta_{1,k}^{Q_y} = |\Delta_1|e^{i\varphi_1}$ and $\Delta_{2,k}^{Q_y} = |\Delta_2|e^{i\varphi_2}$ differ by $\varphi_1 - \varphi_2 = \pm\pi/2$. The selection $\pi/2$ or $-\pi/2$ breaks TRS. In Sec. VI, we analyze GL action for state I beyond mean field by introducing collective variables (by-products of $\Delta_{1,2}$) and search for nonzero expectation values of these variables within the saddle-point approximation. We argue that CDW order develops in three stages, via two intermediate phases, one with pure nematic order and another with additional breaking of TRS. In Sec. VII, we consider the interplay between composite CDW orders, a true CDW order, and superconductivity, and obtain the phase diagram of hole-doped cuprates as a function of hole doping whose increase we identify with the decrease of a magnetic correlation length ξ. Here, we show that $T_{\rm CDW}$, T_n, and T_t decrease with decreasing ξ and vanish at (the same) finite ξ setting up a CDW quantum-critical point at some distance from a quantum-critical point associated with the onset of a magnetic order. In Sec. VIII, we compare our results with the ARPES data both above and below $T_{\rm SC}$. We present our conclusions in Sec. IX. The discussion on several technical issues is moved into the Appendices. For completeness, in Appendix F we also discuss the doping dependence of the onset temperature for bond order and the corresponding phase diagram.

In our consideration, we approximate the electronic structure and collective spin excitations as two dimensional, i.e., neglect fermionic and bosonic dispersions along the k_z direction. We believe that the essential physics is captured within 2D treatment, although a coherent interlayer tunneling may be important for the stabilization of the stripe phase [78]. We also assume that near CDW instability, the system remains a metal, albeit with strong incoherence caused by quantum criticality. A development of stripe CDW order from a quantum antiferromagnet in the strong coupling regime has been recently considered in Ref. [79].

II. MODEL

We use the same spin-fermion model as in earlier studies of magnetically mediated d-wave superconductivity [35,37] and non-Fermi-liquid physics outside of the pseudogap region [38,57]. The model describes low-energy fermions with the FS shown in Fig. 1 and with four-fermion interaction mediated by soft spin collective excitations peaked at or near (π,π). We focus on hot regions on the FS, for which shifting $\mathbf{k}_F$ by $\mathbf{k}_F + (\pi,\pi)$ keeps a fermion near the FS, and expand fermionic dispersion near a hot spot as $\epsilon_k = v_{F,\mathbf{k}}(k_\perp + \kappa k_\parallel^2/k_F)$, where $v_{F,\mathbf{k}}$ is a Fermi velocity at a hot spot, $k_\parallel$ is a deviation from a hot spot along the FS, and dimensionless κ specifies the curvature of the FS. The Fermi velocities at hot spots $\mathbf{k}_1$, $\mathbf{k}_2$ and $\mathbf{k}_3 = \mathbf{k}_1 + (\pi,\pi)$, $\mathbf{k}_4 = \mathbf{k}_2 + (\pi,\pi)$ in Fig. 1 are $\mathbf{v}_{F,\mathbf{k}_1} = (v_x, v_y)$, $\mathbf{v}_{F,\mathbf{k}_2} = (v_x, -v_y)$, $\mathbf{v}_{F,\mathbf{k}_3} = (-v_y, -v_x)$, and $\mathbf{v}_{F,\mathbf{k}_4} = (-v_y, v_x)$. The amplitude of the Fermi velocity $v_{F,\mathbf{k}} = \sqrt{v_x^2 + v_y^2}$ and the value of κ are the same at all hot spots. The effective four-fermion interaction mediated by soft spin excitations is

$$H_{\rm int} = \bar{g}\chi(q) c^\dagger_{k+q,\alpha}\sigma_{\alpha\beta}c_{k,\beta}c^\dagger_{p-q,\gamma}\sigma_{\gamma\delta}c_{p,\delta}, \qquad (1)$$

where $k = (\mathbf{k},\omega_m)$, $q = (\mathbf{q},\Omega_\mathbf{m})$, $\omega_m(\Omega_m)$ are fermionic (bosonic) Matsubara frequencies, and

$$\chi(q) = \chi(\mathbf{q},\Omega_m) = \frac{1}{\mathbf{q}^2 + \xi^{-2} + \gamma|\Omega_m|}, \qquad (2)$$

where the last term in the denominator is the Landau damping with the coefficient $\gamma = 4\bar{g}/(\pi|v_y^2 - v_x^2|)$ [38]. The Landau damping contains the same $\bar{g}$ as in (1) because Landau damping of collective spin excitations also originates from the spin-fermion interaction.

Following earlier works [38,57,58], we assume that the coupling $\bar{g}$ is small compared to the Fermi energy $E_F = v_F k_F/2$ and focus on instabilities which occur at energies well below E_F and at $\xi^{-1} \geqslant 0$, before the system becomes magnetically ordered. One such instability is towards a

d-wave superconductivity [35–37,61]. It involves fermions from hot and lukewarm regions on the FS [with the self-energy $\Sigma(k_\parallel,\omega_m) \propto \sqrt{\omega_m}$ and $\Sigma(k_\parallel,\omega_m) \propto \omega_m/|k_\parallel|$, respectively], and taken alone (i.e., without competition with CDW order) occurs at $T_{SC} = T_{SC}(\xi)$, which is nonzero at all ξ and interpolates between $T_{SC}(\xi) \approx 0.04\bar{g}$ at large ξ, with weak dependence on v_x/v_y [61,80], and BCS-type result $T_{SC}(\xi) \sim (\bar{g}/\lambda^2)e^{-1/\lambda}$, at smaller $\xi \ll E_F/\bar{g}$, when dimensionless coupling $\lambda = 3\bar{g}/(4\pi v_F \xi^{-1})$ is small [see Fig. 17(b)]. Another instability, considered in [57,58], is towards a d-wave charge bond order with diagonal momentum $2k_{hs} = (2Q, \pm 2Q)$, where $k_{hs} = (Q,\pi \pm Q)$. This instability develops at $T_{BO}(\xi)$, which is smaller than $T_{SC}(\xi)$ at any nonzero κ, although rather close to it at $\xi \to \infty$ [57,58]. We analyze the form of $T_{BO}(\xi)$ in Appendix F where we show that $T_{BO}(\xi)$ vanishes at a certain ξ, when $\lambda \ln[E_F/(\bar{g}\kappa)] = O(1)$.

Our goal is to analyze another CDW channel, the one with momentum $Q_x = (2Q,0)$ or $Q_y = (0,2Q)$. This pairing involves fermions from hot/lukewarm regions 1-2, 3-4, etc., in Fig. 1. The analysis of a potential CDW instability involving these fermions is a bit tricky because fermions in the two regions connected by (π,π) (e.g., regions 1-2 and 3-4 in Fig. 1) are different in the sense that parallel (antiparallel) velocities are v_x (v_y) in the first set and $-v_y$ ($-v_x$) in the second. Accordingly, the CDW order parameter $\Delta_k^Q = \langle c^\dagger_{k+Q,\alpha} c_{k-Q,\alpha}\rangle$ does not obey a particular symmetry relation under $k \to k + (\pi,\pi)$, and one has to solve the 2×2 coupled set of equations for Δ_k^Q and $\Delta^Q_{k+(\pi,\pi)}$.

In the next two sections, we consider CDW instability with momentum $\mathbf{Q}$ along either x or y axis near the onset of SDW order, when the magnetic correlation length ξ is near infinite. We consider what happens at smaller ξ later in Sec. VII. We perform our analysis in two stages. In the next section (Sec. III), we solve the set of linearized gap equations for Δ_k^Q and $\Delta^Q_{k+\pi}$ within the ladder approximation and show that this set has nontrivial solution at a nonzero T_{CDW}. In Sec. IV, we rederive the same set by performing Hubbard-Stratonovich transformation from original fermions to bosonic CDW variables and show that the diagrammatic ladder approximation is equivalent to the saddle-point approximation in the Hubbard-Stratonovich approach. We expand around the Hubbard-Stratonovich solution within the CDW subset and show that the saddle-point solution is the minimum of the effective action, i.e., fluctuations around the saddle-point solution do not diverge. We then discuss the interplay between our CDW and superconductivity/bond order. We argue that our CDW order and the other orders can be treated within a generic Ginzburg-Landau functional. Taken alone, each order is stable and is not destroyed by fluctuations. This internal stability implies that the system develops the order which sets up at the highest T. At a mean-field level, $T_{SC} \geqslant T_{BO} > T_{CDW}$, hence superconductivity develops first. However, we show in Sec. VI that composite CDW order develops at $T_n > T_{CDW}$ and this temperature well may exceed T_{SC}. Once this happens, composite charge order provides negative feedback on superconducting/bond order, reducing the corresponding mean-field onset temperatures, and gives positive feedback on T_{CDW} which in some parameter ranges becomes larger than T_{SC}.

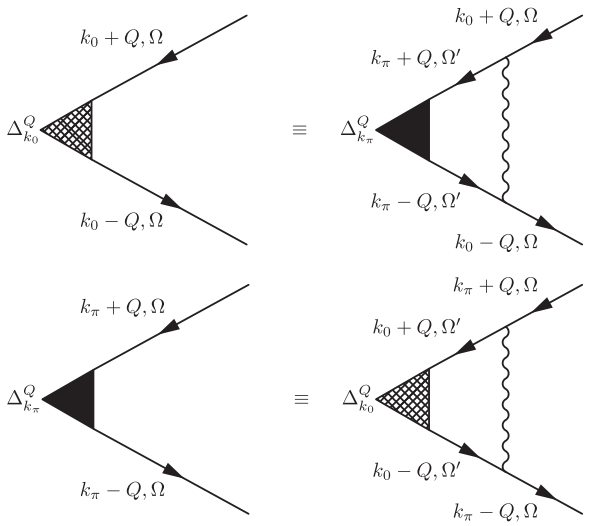

FIG. 2. The set of linearized equations for CDW vertices constructed out of fermions near hot spots. The momenta k_0 and $k_\pi = k_0 + (\pi,\pi)$ are in-between the two neighboring hot spots either along the x or along the y direction, chosen such that $k_0 \pm Q$ and $k_\pi \pm Q$ are right at the hot spots. The solid lines are full fermionic propagators, the wavy lines represent spin-mediated interaction peaked at (π,π).

III. ONSET OF CDW ORDER WITH MOMENTUM $(2Q,0)$ AND $(0,2Q)$ AT $\xi = \infty$

Borrowing notations from superconductivity, we will be calling the equations for Δ_k^Q and $\Delta^Q_{k+(\pi,\pi)}$ as "gap" equations. We will first solve for the onset of CDW instability in the ladder approximation without discussing its validity and later show that nonladder contributions to the gap equation are small numerically. We start with hot regions 1-2 and 3-4 in Fig. 1. These two pairs forms a closed set for the CDW gap equations, and pairing in other hot regions should simply follow due to symmetry.

The gap equations in the ladder approximation are shown in Fig. 2. The CDW order parameters Δ_k^Q and $\Delta^Q_{k+\pi} \equiv \Delta^Q_{k+(\pi,\pi)}$ are expressed via each other, and one needs to solve a set of two coupled gap equations to find an instability. Each equation is, in general, an integral equation in both frequency and momentum. Besides, fermionic propagators in the right-hand side of the gap equations contain the self-energy $\Sigma(k,\Omega_m)$ which is large and depends on frequency Ω_m and on the deviation of an internal fermion from a corresponding hot spot in the direction along the FS [38,57]. We present the calculation of T_{CDW} in which we keep only frequency dependence in the fermionic self-energy and in the gap functions, i.e., approximate $\Sigma(k,\Omega_m) \approx \Sigma(k_{hs},\Omega_m) \equiv \Sigma_{\Omega_m}$, $\Delta_k^Q(\Omega_m) \approx \Delta^Q_{k_0}(\Omega_m)$ when k is near k_0, and $\Delta_k^Q(\Omega_m) \approx \Delta^Q_{k_\pi}(\Omega_m)$ when k is near k_π. Such an approximation has been verified [61] to be a valid one in the calculation of a superconducting T_{SC} and we expect it to be valid also for a CDW instability. The full gap equations, with momentum-dependent CDW order parameters and momentum-dependent self-energy, are presented in Appendix A.

In analytical form, the set of the two linearized integral equations in frequency for $\Delta^Q_{k_0}(\Omega_m)$ and $\Delta^Q_{k_\pi}(\Omega_m)$ is

$$\Delta^Q_{k_0}(\Omega_m) = \frac{3\bar{g}T_{\rm CDW}}{4\pi^2}\sum_{m'}\int \frac{dx\,dy}{\left[i\tilde{\Sigma}(\Omega_{m'}) - v_x y + v_y x\right]\left[i\tilde{\Sigma}(\Omega_{m'}) + v_x y + v_y x\right]}\frac{\Delta^Q_{k_\pi}(\Omega_{m'})}{x^2+y^2+\gamma|\Omega_m-\Omega_{m'}|}, \tag{3}$$

$$\Delta^Q_{k_\pi}(\Omega_m) = \frac{3\bar{g}T_{\rm CDW}}{4\pi^2}\sum_{m'}\int \frac{dx\,dy}{\left[i\tilde{\Sigma}(\Omega_{m'}) - v_x x + v_y y\right]\left[i\tilde{\Sigma}(\Omega_{m'}) - v_x x - v_y y\right]}\frac{\Delta^Q_{k_0}(\Omega_{m'})}{x^2+y^2+\gamma|\Omega_m-\Omega_{m'}|}, \tag{4}$$

where $\gamma = 4\bar{g}/[\pi(v_y^2 - v_x^2)]$, x and y are momentum deviations from the corresponding hot spots, $\tilde{\Sigma}(\Omega_m) = \Omega_m + \Sigma(\Omega_m)$, and the fermionic self-energy $\Sigma(\Omega_m)$ is the solution of the self-consistent equation

$$\Sigma(\Omega_m) = \frac{3\bar{g}T}{4\pi}\sum_{\Omega_{m'}}\int dy \frac{\mathrm{sgn}(\Omega_{m'})}{\sqrt{y^2+\gamma|\Omega_m-\Omega_{m'}|}}\frac{1}{\sqrt{y^2+\gamma|\Omega_m-\Omega_{m'}|}+|\tilde{\Sigma}(\Omega'_m)|/v_F}. \tag{5}$$

The fermionic Green's function $G(k,\Omega_m)$ is related to $\tilde{\Sigma}(\Omega_m)$ as

$$G^{-1}(k,\Omega_m) = i\tilde{\Sigma}(\Omega_m) - \epsilon_k, \tag{6}$$

where ϵ_k is the fermionic dispersion which in Eqs. (3) and (4) we expanded around hot spots. For hot fermions in regions 1 and 2 in Fig. 1, k_0 is near $(0,\pi)$, in which case $v_x < v_y$.

At $T = 0$, the summation over frequency in (5) can be replaced by the integration. The equation for the fermionic self-energy becomes

$$\Sigma(\Omega_m) = \frac{3\bar{g}}{8\pi^2}\int d\Omega_{m'}\int dy \frac{\mathrm{sgn}(\Omega_{m'})}{\sqrt{y^2+\gamma|\Omega_m-\Omega_{m'}|}}\frac{1}{\sqrt{y^2+\gamma|\Omega_m-\Omega_{m'}|}+|\tilde{\Sigma}(\Omega'_m)|/v_F}. \tag{7}$$

One can easily make sure that $\Sigma(\Omega_m) \propto \mathrm{sgn}(\Omega_{m'})\sqrt{|\Omega_{m'}|}$ at small enough frequencies. Earlier calculations [38,57] of $\Sigma(\Omega_m)$ neglected self-energy in the right-hand side of (7). In this approximation, the equation for $\Sigma(\Omega_m)$ is no longer of self-consistent form, and integration over y and over $\Omega_{m'}$ yields

$$\Sigma(\Omega_m) = \mathrm{sgn}(\Omega_{m'})\sqrt{\omega_0|\Omega_{m'}|}, \tag{8}$$

where $\omega_0 = 9\bar{g}/(16\pi) \times [(v_y^2 - v_x^2)/v_F^2]$. By order of magnitude, ω_0 coincides with the spin-fermion coupling constant $\bar{g}$. For consistency with previous works, following we will use ω_0 as the overall scale for the self-energy.

When the self-energy is kept in the right-hand side of (7), the self-energy at frequencies $|\Omega_m| < \omega_0$ retains the same functional form as in (8), but with the extra prefactor

$$\Sigma(\Omega_m) = A\,\mathrm{sgn}(\Omega_{m'})\sqrt{\omega_0|\Omega_{m'}|}, \tag{9}$$

where, to a good numerical accuracy, $A = \frac{2}{3}$.

To get an insight as to where the instability comes from, consider momentarily the case $v_x = 0$, $v_y = v_F$. Then, Fermi velocities at the two hot spots near $(\pi,0)$ (points 1 and 2 in Fig. 1) are antiparallel to each other, while the ones at the two hot spots near $(0,\pi)$ (points 3 and 4 in Fig. 1) are parallel. In this limit, Eqs. (3) and (4) reduce to

$$\Delta^Q_{k_0}(\Omega_m) = \frac{3\bar{g}T_{\rm CDW}}{4\pi^2}\sum_{m'}\int \frac{dx\,dy}{\left[i\tilde{\Sigma}(\Omega_{m'}) + v_F x\right]^2} \times \frac{\Delta^Q_{k_\pi}(\Omega_{m'})}{x^2+y^2+\gamma|\Omega_m-\Omega_{m'}|}, \tag{10}$$

$$\Delta^Q_{k_\pi}(\Omega_m) = -\frac{3\bar{g}T_{\rm CDW}}{4\pi^2}\sum_{m'}\int \frac{dx\,dy}{\left[\tilde{\Sigma}^2(\Omega_{m'}) + (v_F y)^2\right]} \times \frac{\Delta^Q_{k_0}(\Omega_{m'})}{x^2+y^2+\gamma|\Omega_m-\Omega_{m'}|}. \tag{11}$$

In earlier large-N calculations of $T_{\rm SC}$ (Refs. [37,38,57]), the dependence of the bosonic propagator on the momentum transverse to the FS [i.e., the x dependence in the last term in Eq. (10) and the y dependence in Eq. (11)] was neglected. If we used the same approximation here, we would obtain no CDW instability because the integral over x in Eq. (10) would vanish. However, in our case the bosonic propagator does depend on x and its poles are in both upper and lower half-planes of complex x. As a consequence, the momentum integration over x in the right-hand side of (10) gives a nonzero result even if we assume that Fermi velocities at points 3 and 4 in Fig. 1 are parallel. Furthermore, because at $\Omega_m < \omega_0$, $|\tilde{\Sigma}(\Omega_m)|/v_F \approx \Sigma(\Omega_m) \sim (\bar{g}|\Omega_m|/v_F^2)^{1/2} \sim (\gamma|\Omega_m|)^{1/2}$, the poles in the bosonic propagator are located at x comparable to that of the double pole. As a result, the result of the integration over x is comparable to what one would get from integrating over x in the two fermionic Green's functions, if the poles there were in different half-planes of x. In other words, the fact that the velocities at the hot spots at points 3 and 4 in Fig. 1 are parallel does not make the right-hand side of Eq. (10) parametrically smaller compared to the case in Eq. (11), where the velocities at the two hot spots are antiparallel and the momentum integral over the product of the two Green's function already gives a nonzero result. In Eq. (11), the contributions from the poles in the Green's function and in the bosonic propagator are of the same order and just add up in the overall prefactor.

We now return back to Eqs. (3) and (4) for $\Delta^Q_{k_0}(\Omega_m)$ and $\Delta^Q_{k_\pi}(\Omega_m)$. We first integrate over x in Eq. (3) and obtain

$$\Delta^Q_{k_0}(\Omega_m) = -\frac{3\bar{g}T_{\rm CDW}}{8\pi}\sum_{m'}\int_0^\infty \frac{dy}{\sqrt{y^2+\gamma|\Omega_m-\Omega_{m'}|}}\frac{\Delta^Q_{k_\pi}(\Omega_{m'})}{v_x^2y^2+\left[v_y\sqrt{y^2+\gamma|\Omega_m-\Omega_{m'}|}+\tilde{\Sigma}(\Omega_{m'})\right]^2}. \quad (12)$$

Introducing then $z = y/\sqrt{\gamma|\Omega_{m'}|}$ and $\varphi = \arctan(v_x/v_y)$ and using zero-temperature form of $\Sigma(\Omega_m) \approx (2/3)\mathrm{sgn}(\Omega_{m'})\sqrt{\omega_0|\Omega_{m'}|}$, we rewrite (12) as

$$\Delta^Q_{k_0}(\Omega_m) = -\frac{3\cos 2\varphi}{8}T_{\rm CDW}\sum_{m'}\frac{\Delta^Q_{k_\pi}(\Omega_{m'})}{|\Omega_{m'}|}\int_0^\infty \frac{dz}{\sqrt{z^2+|1-\Omega_m/\Omega_{m'}|}} \times \frac{1}{z^2\sin^2\varphi+[\sqrt{z^2+|1-\Omega_m/\Omega_{m'}|}\cos\varphi+(1/4)\cos 2\varphi(1+\sqrt{\Omega_{m'}/\omega_0})]^2}. \quad (13)$$

Integrating over x in Eq. (4) and rewriting the result in the same variables z and φ we obtain

$$\Delta^Q_{k_\pi}(\Omega_m) = -\frac{3\cos 2\varphi}{8}T_{\rm CDW}\sum_{m'}\frac{\Delta^Q_{k_0}(\Omega_{m'})}{|\Omega_{m'}|}\int_0^\infty \frac{dz}{\sqrt{z^2+|1-\Omega_m/\Omega_{m'}|}} \times \frac{1}{z^2\cos^2\varphi+[\sqrt{z^2+|1-\Omega_m/\Omega_{m'}|}\sin\varphi+(1/4)\cos 2\varphi(1+\sqrt{\Omega_{m'}/\omega_0})]^2}. \quad (14)$$

The value of φ depends on the geometry of the FS. When Fermi velocities at hot spots 1 and 2 in Fig. 1 are nearly antiparallel, and the ones at hot spots 3 and 4 are nearly parallel, we have $\varphi \approx 0$. When Fermi velocities at hot spots 1 and 2 are nearly perpendicular to each other, we have $\varphi \approx \pi/4$. For the FS as in hole-doped cuprates, φ is nonzero, but small numerically.

The negative signs in the right-hand sides of (13) and (14) imply that the solution is only possible when $\Delta^Q_{k_0}(\Omega_m)$ and $\Delta^Q_{k_\pi}(\Omega_m)$ have opposite signs, i.e., CDW order parameter $\Delta^Q_k(\Omega_m)$ changes sign under $\mathbf{k} \to \mathbf{k}+(\pi,\pi)$. This does not imply, however, that the order has only a bond component $\langle c^\dagger(\mathbf{r}+\mathbf{a})c(\mathbf{r})\rangle$ [57]. In our case, $\Delta^Q_{k_0}(\Omega_m)$ and $\Delta^Q_{k_\pi}(\Omega_m)$ differ in magnitude, and both onsite and bond components are present. For the onsite charge density we have

$$\langle c^\dagger(\mathbf{r})c(\mathbf{r})\rangle = \sum_{\mathbf{k},\mathbf{Q}}\Delta^Q_k e^{i\mathbf{Qr}} = \sum_Q\left(\Delta^Q_{k_0}+\Delta^Q_{k_\pi}\right)e^{i\mathbf{Qr}}. \quad (15)$$

A. Gap equations to logarithmic accuracy

1. *Neglecting frequency dependencies of $\Delta^{\mathbf{Q}}_{k_0}(\Omega_m)$ and $\Delta^{\mathbf{Q}}_{k_\pi}(\Omega_m)$*

As a first pass on Eqs. (13) and (14), we approximate gap functions as frequency-independent constants $\Delta^{\mathbf{Q}}_{k_0}$ and $\Delta^{\mathbf{Q}}_{k_\pi}$, set the lower limit of integration over internal fermionic frequency to $\pi T_{\rm CDW}$, and neglect the dependence on external frequency in (13) and (14). Evaluating the integrals with two fermionic and one bosonic propagators, we find that they are logarithmically singular, no matter what φ is. To logarithmical accuracy, we obtain

$$\Delta^Q_{k_0} = -S_1(\varphi)\ln\frac{\omega_0}{T_{\rm CDW}}\Delta^Q_{k_\pi}, \qquad \Delta^Q_{k_\pi} = -S_2(\varphi)\ln\frac{\omega_0}{T_{\rm CDW}}\Delta^Q_{k_0}, \quad (16)$$

where

$$S_1(\varphi) = \frac{3\cos 2\varphi}{8\pi}\int_0^\infty \frac{dz}{\sqrt{z^2+1}}\frac{1}{z^2\sin^2\varphi+[\sqrt{z^2+1}\cos\varphi+(1/4)\cos 2\varphi]^2},$$
$$S_2(\varphi) = \frac{3\cos 2\varphi}{8\pi}\int_0^\infty \frac{dz}{\sqrt{z^2+1}}\frac{1}{z^2\cos^2\varphi+[\sqrt{z^2+1}\sin\varphi+(1/4)\cos 2\varphi]^2}. \quad (17)$$

We emphasize that these two functions remain finite even if we set $\varphi = 0$ (i.e., set the velocities at hot spots 3 and 4 in Fig. 1 to be parallel to each other). Note also that S_1 and S_2 depend on the ratio of v_x/v_y but not on $\bar{g}$, which cancels out between the overall factor in the spin-fermion interaction and in the Landau damping. This cancellation is typical for an instability mediated by a massless Landau-overdamped collective mode [80].

Evaluating S_1 and S_2 numerically, we found (see Fig. 3) that $S_2 > S_1 > 0$ as long as $\varphi < \pi/4$. In the limit when $\varphi = 0$ (i.e., when the velocities at hot spots 1 and 2 are antiparallel, and the ones at hot spots 3 and 4 are parallel), we have $S_1 = 0.084$ and $S_2 = 0.650$ ($\sqrt{S_1S_2} = 0.234$). At nonzero φ, the values of S_1 and S_2 are closer to each other. That $S_2 > S_1$ implies that the CDW order parameter in the region with nearly antiparallel Fermi velocities (region 1-2 in our case) is smaller than in the

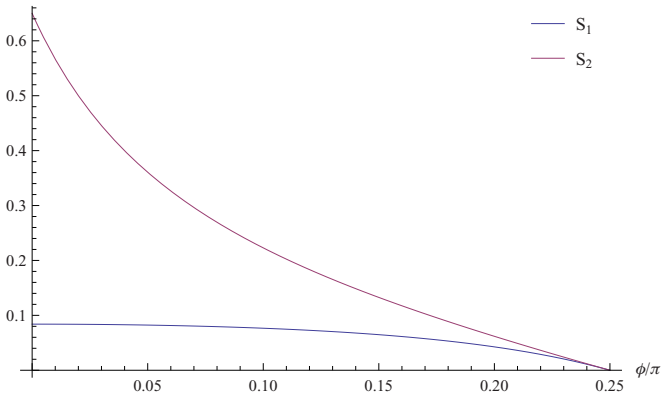

FIG. 3. (Color online) The integrals S_1 and S_2 as functions of the angle φ. Both integrals vanish at $\varphi = \pi/4$ because at this φ the Landau damping coefficient diverges.

region with nearly parallel velocities (region 3-4 in our case). Solving the set (16) we immediately obtain that the linearized gap equation has a nonzero solution at

$$1 = S_1 S_2 \left(\ln \frac{\omega_0}{T_{\rm CDW}} \right)^2, \tag{18}$$

i.e., at $T_{\rm CDW} \sim \omega_0 e^{-1/\sqrt{S_1 S_2}}$. This $T_{\rm CDW}$ is of the same order of magnitude as superconducting $T_{\rm SC}$, which at the onset of SDW order is also of order ω_0 [37,61]. Right at $T = T_{\rm CDW}$ we have from (16)

$$\Delta^Q_{k_0} = -\Delta^Q_{k_\pi} \sqrt{\frac{S_2}{S_1}}. \tag{19}$$

2. *Keeping frequency dependencies of $\Delta^Q_{k_0}(\Omega_m)$ and $\Delta^Q_{k_\pi}(\Omega_m)$*

Equation (18) has been obtained within the approximations that (i) CDW order parameters Δ_{k_0} and Δ_{k_π} do not depend on frequency, and (ii) one can neglect the dependence on external Ω in the right-hand side of Eqs. (13) and (14). For a more accurate treatment, we need to keep the frequency dependence in $\Delta^Q_{k_0}(\Omega_m)$ and in $\Delta^Q_{k_\pi}(\Omega_m)$.

Plugging Eq. (14) into (13), we get rid of $\Delta^Q_{k_\pi}(\Omega_m)$ and obtain the integral equation for $\Delta^Q_{k_0}(\Omega)$ in the form

$$\Delta^Q_{k_0}(\Omega_m) = T \sum_{m'} I(\Omega_m, \Omega_{m'}) \Delta^Q_{k_0}(\Omega_{m'}), \tag{20}$$

where the kernel $I(\Omega_m, \Omega_{m'})$ depends on both external and internal frequencies.

We first analyze the pairing susceptibility. For this we add the source term Δ_0 to the right-hand side of Eq. (20) and search for the divergence of $\Delta^Q_{k_0}/\Delta_0$ at $T = T_{\rm CDW}$. At first order of iterations we replace $\Delta^Q_{k_0}(\Omega_{m'})$ by Δ_0 in the integral part and obtain $\Delta^Q_{k_0}(\Omega_m = \pi T) = \Delta_0(1 + \frac{1}{2} S_1 S_2 \log^2 \frac{\omega_0}{T})$. This is the same result as we had before, except for the additional $\frac{1}{2}$ factor which is due to the requirement that, when we compute $\sum_{m'} I(\Omega_m, \Omega_{m'})$, the internal frequency must be much larger than the external one in order to obtain the $\log^2$ correction. If subsequent iterations would transform $1 + 0.5 S_1 S_2 \log^2 \frac{\omega_0}{T}$ into $1/(1 - 0.5 S_1 S_2 \log^2 \frac{\omega_0}{T})$, as it happens in BCS theory, we would obtain $T_{\rm CDW}$ similar to Eq. (18). However, we found that in our case the series of $\log^2$ terms actually sum up into a power-law form $\Delta^Q_{k_0} = \Delta_0 \cosh(\sqrt{S_1 S_2} \log \frac{\omega_0}{T}) \sim \Delta_0 (\frac{\omega_0}{T})^{\sqrt{S_1 S_2}}$. The implication is that, within the logarithmic approximation, the ratio $\Delta^Q_{k_0}/\Delta_0$ does not diverge at any finite T, i.e., Eq. (18) is an artifact of neglecting frequency dependence of Δ^Q. A similar situation holds in the superconducting channel. There, previous works have found [37,61,81] that the instability does develop, but to detect it one has to go beyond logarithmic accuracy, solve the full integral equation in frequency, and search whether or not there is an instability at $T > 0$. This is what we do next.

B. Beyond logarithmic approximation

1. *Pairing susceptibility at $T = 0$*

The first step in the analysis is to consider $T = 0$, when the summation over Matsubara frequencies can be replaced by integration. At $T = 0$, the lower cutoff of the logarithm is set by frequency rather than by T, hence within the logarithmic approximation

$$\Delta^Q_{k_0}(\Omega_m), \Delta^Q_{k_\pi}(\Omega_m) \propto \Delta_0 \left(\frac{\omega_0}{|\Omega_m|} \right)^{\sqrt{S_1 S_2}}. \tag{21}$$

We now verify whether the actual pairing susceptibility at $T = 0$ behaves similarly to (21) or changes sign, at least in some frequency ranges. The latter would indicate that the normal state is unstable, hence $T_{\rm CDW}$ is nonzero.

A similar strategy has been applied to the superconducting problem at the onset of SDW order, when magnetic $\xi = \infty$ [37,61]. We briefly discuss how it worked there and then apply it to our case. Like in our case, the summation of the leading logarithms for the superconducting problem does not lead to the instability and instead yields for the superconducting order parameter $\Delta_{\rm SC}(\Omega_m) \propto \Delta_0 (\frac{\omega_0}{|\Omega_m|})^{\alpha_0}$, where Δ_0 is again a source term and α_0 is some positive number of order one [82]. The solution of the full integral equation for $\Delta_{\rm SC}(\Omega_m)$ at $T = 0$ also yields a power-law form $\Delta_{\rm SC}(\Omega_m) \propto \Delta_0 (\frac{\omega_0}{|\Omega_m|})^{\alpha}$ at $\Omega_m < \omega_0$, like in (21), however, α turns out to be a complex number. In this situation, there are two solutions, one with α, another with α^*. The linear combination of these two solutions yields oscillating

$$\Delta^Q_{k_0} \propto \Delta_0 \cos[{\rm Im}(\alpha) \ln \omega + \theta] / |\Omega_m|^{{\rm Re}\alpha} \tag{22}$$

with a "free" phase variable θ. The presence of θ plays the crucial role when the analysis is extended to finite T and the source term Δ_0 is set to zero. The power-law behavior at a finite T exists in the frequency range between ω_0 and T and has to satisfy boundary conditions at the two edges. This requires two adjustable parameters. The temperature is one of them and the phase θ is the other one. Solving for the two boundary conditions requires care, but the result is that, very likely, they can be satisfied at a nonzero T, i.e., at this T the linearized gap equation has a solution. Whether this is the actual $T_{\rm SC}$ is a more subtle issue as there may exist some other solution of the linearized gap equation, with different behavior at small frequencies. In any case, however, the fact that Eq. (22) is the solution of the linearized gap equation at a

finite T implies that T_{SC} must be finite. From this perspective, the fact that the exponent α is complex is a sufficient condition for the existence of the pairing instability at a finite T_{SC} in the quantum-critical regime.

We follow the same strategy for the CDW case. We keep the frequency dependencies of $\Delta^Q_{k_0}$ and $\Delta^Q_{k_\pi}$ in Eqs. (13) and (14), solve these two equations as integral equations in frequency, search for a power-law solution, and analyze whether or not the exponent is complex. To shorten the presentation, we only consider the limiting case $\varphi = 0$, and replace the soft upper cutoff at ω_0 with a hard one. With this simplification, we obtain, replacing the sums by integrals,

$$\Delta^Q_{k_0}(\Omega_m) = \frac{-3}{16\pi}\int_{-\omega_0}^{\omega_0}\frac{d\Omega_{m'}\Delta^Q_{k_\pi}(\Omega_{m'})}{|\Omega_{m'}|}\int_0^\infty \frac{dz}{\sqrt{z^2+|1-\Omega_{m'}/\Omega_m|}(\sqrt{z^2+|1-\Omega_{m'}/\Omega_m|}+1/4)^2}, \tag{23}$$

$$\Delta^Q_{k_\pi}(\Omega_m) = \frac{-3}{16\pi}\int_{-\omega_0}^{\omega_0}\frac{d\Omega_{m'}\Delta^Q_{k_0}(\Omega_{m'})}{|\Omega_{m'}|}\int_0^\infty \frac{dz}{\sqrt{z^2+|1-\Omega_{m'}/\Omega_m|}}\frac{1}{z^2+1/16}. \tag{24}$$

We search for the solution in the form $\Delta^Q_{k_0}, \Delta^Q_{k_\pi} \sim |\Omega_m|^{-\alpha}$. One can easily verify that convergence of integrals requires $0 < \mathrm{Re}\,\alpha < 0.5$. Substituting this trial solution into (23) and (24), we find after simple algebra a self-consistency condition

$$g_{\mathrm{eff}} F(\alpha) G(\alpha) = 1, \tag{25}$$

where $g_{\mathrm{eff}} = \frac{9}{64}$ is the universal dimensionless coupling constant for our quantum-critical problem and

$$\begin{aligned} F(\alpha) &= \frac{1}{2\pi}\int_{-\infty}^{\infty}\frac{d\omega}{|\omega|^{1+\alpha}}\int_0^\infty \frac{dz}{\sqrt{z^2+|1-1/\omega|}(\sqrt{z^2+|1-1/\omega|}+1/4)^2}, \\ G(\alpha) &= \frac{1}{2\pi}\int_{-\infty}^{\infty}\frac{d\omega}{|\omega|^{1+\alpha}}\int_0^\infty \frac{dz}{\sqrt{z^2+|1-1/\omega|}}\frac{1}{z^2+1/16}. \end{aligned} \tag{26}$$

We solved Eq. (25) for α and found that the solution is a complex number: $\alpha = 0.288 \pm 0.185i$. The corresponding eigenfunction has the form $\Delta^Q_{k_0}, \Delta^Q_{k_\pi} \sim \cos[0.185 \ln|\Omega_m| + \theta]/|\Omega_m|^{-0.288}$, where θ is a free phase factor. Like we said, this is the sufficient condition for a CDW instability at a nonzero T_{CDW}.

2. *Computation of T_{CDW}*

Because the effective coupling g_{eff} is of order one, the only relevant energy scale in the quantum-critical regime is ω_0, hence, T_{CDW} must be of order ω_0. From this perspective, the estimate of T_{CDW} in Eq. (18) is actually not far off as it also gives T_{CDW} of order ω_0. To get the right ratio of $T_{\mathrm{CDW}}/\omega_0$, one needs to solve the set of the two linearized gap equations numerically.

There is one caveat, however, associated with the special role of zero bosonic Matsubara frequency term in the gap equation. Indeed, the frequency sum in each of Eqs. (23) and (24) contains the term with $\Omega_{m'} = \Omega_m$. For this particular Matsubara frequency, the integral over z diverges logarithmically, as $\ln\xi$, and, if there was no counterterm, T_{CDW} would vanish at $\xi = \infty$.

This issue is known in the superconducting problem [37,80,83]. The term with zero Matsubara frequency represents scattering with zero frequency transfer and a finite momentum transfer and from this perspective acts like an "impurity." The logarithmical divergence of the integral over dz in (23) and (24) implies that "impurity" has an infinite strength at $\xi = \infty$. Still, for an s-wave superconductor, the contribution to T_{SC} from impurities must vanish by Anderson theorem. To see this vanishing in our formalism, one needs to do calculations more accurately than we did so far and reevaluate fermionic self-energy at a finite T, as it also contains a $\ln\xi$ contribution coming from zero bosonic Matsubara frequency. For an s-wave superconductor, the two contributions cancel each other. For other cases, the situation is less obvious. For p-wave pairing, the divergent terms coming from zero bosonic Matsubara frequency do not cancel out within the Eliashberg approximation and this eventually gives rise to first-order superconducting transition [37]. For d-wave pairing, earlier calculations within the spin-fermion model used the Eliashberg approximation, in which the momentum integration is factorized; the one transverse to the FS is performed over the two fermionic propagators, while the one along the FS is performed over the bosonic propagator. Within this approximation, the contributions from zero Matsubara frequency to the pairing vertex and to the fermionic self-energy either completely cancel out in the gap equation [37,83], when fermionic self-energy is approximated by its value at a hot spot, or the divergent terms cancel out and the remaining nondivergent terms give rise to a modest reduction of T_{SC}, when the momentum dependence of the fermionic self-energy on $\mathbf{k}$ along the FS is kept [80]. On the other hand, in our solution of the CDW problem, it was crucial to go beyond Eliashberg approximation and include the contributions from the poles in the bosonic propagator in the integration along and transverse to the FS. (We recall that, for interactions mediated by collective modes of fermions, there is no small parameter to justify Eliashberg approximation, except for special cases near three dimensions [84,85]). To see whether or not the cancellation of the divergent contributions from zero Matsubara frequency holds in our case we have to keep the summation over Matsubara frequencies not only in the

equations for Δ_k^Q, but also in the self-energy. For definiteness, we consider the case $\varphi = 0$, when Fermi velocities at one pair of hot spots are antiparallel to each other and at the other are parallel. Like before, we neglect momentum dependencies of $\Delta_{k_0}^Q$, $\Delta_{k_\pi}^Q$ and the fermionic self-energy, i.e., approximate these quantities by their values at hot spots. The inclusion of the T dependence of the self-energy modifies Eqs. (23) and (24) to

$$\Delta_{k_0}^Q(\Omega_m^*) = -\frac{3T_{\rm CDW}^*}{8}\sum_{|\Omega_{m'}^*|<1}\Delta_{k_\pi}^Q(\Omega_{m'}^*)\int_0^\infty \frac{dy^*}{\sqrt{(y^*)^2+|\Omega_m^*-\Omega_{m'}^*|}}\frac{1}{\left[\sqrt{(y^*)^2+|\Omega_m^*-\Omega_{m'}^*|}+\frac{3}{8}\left|\tilde\Sigma^*(\Omega_{m'}^*)\right|\right]^2}, \tag{27}$$

$$\Delta_{k_\pi}^Q(\Omega_m^*) = -\frac{3T_{\rm CDW}^*}{8}\sum_{|\Omega_{m'}^8|<1}\Delta_{k_0}^Q(\Omega_{m'}^*)\int_0^\infty \frac{dy^*}{\sqrt{(y^*)^2+|\Omega_m^*-\Omega_{m'}^*|}}\frac{1}{(y^*)^2+\frac{9}{64}\left|\tilde\Sigma^*(\Omega_{m'})\right|^2}, \tag{28}$$

where $\tilde\Sigma^*(\Omega_m^*) = \Omega_m^* + \Sigma^*(\Omega_m^*)$, and

$$\Sigma^*(\Omega_m^*) = T_{\rm CDW}^*\sum_{|\Omega_{m'}^*|<\omega_0}\int_0^\infty dy^*\frac{{\rm sgn}(\Omega_{m'}^*)}{\sqrt{(y^*)^2+|\Omega_m-\Omega_{m'}|}}\frac{1}{\sqrt{(y^*)^2+|\Omega_m-\Omega_{m'}|}+\frac{3}{8}\left|\tilde\Sigma^*(\Omega_{m'})\right|}. \tag{29}$$

In (27)–(29) we used rescaled variables $\Omega_m^* = \Omega_m/\omega_0$, $\Sigma^* = \Sigma/\omega_0$, $T_{\rm CDW}^* = T_{\rm CDW}/\omega_0$, and $y^* = y/(\gamma\omega_0)^{1/2} = 2\pi v_F y/(3\bar g)$. Let us first analyze the equation for the self-energy Σ^*. We recall that at $T=0$ we have $\Sigma^*(\Omega^*) = \Omega^* + (2/3)\sqrt{|\Omega^*|}{\rm sgn}(\Omega^*)$. At a finite T, the leading contribution to the sum in the right-hand side of (29) is $\ln\xi$ from the term with $\Omega_{m'}^* = \Omega_m^*$. Restricting with only this term and neglecting bare Ω^* (i.e., neglecting the difference between $\tilde\Sigma^*$ and Σ^*), we obtain from (29)

$$\Sigma^*(\Omega_m^*) \approx \frac{8T_{\rm CDW}^* L\,{\rm sgn}(\Omega_m^*)}{3\left|\Sigma^*(\Omega_m^*)\right|}, \tag{30}$$

where $L = \ln\xi$. Solving (30) we obtain

$$\Sigma^*(\Omega_m^*) \approx \left(\frac{8T_{\rm CDW}^* L}{3}\right)^{1/2}{\rm sgn}(\Omega_m^*) + \ldots, \tag{31}$$

where the ellipsis stands for terms of order one. This formula is valid when $T_{\rm CDW}^* L$ is a large number.

Substituting this $\Sigma^*(\Omega_m^*)$ into the first two equations and assuming that relevant $\Omega_m^* - \Omega_{m'}^*$ and y are of order one (we later verify this), we pull out $\Sigma^*(\Omega_m^*)$ and after integration over y obtain

$$\Delta_{k_0}^Q(\Omega_m^*) \approx -\frac{8T_{\rm CDW}^*}{3}\sum_{|\Omega_{m'}^*|<1}\frac{\Delta_{k_\pi}^Q(\Omega_{m'}^*)}{(\Sigma^*)^2}\ln\frac{(\Sigma^*)^2}{|\Omega_m^*-\Omega_{m'}^*|}+\ldots,$$
$$\Delta_{k_\pi}^Q(\Omega_m^*) \approx -\frac{8T_{\rm CDW}^*}{3}\sum_{|\Omega_{m'}^*|<1}\frac{\Delta_{k_0}^Q(\Omega_{m'}^*)}{(\Sigma^*)^2}\ln\frac{(\Sigma^*)^2}{|\Omega_m^*-\Omega_{m'}^*|}+\ldots, \tag{32}$$

where $(\Sigma^*)^2 = [\Sigma^*(\Omega_m^*)]^2 = 8T_{\rm CDW}^* L/3$. We see that, as long as we neglect nonlogarithmic terms, $\Delta_{k_0}^Q = -\Delta_{k_\pi}^Q$. As a result, in this approximation CDW with Q_x/Q_y has pure d-wave form factor and in real space represents a bond order, just like CDW with diagonal Q. A site component (a true CDW) appears once we include corrections to (32) [labeled as ellipses in (32)], and is small in $1/L$. Such a structure of the charge order parameter is consistent with Refs. [64,65,86] and with the form of Δ_k^Q extracted from recent measurements [5,62].

The reason why $\Delta_{k_0}^Q$ and $\Delta_{k_\pi}^Q$ become almost equal by magnitude in spite of the difference in the arrangements of Fermi velocities in regions 1-2 and 3-4 in Fig. 1 is that at large T^*L, the $\tilde\Sigma$ term in the fermionic propagator $G^{-1}(k,\omega) = i\tilde\Sigma(\Omega) - \mathbf{v}\cdot\mathbf{k}$ becomes larger than the $\mathbf{v}\cdot\mathbf{k}$ term. Then, the difference between nesting and antinesting becomes almost irrelevant as each fermionic propagator can be approximated by $G^{-1}(k,\omega) = i\tilde\Sigma(\Omega)$.

The right-hand side of each of the two equations (32) contains $1/L$ coming from $(\Sigma^*)^2$ in the denominator and the logarithmical term in the numerator due to the presence of zero bosonic Matsubara frequency term in the summation over $\Omega_{m'}^*$. The logarithmical terms in the numerator and denominator exactly cancel each other, i.e., at this level there is no information as to what $T_{\rm CDW}$ is. To obtain $T_{\rm CDW}$ one has to keep terms with $\Omega_m \neq \Omega_{m'}$ in the formulas for $\Delta_{k_0}^Q(\Omega_m^*), \Delta_{k_\pi}^Q(\Omega_m^*)$ and for $\Sigma(\Omega_m^*)$. We follow the strategy used in Eliashberg-type theories and introduce $\bar\Delta_{k_0}^Q(\Omega_m^*) = \Omega_m^*\Delta_{k_0}^Q(\Omega_m^*)/\tilde\Sigma^*(\Omega_m^*)$ and $\bar\Delta_{k_\pi}^Q(\Omega_m^*) = \Omega_m^*\Delta_{k_\pi}^Q(\Omega_m^*)/\tilde\Sigma^*(\Omega_m^*)$. Substituting this into any of the two equations in (32) and using $\Delta_{k_0}^Q = -\Delta_{k_\pi}^Q$ we obtain $[\bar\Delta(\Omega_m^*) \equiv \bar\Delta_{k_0}^Q(\Omega_m^*)]$

$$\bar\Delta(\Omega_m^*) = \lambda T_{\rm CDW}^*\sum_{|\Omega_{m'}^*|<1}\ln\frac{(\Sigma^*)^2}{|\Omega_m^*-\Omega_{m'}^*|}\times\left(\frac{\bar\Delta(\Omega_{m'}^*)}{|\Omega_{m'}^*|}-\frac{\bar\Delta(\Omega_m^*)}{\Omega_m^*}\frac{\Omega_{m'}^*}{|\Omega_{m'}^*|}\right), \tag{33}$$

where we defined $\lambda = 8/(3|\Sigma^*|) = \sqrt{8/(3T_{\rm CDW}^* L)}$. The second term in the last bracket in the right-hand side of this equation [the one with $\bar\Delta(\Omega_m^*)$] comes from the self-energy, once we express $\Delta_{k_0}^Q$ and $\Delta_{k_\pi}^Q$ in the left-hand side of the two equations in (32) via $\bar\Delta$. We see that the term with zero Matsubara frequency vanishes, in agreement with what we found a few lines above [the term inside the parentheses in the right-hand side of (33) vanishes when $\Omega_{m'} = \Omega_m$), and the value of $T_{\rm CDW}$ is determined by the contributions from nonzero bosonic Matsubara frequencies. The vanishing of the $\Omega_{m'} = \Omega_m$ term is similar to what happens in an s-wave

superconductor. However, contrary to an s-wave case, here the effective coupling λ in (33) does depend on L.

Equation (33) has been studied in the context of color superconductivity [87] and of the pairing mediated by collective excitations in $D = 3$ [42,69,81,84,85] and we just borrow the result: at weak coupling (small λ), $T_{\rm CDW}$ is determined by

$$\ln \frac{(\Sigma^*)^2}{T^*_{\rm CDW}} \sim \frac{1}{\lambda^{1/2}}. \tag{34}$$

Solving this equation, we obtain, in actual units,

$$T_{\rm CDW} \sim \omega_0 \frac{(\ln L)^4}{L}. \tag{35}$$

We see that thermal fluctuations reduce the CDW instability temperature by a factor $(\ln L)^4/L$ compared to what we would obtain by using the zero-temperature gap equation and just setting T as the lower cutoff.

C. Interplay between $T_{\rm CDW}$ and $T_{\rm SC}$

There is another consequence of strong effect of thermal fluctuations: the onset temperature for CDW order with Q_x/Q_y becomes almost indistinguishable from the onset temperatures for superconductivity and for bond order with diagonal Q. Indeed, the equation for superconducting $T_{\rm SC}$ is the same as Eq. (28) if we replace $\Delta^Q_{k_0} \to \Delta_{\rm SC}$ and $\Delta^Q_{k_\pi} \to -\Delta_{\rm SC}$. To logarithmic accuracy, this leads to the same gap equation for $\bar{\Delta}_{\rm SC}(\Omega_m) = \Delta_{\rm SC}(\Omega^*_m)(\Omega_m)/\Sigma^*(\omega_m)$ as Eq. (33). This is an expected result as the superconducting problem and CDW problem with Q_x/Q_y differ in the interplay between the directions of Fermi velocities in the two hot regions connected by (π,π). For the superconducting problem, the velocities at hot spots at $\mathbf{k}$ and $-\mathbf{k}$ are strictly antiparallel, while for CDW they are almost antiparallel in one hot region and almost parallel in the other. In a situation when the frequency-dependent term in the fermionic propagator becomes parametrically larger than $\mathbf{v}\cdot\mathbf{k}$, the difference in the directions of Fermi velocities becomes irrelevant and superconducting and CDW onset temperatures are both given by Eq. (35) to leading order in $L = \ln\xi$, and differ only in the subleading terms, which are small in $1/L$, i.e.,

$$T_{\rm SC} = T_{\rm CDW}\,[1 + f(1/L)]\,, \quad f(0) = 0. \tag{36}$$

In real quasi-three-dimensional (quasi-3D) systems, the logarithm remains finite even when magnetic $\xi = \infty$. In this situation, both $T_{\rm CDW}$ and $T_{\rm SC}$ remain finite at the onset of CDW order (i.e., on a phase diagram they both cross $T_{\rm SDW}$ line at finite T) and both are of order ω_0. Still, if L is large enough, $T_{\rm CDW}$ is close to $T_{\rm SC}$, and the relative difference between the two temperatures is parametrically small in $1/L$.

D. Role of nonladder diagrams for $T_{\rm CDW}$

So far, in our consideration of the onset temperature for CDW instability, we analyzed the set of gap equations within ladder approximation, i.e., used the same type of diagrams as in BSC/Eliashberg theory of superconductivity, only in the particle-hole channel. The ladder approximation is justified either at weak coupling, when the kernel in the gap equation is logarithmically singular and ladder diagrams contain higher powers of logarithms than nonladder diagrams, or in the Eliashberg theory, when the coupling is not small but bosons, which mediate pairing, are slow modes compared to electrons. In this last case, nonladder diagrams for the pairing vertex are small in the Eliashberg parameter. Neither of these approximations can be justified in our case: the effective coupling is of order one and the Eliashberg parameter is also of order one because the interaction in the CDW channel is mediated by collective modes of electrons, which have the same Fermi velocity as fermions themselves. The Eliashberg parameter can be artificially made small by extending theory to large N [38,57,84], but we do not use this extension in our analysis.

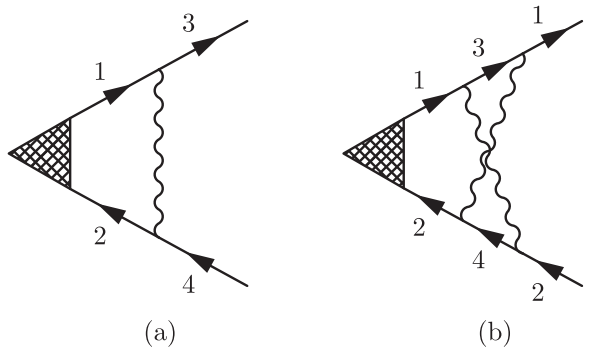

FIG. 4. The one-loop ladder diagram and the two-loop nonladder diagram for the renormalization of the CDW vertex. Both diagrams are logarithmical and, parameter-wise, of the same order, however, the numerical prefactor for the two-loop diagram is much smaller.

In the absence of any small parameter, nonladder diagrams for the CDW order parameter Δ^Q_k are of the same order as the ladder ones, and one has to check whether they can significantly affect the result for $T_{\rm CDW}$. We do a simple check to verify this. Namely, we return back to the logarithmical approximation and check how much the prefactor of the logarithm obtained from the one-loop ladder diagram changes when we include two-loop nonladder diagrams. Specifically, we compare the prefactors from the two diagrams shown in Fig. 4. The one-loop diagram has been analyzed above [see Eqs. (16)]. To logarithmical accuracy it yields

$$\sqrt{S_1 S_2}\,\Delta^Q_{k_0} \ln\frac{\omega_0}{T}, \tag{37}$$

where we used the fact that $\Delta^Q_{k_\pi} = -\Delta^Q_{k_0}\sqrt{S_2/S_1}$. For the case when Fermi velocities at hot spots 1 and 2 in Fig. 1 are antiparallel, $\sqrt{S_1 S_2} = 0.234$. For the same geometry, the two-loop diagram in Fig. 4 yields, to logarithmic accuracy,

$$0.024\,\Delta^Q_{k_0} \ln\frac{\omega_0}{T}. \tag{38}$$

We see that the prefactor in Eq. (38) is 10 times smaller than in Eq. (37), i.e., at least at this level of consideration, the two-loop nonladder diagram in Fig. 4 only contributes a small correction to the one-loop ladder diagram. We take this result as an indication that the ladder approximation for the CDW order, while not justified parametrically, is reasonably well justified numerically.

IV. STABILITY OF THE CDW SOLUTION

The existence of the solution of the gap equation for CDW order parameter by itself does not guarantee that there is an instability towards a CDW state. To prove that the system is truly unstable, one has to verify that the solution with a nonzero CDW order parameter corresponds to a minimum of the free energy, rather than a maximum. For a single order parameter Δ, bilinear in fermionic operators, a way to verify the stability is to use Hubbard-Stratonovich (HS) transformation, introduce Δ as a real HS field, integrate out fermions, and expand the effective action $S_{\rm eff}(\Delta)$ in powers of Δ. The expansion generally has the form

$$S_{\rm eff}(\Delta) = \alpha\Delta^2 + \beta\Delta^4, \tag{39}$$

where $\alpha = a(T - T_0)$ and $\beta > 0$ must be positive for a continuous transition. The saddle-point solution $\partial S_{\rm eff}/\partial\Delta$ yields a conventional result $\Delta^2 = -\alpha/(2\beta)$. Expanding around the saddle point to quadratic order in fluctuations and evaluating fluctuating contribution to the free energy, one finds that fluctuations increase $S_{\rm eff}$ and the Gaussian integral over fluctuations of Δ nicely converges, i.e., the saddle-point solution is a stable minimum. This simple reasoning, however, implies that $a > 0$. If a was negative, saddle-point solutions with $\langle\Delta\rangle = 0$ at $T > T_0$ and $\langle\Delta\rangle \neq 0$ at $T < T_0$ would correspond to a maximum rather than a minimum of the effective action. One can formally convert these states into minima, but for this one has to transform the integration contour over Δ from a real to imaginary axis.

In our case, there are two CDW orders $\Delta^Q_{k_0}$ and $\Delta^Q_{k_\pi}$, hence, one has to introduce two HS fields. We show in the following that the saddle-point solution for $\Delta^Q_{k_0} - \Delta^Q_{k_\pi}$ is along the real axis, while the saddle-point solution for $\Delta^Q_{k_0} + \Delta^Q_{k_\pi}$ is along the imaginary axis. Given that solutions along the real and imaginary axes have very different physical meaning in the case of a single field, one has to perform a more detailed analysis of fluctuations around the saddle-point solution to verify whether in our case a disordered state is stable at $T > T_{\rm CDW}$ and the ordered state is stable at $T < T_{\rm CDW}$.

Another complication in our case is associated with the fact that there are several directions of fluctuations around the CDW solution. The system can fluctuate in the CDW subset (i.e., within the plane set by $\Delta^Q_{k_0}$ and $\Delta^Q_{k_\pi}$), but it also can fluctuate in the directions of different orders, including superconductivity and bond order. All these fluctuations must be included in the full analysis of stability of CDW order [88].

We perform the stability analysis in several stages. First, we analyze the solution of the set of nonlinear ladder equations and show that the mean-field solution with a nonzero Δ^Q_k appears continuously below $T_{\rm CDW}$. Then, we analyze fluctuations around the mean-field solution in the $\Delta^Q_{k_0}$ and $\Delta^Q_{k_\pi}$ planes. Finally, we discuss the interplay with bond order and superconductivity.

To simplify the analysis, following we neglect the complications associated with the frequency dependence of $\Delta^Q_k(\Omega)$ and with pair-breaking effects of thermal fluctuations, i.e., approximate $\Delta^Q_k(\Omega)$ by Δ^Q_k as set T as the lower cutoff of $T = 0$ formulas. Within this approximation, $T_{\rm CDW} = \omega_0 e^{-1/\sqrt{S_1(0)S_2(0)}}$. The inclusion of the frequency dependence of Δ^Q_k and thermal fluctuations will complicate the analysis but not change the conclusions.

A. Nonlinear gap equations at $T < T_{\rm CDW}$

The set of nonlinear gap equations for CDW order with Q_x/Q_y has been obtained in Ref. [89] and we reproduced their formula. For completeness, we briefly outline the details of our derivation. We again assume that Fermi velocities at hot spots 1 and 2 in Fig. 1 are antiparallel, while the velocities of hot spots 3 and 4 are parallel. In regions 1 and 2, a nonzero $\Delta^Q_{k_0}$ acts in the same way as the superconducting order parameter, i.e., $(v_F y)^2$ is replaced by $(v_F y)^2 + (\Delta^Q_{k_0})^2$. In regions 3 and 4, a nonzero $\Delta^Q_{k_\pi}$ just shifts quasiparticle dispersions by $\pm\Delta^Q_{k_\pi}$, and the new fermionic operators which diagonalize the quadratic form are $(c_3 + c_4)/\sqrt{2}$ and $(c_3 - c_4)/\sqrt{2}$. In both regions, we have normal Green's functions of original fermions $\langle T c_i c_i^\dagger\rangle$ $(i = 1,2,3,4)$ and "anomalous" Green's functions $\langle T c_1 c_2^\dagger\rangle$ and $\langle T c_3 c_4^\dagger\rangle$. Combining the contributions to the ladder renormalizations of $\Delta^Q_{k_0}$ and $\Delta^Q_{k_\pi}$ from diagrams with two normal and two anomalous Green's functions, we obtain, restoring momentarily the frequency dependence of Δ^Q_k,

$$\Delta^Q_{k_0}(\Omega_m) = \frac{3\bar{g}T}{4\pi^2}\sum_{m'}\int \frac{dx\,dy}{x^2 + y^2 + \gamma|\Omega_m - \Omega_{m'}|}\,\frac{\Delta^Q_{k_\pi}(\Omega_{m'})}{\left[i\tilde{\Sigma}(\Omega_{m'}) + v_F x + \Delta^Q_{k_\pi}(\Omega_m)\right]\left[i\tilde{\Sigma}(\Omega_{m'}) + v_F x - \Delta^Q_{k_\pi}(\Omega_m)\right]}, \tag{40}$$

$$\Delta^Q_{k_\pi}(\Omega_m) = -\frac{3\bar{g}T}{4\pi^2}\sum_{m'}\int \frac{dx\,dy}{x^2 + y^2 + \gamma|\Omega_m - \Omega_{m'}|}\,\frac{\Delta^Q_{k_0}(\Omega_{m'})}{\tilde{\Sigma}^2(\Omega_{m'}) + (v_F y)^2 + \left[\Delta^Q_{k_0}(\Omega_{m'})\right]^2}. \tag{41}$$

For definiteness, we set both $\Delta^Q_{k_0}(\Omega_m)$ and $\Delta^Q_{k_\pi}(\Omega_m)$ to be real.

At T slightly below $T_{\rm CDW}$, one can expand the right-hand side of (40) and (41) in powers $\Delta^Q_{k_0}$ and $\Delta^Q_{k_\pi}$. Approximating now $\Delta^Q_k(\Omega)$ by frequency-independent values and restricting with the logarithmic approximation, we obtain to order Δ^3

$$\begin{aligned}\Delta^Q_{k_0} &= -S_1(0)\Delta^Q_{k_\pi}\left[\ln\frac{\omega_0}{T} + \frac{\pi C_1}{4T}\left(\Delta^Q_{k_\pi}\right)^2\right],\\ \Delta^Q_{k_\pi} &= -S_2(0)\Delta^Q_{k_0}\left[\ln\frac{\omega_0}{T} + \frac{\pi C_2}{4T}\left(\Delta^Q_{k_0}\right)^2\right],\end{aligned} \tag{42}$$

where $C_1 = 0.43$ and $C_2 = 9.03$. Eliminating $\Delta^Q_{k_\pi}$ from these equations we obtain

$$\left(\Delta^Q_{k_0}\right)^2 = -\frac{\alpha}{\beta}, \tag{43}$$

where

$$\begin{aligned} \alpha &= 1 - S_1(0)S_2(0)\log^2 \omega_0/T = a(T - T_{\rm CDW}); \\ a &= 2\sqrt{S_1(0)S_2(0)}/T_{\rm CDW} > 0, \\ T_{\rm CDW} &= \omega_0 e^{-1/\sqrt{S_1(0)S_2(0)}}, \end{aligned} \tag{44}$$

and

$$\beta = \left[C_2 + C_1\frac{S_2(0)}{S_1(0)}\right]\frac{\pi S_1(0)S_2(0)}{4T_{\rm CDW}}\ln\frac{\omega_0}{T_{\rm CDW}}. \tag{45}$$

We see that $\beta > 0$, hence, the CDW transition is continuous.

B. Fluctuations within the CDW subset

To analyze fluctuations within the CDW subset, we derive the effective action in terms of fields $\Delta^Q_{k_0}$ and $\Delta^Q_{k_\pi}$, show that the saddle-point solution is equivalent to the solution that we found by summing up ladder diagrams, and then expand $\Delta^Q_{k_0}$ and $\Delta^Q_{k_\pi}$ around the saddle-point solution and analyze the stability of the effective action.

To make the presentation easier to follow, we temporarily replace the actual momentum and frequency-dependent spin-mediated interaction $3\bar{g}\chi(q,\Omega)$ by a constant $\bar{\chi}$. We restore the actual momentum and frequency dependence of the interaction in the final formulas for the effective action.

Consider for definiteness the ordering with $\mathbf{Q} = Q_y$, between regions 1-2 and 3-4. The four-fermion interaction, which provides the glue for CDW, is

$$H' = \bar{\chi}c^\dagger_{k_0-Q}c_{k_0+Q}c^\dagger_{k_\pi+Q}c_{k_\pi-Q} + \text{H.c.} \tag{46}$$

We define $\rho_{k_0} = c^\dagger_{k_0+Q}c_{k_0-Q}$, and $\rho_{k_\pi} = c^\dagger_{k_\pi+Q}c_{k_\pi-Q}$, and rewrite the four-fermion interaction as

$$\begin{aligned} H' &= \bar{\chi}\left(\bar{\rho}_{k_0}\rho_{k_\pi} + \bar{\rho}_{k_\pi}\rho_{k_0}\right) \\ &= \frac{\bar{\chi}}{2}\left(\bar{\rho}_{k_0} + \bar{\rho}_{k_\pi}\right)\left(\rho_{k_0} + \rho_{k_\pi}\right) - \frac{\bar{\chi}}{2}\left(\bar{\rho}_{k_0} - \bar{\rho}_{k_\pi}\right)\left(\rho_{k_0} - \rho_{k_\pi}\right). \end{aligned} \tag{47}$$

The free energy $F = -T\ln Z$ and the partition function is $Z = \prod_k \int dc^\dagger_k dc_k e^{-(H_0+H')/T}$.

We use the HS identities [71,90]

$$\begin{aligned} &\exp\left(\frac{\bar{\chi}}{2}\bar{z}_+z_-\right) \\ &\quad= \int \frac{d\Delta_+ d\bar{\Delta}_+}{2\pi\bar{\chi}}\exp\left[-\frac{|\Delta_+|^2}{2\bar{\chi}} + \frac{i}{2}(\Delta_+ z_+ + \bar{\Delta}_+\bar{z}_+)\right], \\ &\exp\left(\frac{\bar{\chi}}{2}\bar{z}_-z_-\right) \\ &\quad= \int \frac{d\Delta_- d\bar{\Delta}_-}{2\pi\bar{\chi}}\exp\left[-\frac{|\Delta_-|^2}{2\bar{\chi}} + \frac{1}{2}(\Delta_- z_- + \bar{\Delta}_-\bar{z}_-)\right], \end{aligned} \tag{48}$$

where Δ's are in general complex fields, and apply these identities to $z_+ = \rho_{k_0} + \rho_{k_\pi} = c^\dagger_{k_0+Q}c_{k_0-Q} + c^\dagger_{k_\pi+Q}c_{k_\pi-Q}$ and $z_- = \rho_{k_0} - \rho_{k_\pi} = c^\dagger_{k_0+Q}c_{k_0-Q} - c^\dagger_{k_\pi+Q}c_{k_\pi-Q}$ to decouple bilinear terms in ρ in (47). The partition function is now $Z = \prod_k \int dc^\dagger_k dc_k d\Delta_- d\bar{\Delta}_- d\Delta_+ d\bar{\Delta}_+ e^{-S(c^\dagger,c,\Delta_-,\Delta_+)}$ and the action is now quadratic in fermionic fields. Integration over fermionic variables can be carried out explicitly and we obtain

$$Z = \int d\Delta_- d\bar{\Delta}_- d\Delta_+ d\bar{\Delta}_+ e^{-S_{\rm eff}(\Delta_-,\bar{\Delta}_-,\Delta_+,\bar{\Delta}_+)}. \tag{49}$$

We analyze the action in the saddle-point approximation and consider fluctuations around saddle-point solutions. Because Δ_+ and Δ_- couple linearly to z_+ and z_-, nonzero saddle-point solutions for Δ_+ and/or Δ_- imply that the corresponding z_+ and z_- are also nonzero: $z_+ = i\Delta_+/\bar{\chi}$ and $z_- = \Delta_-/\bar{\chi}$. In our notations then, $\Delta^Q_{k_0} = \langle\bar{\chi}c^\dagger_{k_0+Q}c_{k_0-Q}\rangle = (i\Delta_+ + \Delta_-)/2$ and $\Delta^Q_{k_\pi} = \langle c^\dagger_{k_\pi+Q}c_{k_\pi-Q}\rangle = (i\Delta_+ - \Delta_-)/2$. (this does *not* mean that $\Delta^Q_{k_0}$ and $\Delta^Q_{k_\pi}$ are related by complex conjugation since Δ_+ and Δ_- are in general complex). For our CDW solution $\Delta^Q_{k_0} \neq \pm\Delta^Q_{k_\pi}$, hence, we expect nonzero saddle-point values of both Δ_+ and Δ_-.

1. *Fluctuations at $T > T_{\rm CDW}$*

We first consider the situation at $T > T_{\rm CDW}$, when we expect that the minimum of the effective action corresponds to $\Delta_- = \Delta_+ = 0$. Integrating out fermions and expanding the result to quadratic order in Δ_+ and Δ_-, we obtain the effective action in the form

$$S_{\rm eff} = \tfrac{1}{2}[A|\Delta_+|^2 - B|\Delta_-|^2 - iC(\Delta_+\bar{\Delta}_- + \bar{\Delta}_+\Delta_-)], \tag{50}$$

where

$$\begin{aligned} A &= \frac{1}{\bar{\chi}} + \frac{A_1 + A_2}{2}, \\ B &= -\frac{1}{\bar{\chi}} + \frac{A_1 + A_2}{2}, \\ C &= \frac{A_1 - A_2}{2}, \end{aligned} \tag{51}$$

and

$$\begin{aligned} A_1 &= -\sum_{k,\omega}\frac{1}{G^{-1}_{k_0+Q}G^{-1}_{k_0-Q}}, \\ A_2 &= -\sum_{k,\omega}\frac{1}{G^{-1}_{k_\pi+Q}G^{-1}_{k_\pi-Q}}, \end{aligned} \tag{52}$$

where the Green's functions were introduced in (6). We show diagrammatic expressions for A_1 and A_2 in Fig. 5. The overall negative signs in Eq. (52) are due to the presence of fermion loops. Evaluating A_1 and A_2, we find that they are both positive.

The action in (50) contains two terms with real prefactors of different sign (A and B terms) and one term with imaginary prefactor. This apparently leads to some uncertainty as for a single field η fluctuations described by $S_{\rm eff} = D|\eta|^2$ converge if $D > 0$ and diverge if $D < 0$. In our case, the prefactor for the $|\Delta_+|^2$ term is positive and the one for $|\Delta_-|^2$ is negative, i.e., without the coupling provided by the C term in (50) fluctuations of Δ_- field would diverge. We will show,

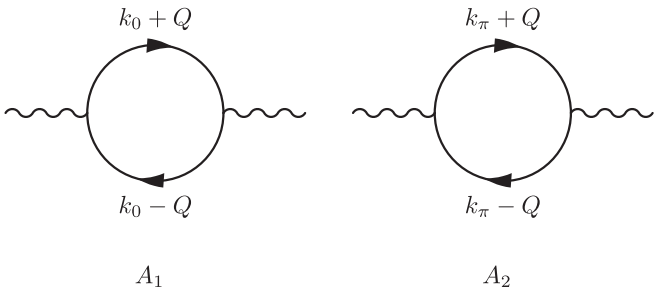

FIG. 5. The diagrams for the coefficients A_1 and A_2 in the effective action, Eq. (52).

however that the C term makes fluctuations of both Δ_+ and Δ_- convergent at $T > T_{\rm CDW}$.

To prove this, we first notice that the effective action in (50) can be written in the form

$$S_{\rm eff} = \frac{1}{2}\Big[A\Big(\bar\Delta_+ - i\frac{C}{A}\bar\Delta_-\Big)\Big(\Delta_+ - i\frac{C}{A}\Delta_-\Big) + \Big(\frac{C^2-AB}{A}\Big)|\Delta_-|^2\Big]. \tag{53}$$

Expressing complex Δ_+ and Δ_- as $\Delta_+ = x+iy$, $\Delta_- = z+iw$, where x,y,z,w are all real, we rewrite

$$\Big(\bar\Delta_+ - i\frac{C}{A}\bar\Delta_-\Big)\Big(\Delta_+ - i\frac{C}{A}\Delta_-\Big) \tag{54}$$

as $(x+izC/A)^2 + (y+iwC/A)^2$. Introducing then $x+izC/A = \bar x$ and $y+iwC/A = \bar y$ as new variables, we find that integration over Δ_+ reduces to

$$\int d\bar x\, d\bar y\, e^{-(A/2)(\bar x^2+\bar y^2)}. \tag{55}$$

This integral obviously converges. Integrating then over $\bar x$ and $\bar y$ before integrating over z and w we obtain that fluctuating part of the effective action reduces to

$$S_{\rm eff} = \Big(\frac{C^2-AB}{2A}\Big)|\Delta_-|^2. \tag{56}$$

The prefactor $(C^2-AB)/(2A)$ is

$$\frac{C^2-AB}{2A} = \frac{1}{\bar\chi}\frac{1-(\bar\chi A_1)(\bar\chi A_2)}{2+\bar\chi(A_1+A_2)}. \tag{57}$$

The combinations $\bar\chi A_1$ and $\bar\chi A_2$ in the numerator have the same forms as the kernels in the gap equations for $\Delta^Q_{k_0}$ and $\Delta^Q_{k_\pi}$. To see this, we note that $\bar\chi A_{1,2}$ is the product of magnetically mediated interaction and two fermionic propagators with momentum difference $2Q$. Restoring frequency and momentum dependence of $\bar\chi = 3\bar g\chi(q,\Omega)$ and evaluating $\bar\chi A_{1,2}$ with logarithmic accuracy, we obtain

$$\bar\chi A_1 = \frac{3\bar g}{8\pi^3}\int \frac{dx\,dy\,d\Omega_{m'}}{\big[i\tilde\Sigma(\Omega_{m'}) - v_x y + v_y x\big]\big[i\tilde\Sigma(\Omega_{m'}) + v_x y + v_y x\big]}\frac{1}{x^2+y^2+\gamma|\Omega_m-\Omega_{m'}|} = -S_1(\varphi)\ln\frac{\omega_0}{T}, \tag{58}$$

$$\bar\chi A_2 = \frac{3\bar g}{8\pi^3}\int \frac{dx\,dy\,d\Omega_{m'}}{\big[i\tilde\Sigma(\Omega_{m'}) - v_x x + v_y y\big]\big[i\tilde\Sigma(\Omega_{m'}) - v_x x - v_y y\big]}\frac{1}{x^2+y^2+\gamma|\Omega_m-\Omega_{m'}|} = -S_2(\varphi)\ln\frac{\omega_0}{T}. \tag{59}$$

Hence,

$$\frac{C^2-AB}{2A} \propto (1-\bar\chi^2 A_1A_2) = 1 - S_1(\varphi)S_2(\varphi)\Big(\ln\frac{\omega_0}{T}\Big)^2. \tag{60}$$

Comparing this with Eq. (18), we immediately find that $(C^2 - AB)/(2A) = a(T-T_{\rm CDW})$, and the prefactor a is positive. This obviously implies that the disordered state is stable at $T > T_{\rm CDW}$.

Another variable, whose fluctuations are convergent, is $\Delta_+ - i\frac{C}{A}\Delta_-$. The prefactor of the corresponding term in the effective action equals $A/2$ and remains positive at $T_{\rm CDW}$. Hence, the combination $\Delta_+ - i\frac{C}{A}\Delta_-$ does not acquire a nonzero value even when $C^2 - AB$ becomes negative and the field Δ_- condenses. Because $\Delta^Q_{k_0}/\Delta^Q_{k_\pi} = (\Delta_- + i\Delta_+)/(\Delta_- - i\Delta_+)$, the condition $\Delta_+ - i\frac{C}{A}\Delta_- = 0$ together with $\bar\chi^2 A_1A_2 = 1$ yields

$$\Delta^Q_{k_0} = -\Delta^Q_{k_\pi}\sqrt{\frac{S_2}{S_1}}. \tag{61}$$

This is exactly the same as Eq. (19), which we obtained by summing up ladder diagrams.

We now pause momentarily and summarize what we just did. We reexpressed the effective action (50) as in (53), shifted variables ${\rm Re}\Delta_+$ and ${\rm Im}\Delta_+$ into the complex plane by adding to them $i(C/A){\rm Re}\Delta_-$ and $i(C/A){\rm Im}\Delta_-$, respectively, and then integrated first over ${\rm Re}\Delta_+$ and ${\rm Im}\Delta_+$ along the direction parallel to the real axis, and then over ${\rm Re}\Delta_-$ and ${\rm Im}\Delta_-$. We found that all Gaussian integrals are convergent at $T > T_{\rm CDW}$, i.e., the disordered state appears as stable at $T > T_{\rm CDW}$.

We could, however, combine the three terms in (50) differently by keeping Δ_+ as one variable and shifting Δ_- by a term proportional to Δ_+. This way, we rewrite (50) as

$$S_{\rm eff} = \frac{1}{2}\Big[-B\Big(\bar\Delta_- + i\frac{C}{B}\bar\Delta_+\Big)\Big(\Delta_- + i\frac{C}{B}\Delta_+\Big) - \Big(\frac{C^2-AB}{A}\Big)|\Delta_+|^2\Big]. \tag{62}$$

Shifting now real and imaginary parts of Δ_- by $-i(C/B){\rm Re}\Delta_+$ and $-i(C/B){\rm Im}\Delta_+$, respectively, and integrating first over ${\rm Re}\Delta_-$ and ${\rm Im}\Delta_-$ parallel to the real axis and then over ${\rm Re}\Delta_+$ and ${\rm Im}\Delta_+$ we obtain two divergent Gaussian integrals. Taken at face value, this would imply that fluctuations of Δ_- and Δ_+ diverge at $T > T_{\rm CDW}$, when

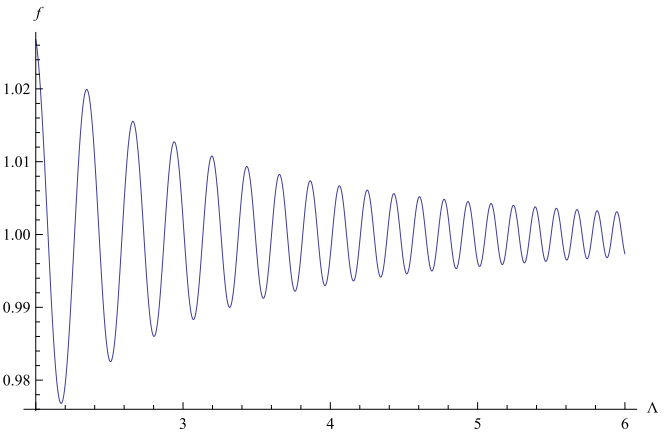

FIG. 6. (Color online) The scaling function $f(\Lambda/A, C^2/AB, A/B)$ from Eq. (64) is plotted as a function of Λ for fixed $A = B = 1$, $C = 2$. The function has a Λ-dependent oscillating component, but clearly converges to $f = 1$ at large Λ.

$C^2 - AB > 0$. In reality, however, fluctuations do not diverge even if we integrate this way. To see this, one has to keep the limits of integration finite and set them to infinity only at the end of the calculation. One can then explicitly verify that in this computational scheme, the Gaussian integral $\int d\Delta_+ d\Delta_- e^{-S_{\rm eff}}$ with $S_{\rm eff}$ as in (62) yields the same result as we found before. Specifically, the integral $W = \int d\bar{\Delta}_+ d\bar{\Delta}_- d(\bar{\Delta}_+)^* d(\bar{\Delta}_-)^* \exp -S_{\rm eff}$, obtained by integrating over $d\bar{\Delta}_+ d(\bar{\Delta}_+)^*$ first, yields

$$W = \frac{4\pi^2}{C^2 - AB}. \tag{63}$$

If, instead, we integrate first over $d\bar{\Delta}_- d(\bar{\Delta}_-)^*$ and then over $d\bar{\Delta}_+ d(\bar{\Delta}_+)^*$, but each time will keep the limits of integration finite, from $-\Lambda$ to Λ, we obtain

$$W = \frac{4\pi^2}{C^2 - AB} f(\Lambda/A, C^2/AB, A/B). \tag{64}$$

In Fig. 6, we plot f as a function of Λ for a fixed set of A, B, C. We see that f has an oscillating component, but clearly tends to one when Λ gets larger. The conclusion here is that, no matter in which the integration is done, the disordered state is stable at $T > T_{CDW}$ and becomes unstable at $T < T_{\rm CDW}$ when $C^2 - AB$ changes sign.

We discuss additional technical aspects of the evaluation of the partition function for the complex effective action in Appendix C.

2. *Fluctuations at $T < T_{\rm CDW}$*

The HS analysis can be straightforwardly extended to $T < T_{\rm CDW}$, however, to perform it we need to expand the effective action $S_{\rm eff}[\Delta_-, \bar{\Delta}_-, \Delta_+, \bar{\Delta}_+]$ up to quartic terms. Applying the HS transformation and expanding to fourth order in Δ we obtain

$$\begin{aligned} S_{\rm eff} =& \tfrac{1}{2}[A|\Delta_+|^2 - B|\Delta_-|^2 - iC(\Delta_+\bar{\Delta}_- + \bar{\Delta}_+\Delta_-)] \\ & - \tfrac{1}{16} I_1 [(\bar{\Delta}_- + i\bar{\Delta}_+)(\Delta_- + i\Delta_+)]^2 \\ & - \tfrac{1}{16} I_2 [(\bar{\Delta}_- - i\bar{\Delta}_+)(\Delta_- - i\Delta_+)]^2. \end{aligned} \tag{65}$$

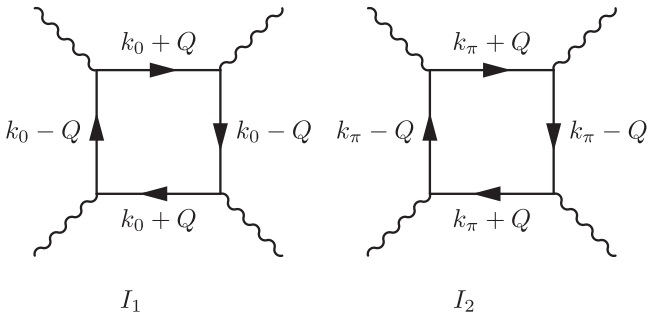

FIG. 7. The diagrammatic representation of the prefactors I_1 and I_2 in Eq. (65).

The coefficients I_1 and I_2 are given by square diagrams made out fermions and are shown in Fig. 7. In analytical form,

$$\begin{aligned} I_1 &= -\frac{1}{2}\sum_{k,\omega} \frac{1}{G^{-2}_{k_0+Q} G^{-2}_{k_0-Q}}, \\ I_2 &= -\frac{1}{2}\sum_{k,\omega} \frac{1}{G^{-2}_{k_\pi+Q} G^{-2}_{k_\pi-Q}}. \end{aligned} \tag{66}$$

The integrals I_1 and I_2 are evaluated in Appendix B using linear dispersion around hot spots. In this approximation, I_1 is negative and finite and $I_2 = 0$. Expanding further the dispersion relation, we find that I_2 is also nonzero, but is smaller than I_1. The discussion below does not rely on the precise numerical values of I_1 and I_2, and we keep both I_1 and I_2 as finite.

Differentiating (65) with respect to Δ_+ we find from $\frac{\delta S}{\delta \bar{\Delta}_+} = 0$ the relation $\Delta_+ = i\tilde{\lambda}\Delta_-$, with the prefactor renormalized from $\lambda = C/A$ by a nonzero Δ_-:

$$\tilde{\lambda} = \frac{C}{A} + \frac{1}{4A}[I_1(1-\lambda)^3 - I_2(1+\lambda)^3]|\Delta_-|^2. \tag{67}$$

Solving then the other saddle-point equation $\frac{\delta S}{\delta \bar{\Delta}_-} = 0$ and using $\Delta_+/(i\Delta_-) = \tilde{\lambda} = (\Delta^Q_{k_0} + \Delta^Q_{k_\pi})/(\Delta^Q_{k_\pi} - \Delta^Q_{k_0})$, we obtain

$$\begin{aligned} \frac{1}{\tilde{\chi}}\Delta^Q_{k_0} + A_1 \Delta^Q_{k_\pi} + 2I_1 \left|\Delta^Q_{k_\pi}\right|^2 \Delta^Q_{k_\pi} = 0, \\ \frac{1}{\tilde{\chi}}\Delta^Q_{k_\pi} + A_2 \Delta^Q_{k_0} + 2I_2 \left|\Delta^Q_{k_0}\right|^2 \Delta^Q_{k_0} = 0. \end{aligned} \tag{68}$$

Restoring the frequency and momentum dependence of $\tilde{\chi}$, like we did before, we immediately find that this set is analogous to Eq. (42), which we obtained by expanding in Δ^Q_k in the set of ladder gap equations (it is important to keep I_2 for this comparison). The equivalence shows that the set of ladder gap equations is equivalent to the saddle point of the effective action.

We next replace Δ_+ in Eq. (65) by its saddle-point value and expand $S_{\rm eff}[\Delta_-]$ in powers of Δ_-. We obtain

$$S_{\rm eff}[\Delta_-] = \left(\frac{C^2 - AB}{2A}\right)|\Delta_-|^2 + \beta'|\Delta_-|^4, \tag{69}$$

where, we remind, $\frac{C^2-AB}{2A} \propto (T - T_{\rm CDW})$ and

$$\beta' = -\tfrac{1}{16}[(1-\lambda)^4 I_1 + (1+\lambda)^4 I_2], \tag{70}$$

where, again, $\lambda = C/A$ and hence $(1+\lambda)/(1-\lambda) = \sqrt{A_1/A_2}$ when $C^2 - AB$ is close to zero. Because I_1 is negative, I_2 is much smaller than $|I_1|$, and λ is also small, it follows from (70) that $\beta' > 0$, as expected. We verified that, if we restore the frequency and momentum dependence of $\tilde{\chi}$, the order parameters $\Delta^Q_{k_0}$ and $\Delta^Q_{k_0}$, obtained by minimizing (69) with respect to Δ_- and using (67) to obtain Δ_+, are equivalent to the solution of the nonlinear ladder equations (43). Gaussian fluctuations around the HS solution can be obtained by usual means and indeed show that the saddle-point solution is a minimum with respect to variations of Δ_-.

In Appendix D, we present an alternative derivation of Eq. (69), using another HS formalism, in which the saddle points for Δ_+ and Δ_- are both located along the real axis.

C. Interplay between CDW order and superconductivity/diagonal bond order

So far, we considered only fluctuations within the CDW subset. The discussion in the preceding section shows that within this subset, the CDW solution is a local minimum and fluctuations are convergent. The order parameters $\Delta^Q_{k_0}$ and $\Delta^Q_{k_\pi}$ are proportional to each other and the effective action can be expressed in terms of one of them, which we label $\Delta_{\rm CDW}$:

$$S_{\rm eff} = \alpha_{\rm CDW}|\Delta_{\rm CDW}|^2 + \beta_{\rm CDW}|\Delta_{\rm CDW}|^4 + \dots \qquad (71)$$

with $\alpha_{\rm CDW} = a(T - T_{\rm CDW})$ and $a > 0$, $\beta_{\rm CDW} > 0$.

There are indeed also fluctuations in the other directions, including the direction of d-wave superconductivity and diagonal bond order. There, fluctuations are longitudinal ones for CDW order and describe the change of $S_{\rm eff}$ when the magnitude of $\Delta_{\rm CDW}$ decreases and the magnitude of superconducting order of diagonal bond order increases. To describe these fluctuations, we extend the GL expansion of the effective action to include the competing channels. To avoid complex formulas, we only consider the superconducting channel with order parameter $\Delta_{\rm SC}$.

A straightforward analysis shows that the full effective action has the form

$$S_{\rm eff} = \alpha_{\rm CDW}|\Delta_{\rm CDW}|^2 + \beta_{\rm CDW}|\Delta_{\rm CDW}|^4 + \alpha_{\rm SC}|\Delta_{\rm SC}|^2 + \beta_{\rm SC}|\Delta_{\rm SC}|^4 + \beta_m|\Delta_{\rm CDW}|^2|\Delta_{\rm SC}|^2 + \dots, \qquad (72)$$

where the ellipsis stands for higher-order terms, $\beta_i > 0$, and $\alpha_{\rm SC} = a(T - T_{\rm SC})$. The effective action of this form has been presented in Ref. [91]. The prefactor a does not have to be the same as for CDW order but can be adjusted to match that of $\alpha_{\rm CDW}$ by rescaling the magnitude of $\Delta_{\rm SC}$.

We know from the analysis in Sec. III that the instability temperature in the superconducting channel is close to $T_{\rm CDW}$, but still larger than $T_{\rm CDW}$ [see Eq. (36)]. Analyzing the effective action (72) within mean-field theory, we find that immediately below $T_{\rm SC}$ only superconducting order emerges, while CDW order emerges at a lower $T = \bar{T}_{\rm CDW}$:

$$\bar{T}_{\rm CDW} = T_{\rm CDW}\frac{\beta_{\rm SC} - \beta_m\frac{T_{\rm SC}}{T_{\rm CDW}}}{\beta_{\rm SC} - \beta_m}, \qquad (73)$$

provided that two conditions are met [73,74,92]:

$$\beta_{\rm SC}\beta_{\rm CDW} > \beta_m^2, \quad \beta_{\rm SC} > \beta_m\frac{T_{\rm SC}}{T_{\rm CDW}}. \qquad (74)$$

The first condition makes certain that the mixed state has lower energy than either of the two pure states and the second one guarantees that $\bar{T}_{\rm CDW} > 0$. If either of these two conditions is not met, the system remains in a pure superconducting state down to $T = 0$ and CDW order does not develop.

We show in the following that beyond mean field the situation is more involved and the first instability upon lowering T can actually happen within the CDW subset, before superconducting order or bond order with diagonal $\mathbf{Q}$ develop. The reason is that the manifold for the CDW order parameter includes one or two additional discrete Z_2 symmetries, depending on the actual structure of the CDW order. We demonstrate this in Sec. V. In Sec. VI, we show that composite charge orders, associated with their Z_2 symmetries, develop at temperatures larger than $T_{\rm CDW}$. Given that $T_{\rm CDW}$ is close to $T_{\rm SC}$, the onset temperature for composite charge order likely exceeds $T_{\rm SC}$. Once a Z_2 composite orders sets in, it gives a negative feedback on superconductivity and reduces $T_{\rm SC}$, and, at the same time, increases the susceptibility for the primary CDW order and hence enhances $T_{\rm CDW}$. It the enhanced $T_{\rm CDW}$ becomes larger than the reduced $T_{\rm SC}$, the same GL analysis as we just did below shows that $T_{\rm SC}$ is further reduced and whether it develops in coexistence of CDW at a lower T depends on the same conditions as in (74).

V. STRUCTURE OF CHARGE ORDER: MEAN-FIELD ANALYSIS

In previous sections we considered CDW order with momentum either $Q_x = (2Q,0)$ or $Q_y = (0,2Q)$ and assumed that Δ^Q_k with a given Q is a single $U(1)$ field, i.e., that $\Delta^Q_{k_0} = \Delta^Q_{-k_0}$. In reality, the CDW order can emerge with either only Q_x or Q_y, or with both momenta, and also $\Delta^Q_{k_0}$ and $\Delta^Q_{-k_0}$ are in general not identical because $\mathbf{k}_0$ is not a high-symmetry point in the Brillouin zone. Indeed, by construction, the order parameter satisfies $(\Delta^Q_k)^* = \Delta^{-Q}_k$. This condition implies that an incommensurate charge order parameter has an overall phase factor associated with the breaking of $U(1)$ symmetry, but does not specify how Δ^Q_k changes under $k \to -k$. For sets 1-2 and 3-4 in Fig. 1, relevant k are near $k_0 = (\pi - Q,0)$ and $k_\pi = (-Q,\pi)$. For the sets 5-6 and 7-8 in Fig. 1, relevant k are near $\bar{k}_0 = -k_0 \equiv (\pi + Q,0)$ and $\bar{k}_\pi = -k_\pi$. As long as typical $|k - k_0|$ are smaller than $2Q$ (i.e., as long as $T_{\rm CDW}$ is smaller than, roughly, $E_F|Q/\pi|$), the two regions are weakly connected and at zero-order approximation can be considered independent of each other, in which case the gap equation does not distinguish between the solutions for Δ^Q_k, which are even and which are odd under $k \to -k$. One can easily check [64] that under time reversal $\Delta^Q_k \to \Delta^Q_{-k}$, hence the odd in k solution changes sign under time reversal, and its emergence therefore implies that CDW order breaks time-reversal symmetry. We emphasize that the possibility to have two types of solutions is specific to CDW order with Q_y (Q_x). For a charge order with a diagonal Q, the center-of-mass momentum is at $k = 0$, and only an even in k solution is possible.

We label the even in k solution as Δ^Q_1 and the odd in k solution as $\Delta^Q_2 \propto {\rm sgn}(k)$. We will show later in this section

that in real space Δ_1^Q describes an incommensurate cite or bond charge density modulation, while Δ_2^Q describes an incommensurate bond current.

Combining two different $\mathbf{Q}$ with two components of Δ_k^Q for a given Q, we find that the full order parameter for CDW order has two components: $\Delta_1^{Q_x}, \Delta_2^{Q_x}, \Delta_1^{Q_y}$, and $\Delta_2^{Q_y}$. In this section, we obtain the effective action for four-component CDW order parameter and analyze it in the mean-field approximation. In Sec. VI, we perform the analysis beyond mean field and study preemptive composite orders.

A. Truncated effective action: Stripe versus checkerboard order

As a first pass on the structure of Δ_k^Q, we assume that Δ_k^Q has only an even in k component Δ_1^Q (i.e., that $\Delta_{k_0}^Q = \Delta_{-k_0}^Q$) and analyze the GL model for two-component order parameter $\Delta_x = \Delta_{k_0}^{Q_x}$ and $\Delta_y = \Delta_{k_0}^{Q_y}$, subject to $\Delta_{k_\pi}^{Q_x} = \mu\Delta_x$ and $\Delta_{k_\pi}^{Q_x} = \mu\Delta_x$. Our goal here is to address the issue whether CDW order develops simultaneously with both Q_x and Q_y, in which case it preserves the underlying lattice C_4 symmetry and gives rise to checkerboard charge order in the real space, or with either Q_x or Q_y, in which case it spontaneously breaks C_4 symmetry down to C_2 and gives rise to stripe order The order with Q_x corresponds to CDW between fermions in regions 1-2 and 3-4 in Fig. 1 and the order with Q_y corresponds to CDW between fermions in regions 1-5 and 3-8. We introduce Δ_x and Δ_y as two HS fields, integrate over fermions, and obtain the effective action $S_{\text{eff}}(\Delta_x, \Delta_y)$. The prefactors for $|\Delta_y|^2$ and $|\Delta_x|^2$ are identical by symmetry, and the full action to order Δ^2 is

$$S_{\text{eff}}^{(2)} = \alpha(|\Delta_x|^2 + |\Delta_y|^2). \tag{75}$$

Extending the result to fourth order in Δ, we obtain

$$S_{\text{eff}}(\Delta_x, \Delta_y) = \alpha\left(\Delta_x^2 + \Delta_y^2\right) + \beta\left(\Delta_x^4 + \Delta_y^4\right) + 2\beta_m \Delta_x^2 \Delta_y^2, \tag{76}$$

where, we remind, $\alpha = a(T - T_{\text{CDW}})$, $a > 0$. At a mean-field level, the effective action (76) gives rise to a checkerboard order when $\beta > \beta_m$, and to a stripe order when $\beta_m > \beta$. The coefficients β and β_m are expressed via the square diagrams with four fermionic propagators as

$$\beta = -2(I_1 + \mu^4 I_2), \quad \beta_m = -2\mu^2(2I_3 + I_4), \tag{77}$$

where μ is the ratio $\Delta_{k_\pi}^{Q_y}/\Delta_{k_0}^{Q_y}$, which, we remind, is $-\sqrt{S_1/S_2}$ [see Eqs. (19) and (61)]. The terms I_i are the convolutions of four fermionic propagators

$$\begin{aligned} I_1 &\equiv -\frac{1}{2}\int G_1^2 G_2^2, \\ I_2 &\equiv -\frac{1}{2}\int G_1^2 G_5^2, \\ I_3 &\equiv -\int G_1 G_5^2 G_6, \\ I_4 &\equiv -\int G_1 G_2 G_5 G_6. \end{aligned} \tag{78}$$

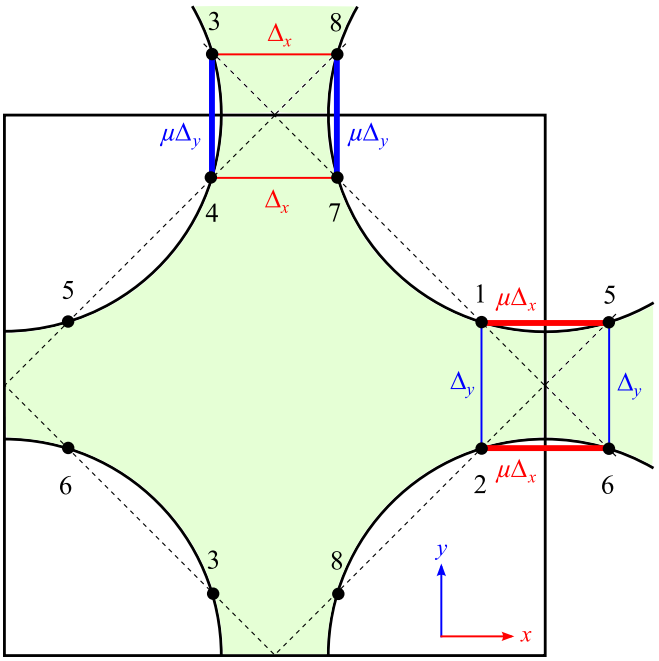

FIG. 8. (Color online) The two order parameters responsible for stripe or checkerboard order.

We show I_i graphically in Fig. 9, using the notations from Fig. 8. The overall minus sign in every line in (78) is due to the presence of a fermionic loop. The abbreviations for the Green's function as $G_1 \equiv G[\omega_m, \mathbf{k_1} + (k_x, k_y)]$, etc., and the integrals are performed over running frequency ω_m and momenta k_x and k_y. The integrals I_1 and I_2 have been already introduced in Sec. II.

We evaluate I_1–I_4 in Appendix B by expanding to linear order in the deviations from hot spots, and here quote the

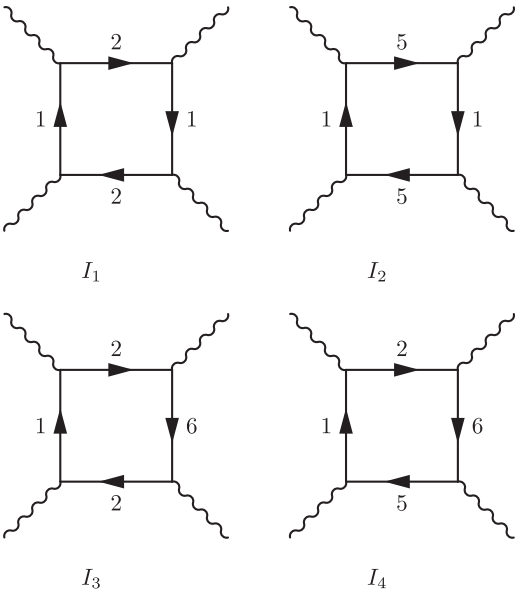

FIG. 9. The diagrammatic representation of the quartic terms in the effective action.

results. We obtain

$$\begin{aligned} I_1 &= -\frac{1}{16\pi^2 v_x^2 v_y}\frac{1}{\Lambda}, \\ I_2 &= 0, \\ I_3 &= -\frac{1}{16\pi^2 v_x^2 v_y}\frac{1}{\Lambda}\ln\frac{\omega_0}{\Lambda}, \\ I_4 &= -\frac{1}{32 v_x v_y}\frac{1}{T}. \end{aligned} \tag{79}$$

Using these results, we find that the prefactors β and β_m in Eq. (B3) are given by

$$\begin{aligned} \beta &= -2(I_1 + \mu^4 I_2) = \frac{1}{8\pi v_x^2 v_y}\frac{1}{\Lambda}, \\ \beta_m &= -2\mu^2(2I_3 + I_4) \approx \frac{\mu^2}{16 v_x v_y}\frac{1}{T}. \end{aligned} \tag{80}$$

Because $\mu > 1$, we have at low $T \ll \Lambda v_x$, $\beta_m \gg \beta$, i.e., the system chooses the stripe order in which only Δ_x or Δ_y emerges. Such an order spontaneously breaks C_4 lattice rotational symmetry.

Phenomenological arguments for stripe charge order in hole-underdoped cuprates have been displayed earlier [76], and our microscopic analysis is consistent with earlier works. We caution, however, that more accurate treatment is needed when CDW order emerges either from a preexisting superconducting state or in an applied magnetic field. Both a superconducting gap and a magnetic field cut the divergencies in I_3 and I_4 at low T, and it may happen that in this situation β becomes larger than β_m, in which case the checkerboard CDW order develops.

B. Full effective action

We next analyze the effective action for the full four-component CDW order parameter. We split Δ_k^Q into even and odd parts as

$$\Delta_k^Q = \Delta_{1,k}^Q + \Delta_{2,k}^Q \mathrm{sgn}(k) \tag{81}$$

and, to shorten notations, define $\Delta_1^{Q_x}$, $\Delta_2^{Q_x}$, $\Delta_1^{Q_y}$, and $\Delta_2^{Q_y}$ as Δ_1^x, Δ_2^x, Δ_1^y, and Δ_2^y, respectively. The four order parameters transform differently under translation along x and y directions in real space, lattice rotation by $\pi/2$, and inversion of time. We list the symmetry properties of the four Δ's in Table I.

We again use the HS transformation from the action written in terms of fermionic operators to the action in terms of collective bosonic variables and obtain the prefactors for quadratic and quartic terms in Δ_i^j by integrating over the loops made out of two and four fermions, respectively. The full analysis is somewhat involved and to give insights what CDW configurations may emerge we first approximate the CDW order parameters by their values at hot spots, which in technical terms implies that we approximate $c^\dagger c\Delta$ vertices in the square diagrams for the prefactors for Δ^4 terms by their values at hot spots. Following the same steps as in the previous subsection, we obtain the effective action in the form

$$\begin{aligned} S_{\rm eff} = {} & \alpha\left(|\Delta_1^x|^2 + |\Delta_1^y|^2 + |\Delta_2^x|^2 + |\Delta_2^y|^2\right) \\ & + \beta\left\{|\Delta_1^x|^4 + |\Delta_1^y|^4 + |\Delta_2^x|^4 + |\Delta_2^y|^4\right. \\ & + \left[(\Delta_1^x)^*\Delta_2^x\right]^2 + \left[(\Delta_2^x)^*\Delta_1^x\right]^2 + 4|\Delta_1^x|^2|\Delta_2^x|^2 \\ & \left. + \left[(\Delta_1^y)^*\Delta_2^y\right]^2 + \left[(\Delta_2^y)^*\Delta_1^y\right]^2 + 4|\Delta_1^y|^2|\Delta_2^y|^2\right\} \\ & + 2\bar\beta_m\left\{\left[|\Delta_1^x|^2 - |\Delta_2^x|^2\right]\left[|\Delta_1^y|^2 - |\Delta_2^y|^2\right]\right. \\ & \left. + \left[\Delta_1^x(\Delta_2^x)^* - (\Delta_1^x)^*\Delta_2^x\right]\left[\Delta_1^y(\Delta_2^y)^* - (\Delta_1^y)^*\Delta_2^y\right]\right\} \\ & + 2\tilde\beta_m\left(|\Delta_1^x|^2 + |\Delta_2^x|^2\right)\left(|\Delta_1^y|^2 + |\Delta_2^y|^2\right), \end{aligned} \tag{82}$$

where $\beta = -2(I_1 + \mu^4 I_2)$, $\bar\beta_m = -2\mu^2 I_4$, and $\tilde\beta_m = -4\mu^2 I_3$. For $\Delta_2^i = 0$, Eq. (82) reduces to (76) with $\beta_m = \bar\beta_m + \tilde\beta_m$. The expressions for I_i are presented in (79). For these I_i, all β's are positive and $\bar\beta_m$ and $\tilde\beta_m$ well exceed β because corresponding I_i are larger and also because μ is larger than one. The ratio of $\bar\beta_m/\tilde\beta_m$ does not depend on μ and is given by I_4/I_3. At low T, this ratio is large, but at $T = T_{\rm CDW}$ it is generally of order one. To account for all possible phases, we will treat $\bar\beta_m$ and $\tilde\beta_m$ as the two parameters of comparable strength, but will keep $\tilde\beta_m, \bar\beta_m \gg \beta$.

We parametrize the four fields Δ_1^x, Δ_2^x, Δ_1^x, and Δ_2^y as

$$\begin{aligned} \Delta_1^x &= |\Delta|\cos\theta\cos\varphi_1 e^{i\psi_1}, \\ \Delta_2^x &= |\Delta|\sin\theta\cos\varphi_2 e^{i\psi_2}, \\ \Delta_1^y &= |\Delta|\cos\theta\sin\varphi_1 e^{i\bar\psi_1}, \\ \Delta_2^y &= |\Delta|\sin\theta\sin\varphi_2 e^{i\bar\psi_2}, \end{aligned} \tag{83}$$

where all angles are taken between 0 and $\pi/2$. Plugging this into Eq. (82) and varying over ψ we find that the action is minimized when

$$\begin{aligned} &\psi_1 - \psi_2 = \frac{\pi}{2}, \quad \bar\psi_1 - \bar\psi_2 = \frac{\pi}{2}, \\ \text{or} \quad &\psi_1 - \psi_2 = -\frac{\pi}{2}, \quad \bar\psi_1 - \bar\psi_2 = -\frac{\pi}{2}. \end{aligned} \tag{84}$$

This condition "locks" the phase difference between Δ_1's and Δ_2's for CDW order parameters along the two directions of $\mathbf{Q}$ to be simultaneously either $\pi/2$ or both $-\pi/2$. Plugging Eqs. (83) and (84) back into Eq. (82), we obtain

$$\begin{aligned} S_{\rm eff} = {} & \alpha|\Delta|^2 + \beta|\Delta|^4[(\cos^2\theta\cos^2\varphi_1 + \sin^2\theta\cos^2\varphi_2)^2 \\ & + (\cos^2\theta\sin^2\varphi_1 + \sin^2\theta\sin^2\varphi_2)^2] \\ & + \frac{\bar\beta_m + \tilde\beta_m}{2}|\Delta|^4(\cos^2\theta\sin 2\varphi_1 - \sin^2\theta\sin 2\varphi_2)^2 \\ & - \frac{\bar\beta_m - \tilde\beta_m}{2}|\Delta|^4[\sin^2 2\theta\sin^2(\varphi_1 + \varphi_2)] \end{aligned}$$

TABLE I. The symmetry properties of the four order parameters Δ_1^x, Δ_2^x, Δ_1^y, and Δ_2^y under translation, C_4 lattice rotation, and time reversal.

	Δ_1^x	Δ_2^x	Δ_1^y	Δ_2^y
Translation along x	$\Delta_1^x e^{2iQ_x x}$	$\Delta_2^x e^{2iQ_x x}$	Δ_1^y	Δ_2^y
Translation along y	Δ_1^x	Δ_2^x	$\Delta_1^y e^{2iQ_y y}$	$\Delta_2^y e^{2iQ_y y}$
C_4 lattice rotation	Δ_1^y	Δ_2^y	Δ_1^x	Δ_2^x
Time reversal	Δ_1^x	$-\Delta_2^x$	Δ_1^y	$-\Delta_2^y$

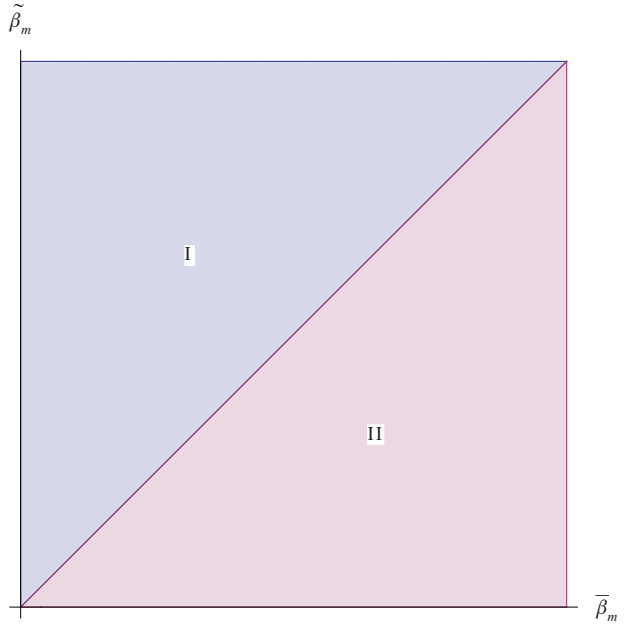

FIG. 10. (Color online) States I and II in the parameter space of $\tilde{\beta}_m$ and $\bar{\beta}_m$.

$$\approx \alpha|\Delta|^2+\frac{\bar{\beta}_m+\tilde{\beta}_m}{2}|\Delta|^4(\cos^2\theta\sin 2\varphi_1-\sin^2\theta\sin 2\varphi_2)^2$$
$$-\frac{\bar{\beta}_m-\tilde{\beta}_m}{2}|\Delta|^4[\sin^2 2\theta\sin^2(\varphi_1+\varphi_2)], \quad (85)$$

where in the last line we have used the approximation $\tilde{\beta}_m, \bar{\beta}_m \gg \beta$.

The structure of the CDW order is now obtained by varying this action over φ_1, φ_2, and θ. We found two types of states, I and II, depending on the interplay between $\tilde{\beta}_m$ and $\bar{\beta}_m$ (see Fig. 10).

For $\tilde{\beta}_m > \bar{\beta}_m$, we find that the minimum of S_{eff} corresponds to $\varphi_1 = \varphi_2 = 0$ or $\varphi_1 = \varphi_2 = \frac{\pi}{2}$, and arbitrary θ. The implication is that CDW order develops either with Q_x or Q_y, i.e., is in the stripe form, like we found before. We see, however, that both Δ_1 and Δ_2 develop, in general, and the relative phase between the two is $\pm\pi/2$. We label this state as state I. The relative magnitude of Δ_1 and Δ_2 is arbitrary at this level of consideration, but we show in the next subsection that it gets fixed when we include the k dependence of $c^\dagger c\Delta_k^Q$ vertices.

For $\tilde{\beta}_m < \bar{\beta}_m$, the action (85) is minimized when $\theta = \pi/4$ and $\varphi_1 + \varphi_2 = \pi/2$. In terms of Δ's, this implies $|\Delta_1^x| = |\Delta_2^y|$ and $|\Delta_1^y| = |\Delta_2^x|$. We label this state as state II. The relative phases of Δ_1^x and Δ_2^x and of Δ_1^y and Δ_2^y are again fixed at either $\pi/2$ or $-\pi/2$ (with the same value for x and y components), but the relative phase of Δ_1^x and Δ_1^y and the relative magnitude of Δ_1^x and Δ_2^x remain arbitrary at this level of consideration. We show in the next subsection that the relative magnitude gets fixed once we include the k dependence of vertices, but the relative phase of Δ_1^x and Δ_1^y still remains arbitrary.

In the next two sections, we present a more detailed study on states I and II.

C. Properties of state I

Suppose for definiteness that the ordering is along Q_y, i.e., Δ_1^y and Δ_2^y become nonzero below T_{CDW}. The corresponding S_{eff} from (82) is

$$S_{\text{eff}} = \alpha\left(|\Delta_1^y|^2+|\Delta_2^y|^2\right)+\beta\left(|\Delta_1^y|^4+|\Delta_2^y|^4+\left[(\Delta_1^y)^*\Delta_2^y\right]^2\right.$$
$$\left.+\left[(\Delta_2^y)^*\Delta_1^y\right]^2+4|\Delta_1^y|^2|\Delta_2^y|^2\right)$$
$$=\alpha\left(|\Delta_1^y|^2+|\Delta_2^y|^2\right)+\beta\left(|\Delta_1^y|^2+|\Delta_2^y|^2\right)^2$$
$$+\beta\left[(\Delta_1^y)^*\Delta_2^y+\Delta_1^y(\Delta_2^y)^*\right]^2. \quad (86)$$

As we already said, at this level, while the phase difference of Δ_1^y and Δ_2^y is locked to be $\pm\pi/2$, the relative magnitude of Δ_1^y and Δ_2^y can be arbitrary, only $|\Delta_1^y|^2+|\Delta_2^y|^2$ is specified by minimizing Eq. (86). In fact, in this approximation one can easily make sure that the fields $\Delta_{k_0}^y = \Delta_1^y + \Delta_2^y$ and $\Delta_{-k_0}^y = \Delta_1^y - \Delta_2^y$ decouple: the first line in (86) exactly reduces to

$$S_{\text{eff}} = \tfrac{1}{2}\left[\alpha\left(|\Delta_{k_0}^y|^2+|\Delta_{-k_0}^y|^2\right)+\beta\left(|\Delta_{k_0}^y|^4+|\Delta_{-k_0}^y|^4\right)\right]. \quad (87)$$

One implication of this equivalence is that in the hot spot approximation, the fact that the phases of Δ_1^y and Δ_2^y are locked at $\pm\pi/2$ does not have a physical consequence in the sense that the parameter manifold is $U(1)\times U(1)\times Z_2$, where the two $U(1)$'s are the two completely decoupled order parameters at k and $-k$, and Z_2 symmetry is for the choice between Q_x and Q_y, and there is no additional Z_2 component associated with the two choices for the phase locking. However, as we will see below, the decoupling between $\Delta_{k_0}^y$ and $\Delta_{-k_0}^y$ is the artifact of the approximation of $\Delta_k^{Q_x}$ by its value at $\mathbf{k} = \mathbf{k}_0 = (\pi - Q, 0)$. Once we go beyond this approximation, Δ_k^y and Δ_{-k}^y become coupled and Z_2 symmetry associated with the two choices of phase locking becomes a physically relevant part of the order parameter manifold.

To account for the effects due to momentum dependence of Δ_k^y, we adopt a simple "toy model" approach and assume that odd and even components of Δ_k^y behave near k_0 as

$$\Delta_{1,k}^y = \Delta_1^y\frac{\cos k}{\cos k_0}, \quad \Delta_{2,k}^y\text{sgn}(k) = \Delta_2^y\frac{\sin k}{\sin k_0}, \quad (88)$$

where k is along the x direction. The correspondent momentum dependence then appears in the vertices in two-fermion and four-fermion loop diagrams for α and β terms. Reevaluating the GL action with these vertices we obtain

$$S_{\text{eff}} = \alpha_1|\Delta_1^y|^2+\alpha_2|\Delta_2^y|^2+\beta_1|\Delta_1^y|^4+\beta_2|\Delta_2^y|^4$$
$$+2\beta_3|\Delta_1^y|^2|\Delta_2^y|^2+\beta_3\left[(\Delta_1^y)^*\Delta_2^y+\Delta_1^y(\Delta_2^y)^*\right]^2, \quad (89)$$

where

$$\alpha_{1,2} = \alpha - J_{\alpha_{1,2}}, \quad \beta_{1,2,3} = \beta + J_{\beta_{1,2,3}}. \quad (90)$$

Here, α and β are GL coefficients in the approximation $\Delta_k^{Q_y} = \Delta_{k_0}^{Q_y}$ and the corrections $J_{\alpha_{1,2}}$ and $J_{\beta_{1,2,3}}$ are

given by

$$J_{\alpha_1}=\int_{-\Lambda}^{\Lambda}dk\left(\frac{\cos^2 k}{\cos^2 k_0}-1\right),\quad J_{\alpha_2}=\int dk\left(\frac{\sin^2 k}{\sin^2 k_0}-1\right),$$
$$J_{\beta_1}=\int_{-\Lambda}^{\Lambda}dk\left(\frac{\cos^4 k}{\cos^4 k_0}-1\right),\quad J_{\beta_2}=\int dk\left(\frac{\sin^4 k}{\sin^4 k_0}-1\right),$$
$$J_{\beta_3}=\int_{-\Lambda}^{\Lambda}dk\left(\frac{\sin^2 k\cos^2 k}{\sin^2 k_0\cos^2 k_0}-1\right), \tag{91}$$

where the integration extends to a finite range Λ around hot spots. Expanding in (91) in $k-k_0$ we obtain

$$J_{\alpha_1}=-2\epsilon\frac{\cos 2k_0}{\cos^2 k_0},\quad J_{\alpha_2}=2\epsilon\frac{\cos 2k_0}{\sin^2 k_0}, \tag{92}$$

$$J_{\beta_1}=2\epsilon(3\cot^2 k_0-1),\quad J_{\beta_2}=2\epsilon(3\tan^2 k_0-1),$$
$$J_{\beta_3}=\epsilon(\cot^2 k_0+\tan^2 k_0-6), \tag{93}$$

where $\epsilon=\int_{-\Lambda}^{\Lambda}(k-k_0)^2dk>0$. In $Bi_2Sr_{2-x}La_xCuO_{6+y}$, $\pi-k_0\approx 0.255\pi$ (Ref. [12]) hence $|\tan k_0|\approx 1.03$ and $\cos 2k_0\approx -0.03$. From Eq. (92) we then find that $\alpha_2>\alpha_1$, i.e., the renormalized mean-field CDW transition temperature for the even component $T_{\mathrm{CDW},e}=T_e$ is larger than that for the odd component $T_{\mathrm{CDW},o}=T_o$. This agrees with Refs. [64,65]. We note, however, that the two are still very close to the original T_{CDW} because J_{α_1} and J_{α_2} are very small numerically. A complementary approach as to how to go beyond hot spot treatment is presented in Appendix E. It also leads to $\alpha_2\geqslant\alpha_1$. We also have

$$\beta_1-\beta_3=\epsilon(4-(\tan k_0)^2+5(\cot k_0)^2),$$
$$\beta_2-\beta_3=\epsilon(4-(\cot k_0)^2+5(\tan k_0)^2). \tag{94}$$

For $|\tan k_0|\approx|\cot k_0|\approx 1$, $\beta_1\approx\beta_2>\beta_3$.

Analyzing the effective action (89) in the mean-field approximation, we observe that a relative phase between $\Delta_1^y=|\Delta_1^y|e^{i\psi_1}$ and $\Delta_2^y=|\Delta_2^y|e^{i\psi_2}$ is locked at $\pm\pi/2$, like in the case of a constant Δ_k^x. In other words, if Δ_1^x is real, Δ_2^x should be imaginary. From $\partial S_{\mathrm{eff}}/\partial\Delta_1^y=\partial S_{\mathrm{eff}}/\partial\Delta_2^y=0$, we obtain

$$\Delta_1^y\left(\alpha_1+2\beta_1\left|\Delta_1^y\right|^2+2\beta_3\left|\Delta_2^y\right|^2\right)=0,$$
$$\Delta_2^y\left(\alpha_2+2\beta_2\left|\Delta_2^y\right|^2+2\beta_3\left|\Delta_1^y\right|^2\right)=0. \tag{95}$$

Assuming that both orders are nonzero, we obtain from (95)

$$\left|\Delta_1^y\right|^2=\frac{1}{2}\frac{\alpha_2\beta_3-\alpha_1\beta_2}{\beta_1\beta_2-\beta_3^2},$$
$$\left|\Delta_2^y\right|^2=\frac{1}{2}\frac{\alpha_1\beta_3-\alpha_2\beta_1}{\beta_1\beta_2-\beta_3^2}. \tag{96}$$

An elementary analysis shows that this solution is a minimum of the effective action when $\beta_1\beta_2>\beta_3^2$. In our case,

$$\beta_1\beta_2-\beta_3^2=\frac{16\beta\epsilon}{(\sin 2k_0)^2}>0, \tag{97}$$

i.e., this condition is satisfied. The temperature at which Δ_2^x acquires a nonzero value is

$$T_{co}=T_o\frac{\beta_1-\beta_3}{\beta_1-\beta_3\frac{T_o}{T_e}}\approx T_o. \tag{98}$$

Below this temperature, both order parameters acquire nonzero values and the relative phase $\psi_1-\psi_2$ is either $\pi/2$ or $-\pi/2$. The broken symmetry in the phase when both Δ_1^y and Δ_2^y are nonzero is $U(1)\times Z_2$, where continuous $U(1)$ corresponds to the common phase $\bar\varphi_1+\bar\varphi_2$ of Δ_1^y and Δ_2^y and Ising Z_2 corresponds to the choice $\pi/2$ or $-\pi/2$ for the relative phase.

What happens at lower T depends on the sign of $\beta_2-\beta_3>0$, and the two orders coexist down to $T=0$. Interestingly, when $\beta_2<\beta_3$, there is another temperature

$$\bar T_{co}=T_o\frac{\beta_3-\beta_2}{\beta_3-\beta_2\frac{T_o}{T_e}}<T_o \tag{99}$$

at which Δ_1^y disappears and at smaller T only Δ_2^y is nonzero.

It is also instructive to rewrite the effective action (89) in terms of the original CDW order parameters $\Delta_{k_0}^y$ and $\Delta_{-k_0}^y$ at the hot spots. From Eqs. (81) and (88), we have $\Delta_1^y=(\Delta_{k_0}^y+\Delta_{-k_0}^y)/2$ and $\Delta_2^y=(\Delta_{k_0}^y-\Delta_{-k_0}^y)/2$, which is the same relation as in the hot spot approximation. Plugging them into Eq. (89), we obtain

$$\begin{aligned}S_{\mathrm{eff}}=&\left(\frac{\alpha_1+\alpha_2}{4}\right)\left(\left|\Delta_{k_0}^y\right|^2+\left|\Delta_{-k_0}^y\right|^2\right)\\&+\left(\frac{\alpha_1-\alpha_2}{4}\right)\left[\Delta_{k_0}^y\left(\Delta_{-k_0}^y\right)^*+\Delta_{-k_0}^y\left(\Delta_{k_0}^y\right)^*\right]\\&+\left(\frac{3\beta_3}{8}+\frac{\beta_1+\beta_2}{16}\right)\left(\left|\Delta_{k_0}^y\right|^2+\left|\Delta_{-k_0}^y\right|^2\right)^2\\&-\left(\frac{3\beta_3}{8}-\frac{\beta_1+\beta_2}{16}\right)\left[\Delta_{k_0}^y\left(\Delta_{-k_0}^y\right)^*+\Delta_{-k_0}^y\left(\Delta_{k_0}^y\right)^*\right]^2\\&+\frac{\beta_1-\beta_2}{8}\left(\left|\Delta_{k_0}^y\right|^2+\left|\Delta_{-k_0}^y\right|^2\right)\\&\times\left[\Delta_{k_0}^y\left(\Delta_{-k_0}^y\right)^*+\Delta_{-k_0}^y\left(\Delta_{k_0}^y\right)^*\right]\\&+\frac{\beta_3}{4}\left[\Delta_{k_0}^y\left(\Delta_{-k_0}^y\right)^*-\Delta_{-k_0}^y\left(\Delta_{k_0}^y\right)^*\right]^2.\end{aligned} \tag{100}$$

For momentum-independent vertices, $\Delta_{k_0}^y$ and $\Delta_{-k_0}^y$ decouple in the effective action (87). However, we see that the fields Δ_k^y and $\Delta_{-k_0}^y$ now interact with each other. To make this more clearly visible, let us neglect small differences between α and $\alpha_{1,2}$ and between β_1 and β_2, but keep a larger difference between β_1 and β_3. In this approximation, the effective action reduces to

$$\begin{aligned}S_{\mathrm{eff}}=&\frac{\alpha}{2}\left(\left|\Delta_{k_0}^y\right|^2+\left|\Delta_{-k_0}^y\right|^2\right)\\&+\left(\frac{3\beta_3+\beta_1}{8}\right)\left(\left|\Delta_{k_0}^y\right|^4+\left|\Delta_{-k_0}^y\right|^4\right)\\&+\left(\frac{\beta_1-\beta_3}{8}\right)\left(6\left|\Delta_{k_0}^y\right|^2\left|\Delta_{-k_0}^y\right|^2\right.\\&\left.+\left[\Delta_{k_0}^y\left(\Delta_{-k_0}^y\right)^*-\Delta_{-k_0}^y\left(\Delta_{k_0}^y\right)^*\right]^2\right).\end{aligned} \tag{101}$$

This can be equivalently reexpressed as

$$S_{\rm eff} = \frac{\alpha}{2}\left(|\Delta^y_{k_0}|^2 + |\Delta^y_{-k_0}|^2\right) + \frac{\beta_1}{4}\left(|\Delta^y_{k_0}|^2 + |\Delta^y_{-k_0}|^2\right)^2 + \left(\frac{3\beta_3-\beta_1}{8}\right)\left(|\Delta^y_{k_0}|^2 - |\Delta^y_{-k_0}|^2\right)^2 - \left(\frac{\beta_1-\beta_3}{8}\right) \times \left\{i\left[\Delta^y_{k_0}\left(\Delta^y_{-k_0}\right)^* - \Delta^y_{-k_0}\left(\Delta^y_{k_0}\right)^*\right]\right\}^2. \quad (102)$$

The advantage of this last expression is that it clearly shows that, for $\beta_1 > \beta_3$, $S_{\rm eff}$ is reduced when $\Delta^y_{k_0}$ and $\Delta^y_{-k_0}$ appear together, and $\Delta^y_{k_0} = \Delta^y_1 \pm i|\Delta^y_2|$ and $\Delta^y_{-k_0} = \Delta^y_1 \mp i|\Delta^y_2|$ because then the last term in (102) becomes $-[(\beta_1-\beta_3)/2]|\Delta^y_1||\Delta^y_2|$. At the same time, the prefactor for the "nematic" term $(|\Delta^y_{k_0}|^2 - |\Delta^y_{-k_0}|^2)^2$ is positive, which implies that $|\Delta^y_{k_0}|$ and $|\Delta^y_{-k_0}|$ must be equal. This holds when Δ^y_1 and Δ^y_2 are orthogonal to each other.

1. Physical properties of the coexistence state

We now consider physical properties of the coexistence state, when both even and odd CDW order parameters are nonzero. The generic condition $(\Delta^Q_k)^* = \Delta^{-Q}_k$ imposes the constraint that Δ^Q_1 must be even in Q and Δ^Q_2 must be odd in Q. We then reexpress the Δ^Q_k at hot spots 1-2 and 3-4 as (for $\mathbf{Q} = \pm Q_y$)

$$\Delta^Q_k = \Delta_1 \pm i\Delta_2 {\rm sgn}(k){\rm sgn}(Q), \quad (103)$$

where Δ_1 and Δ_2 are numbers. This Δ^Q_k breaks time-reversal symmetry because under time reversal Δ^Q_k transforms into $(\Delta^{-Q}_{-k})^* = \Delta^Q_{-k}$. The choice of relative sign in (103) specifies one of two nonequivalent solutions which transform into each other under time inversion. On the other hand, the parity is not broken as under parity operation Δ^Q_k transforms into $\Delta^{-Q}_{-k} = \Delta^Q_k$. Note that the order parameter (103) is similar, but not equivalent, to incommensurate complex d-density wave order proposed in [93,94].

Converting to real space, we find that the term Δ_1 corresponds to an incommensurate modulation of local charge and bond density in the y direction:

$$\begin{aligned}\delta\rho(r) &= {\rm Re}\langle c^\dagger(r)c(r)\rangle \\ &= \sum_k \langle c^\dagger(k+Q_y)c(k-Q_y)\rangle e^{i(k+Q_y)r}e^{-i(k-Q_y)r} + {\rm H.c.} \\ &\propto \Delta_1 \cos 2Qr_y, \\ \delta\rho(r,a_x) &= {\rm Re}[\langle c^\dagger(r+a_x/2)c(r-a_x/2)\rangle] \\ &\propto \Delta_1 \cos 2Qr_y \cos k_0 a_x \approx -\Delta_1 \cos 2Qr_y, \\ \delta\rho(r,a_y) &= {\rm Re}[\langle c^\dagger(r+a_y/2)c(r-a_y/2)\rangle] \\ &\propto \Delta_1 \cos 2Q(r_y+a_y/2) \approx \Delta_1 \cos 2Qr_y. \end{aligned} \quad (104)$$

The term Δ_2 corresponds to an incommensurate bond current, which flows along the x direction and has incommensurate modulation in the y direction [see Fig. 11(a)]:

$$\begin{aligned} j_x(r) &= {\rm Re}[i\langle c^\dagger(r-a_x/2)c(r+a_x/2)\rangle] \\ &= {\rm Re}\left[i\sum_k \langle c^\dagger(k+Q_y)c(k-Q_y)\rangle e^{i(k+Q_y)(r-a_x/2)}e^{-i(k-Q_y)(r+a_x/2)} + (Q_y \to -Q_y)\right] \\ &= {\rm Re}\left[i\sum_k \left(\Delta^Q_k e^{2iQr_y} + \Delta^{-Q}_k e^{-2iQr_y}\right)e^{-ika_x}\right] \\ &= 2\,{\rm Re}\left[i\Delta_1\cos(2Qr_y)\sum_k e^{-ika_x} - i|\Delta_2|\sin(2Qr_y)\sum_k {\rm sgn}(k)e^{-ika_x}\right] \\ &\propto |\Delta_2|\sin 2Qr_y \sin k_0 a_x = |\Delta_2|\sin 2Qr_y \sin Qa_x. \end{aligned} \quad (105)$$

Note that the bond current modulation is in antiphase with the density modulation. An incommensurate bond current in turn creates an incommensurate magnetic field $H_z(r) \propto |\Delta_2|\cos 2Qr_y$. This, however, does not lead to orbital ferromagnetism as the total magnetic field, integrated over the volume of the system, vanishes: $(1/V)\int H_z dV = 0$. To be more precise, current lines have to close at the boundary of a sample, and it is natural to expect that they close through the regions of excess charge, as shown in Fig. 11(b). This gives rise to a set of loop currents with circulation along the same direction, which do create a uniform magnetic field. However, a uniform field scales as the area of the sample rather than its volume and vanishes in the thermodynamic limit. This is very different from triangular loop currents proposed in Ref. [46].

D. Properties of state II

We recall that in the hot spot approximation, the minimum of the effective action (85) for $\tilde{\beta}_m > \tilde{\beta}_m$ (state II) is at $\theta = \pi/4$ and $\varphi_1 + \varphi_2 = \pi/2$, which in terms of Δ's implies that $|\Delta^x_1| = |\Delta^y_2|$ and $|\Delta^y_1| = |\Delta^x_2|$. The relative phases between Δ^x_1 and Δ^x_2 and between Δ^y_1 and Δ^y_2 are either both $\pi/2$ or $-\pi/2$.

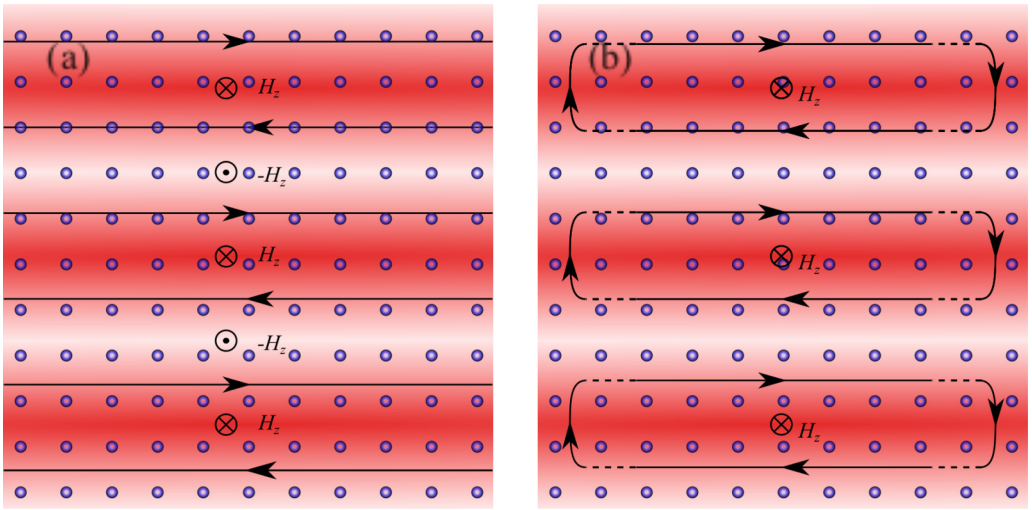

FIG. 11. (Color online) (a) The structure of density and current modulations in state I. The regions of higher and lower fermionic density are shown by darker and lighter color, respectively. The direction of the current is shown by arrows. The current vanishes when the density fluctuation has either the highest or the lowest value. An oscillating current gives rise to an oscillating magnetic field, whose values are shown by dots and crosses. (b) Current loops, formed by connecting oscillating currents in the bulk via the regions of higher local charge density on the surface.

Substituting these relations into (85) and using Δ_1^y and Δ_2^y as two variables, we obtain the same effective action (86) as for state I, namely,

$$S_{\text{eff}} = \alpha\left(\left|\Delta_1^y\right|^2 + \left|\Delta_2^y\right|^2\right) + \beta\left(\left|\Delta_1^y\right|^2 + \left|\Delta_2^y\right|^2\right)^2 \qquad (106)$$

Like for state I, the relative magnitude between Δ_1^y and Δ_2^y is not fixed in the hot spot approximation, and to find the actual CDW ordering one has to include the k dependence of $c^\dagger c\Delta_k^Q$ vertices. This gives rise to an effective action similar to Eq. (89), however, for state II the full effective action is more involved as all four CDW components are different from zero. We will not discuss the full form of the action because we believe that the state II is less relevant to the cuprates than the state I, and rather describe two potential realizations of the freezing of the relative magnitude of $|\Delta_1^y|$ and $|\Delta_2^y|$, i.e., the breaking of the freedom associated with the realization of $\varphi_1 + \varphi_2 = \pi/2$. One obvious choice is $\varphi_1 = \varphi_2 = \pi/4$, another is $\varphi_1 = \pi/2$, $\varphi_2 = 0$ or $\varphi_1 = 0$, $\varphi_2 = \pi/2$.

1. $\theta = \pi/4$, $\varphi_1 = \pi/4$, $\varphi_2 = \pi/4$

In this case, all four CDW components Δ_1^x, Δ_2^x, Δ_1^y, Δ_2^y develop with the same magnitude Δ. In real space, this order corresponds to a checkerboard-type incommensurate charge-density modulation and incommensurate current in both x and y directions. We show this in Fig. 12(a). The order parameter manifold is $U(1) \times U(1) \times Z_2$, where two continuous $U(1)$ symmetries are associated with the phases of Δ_1^x and Δ_1^y, and the Ising Z_2 is associated with the relative phase between Δ_1 and Δ_2, which is $\pi/2$ or $-\pi/2$, simultaneously for x and y

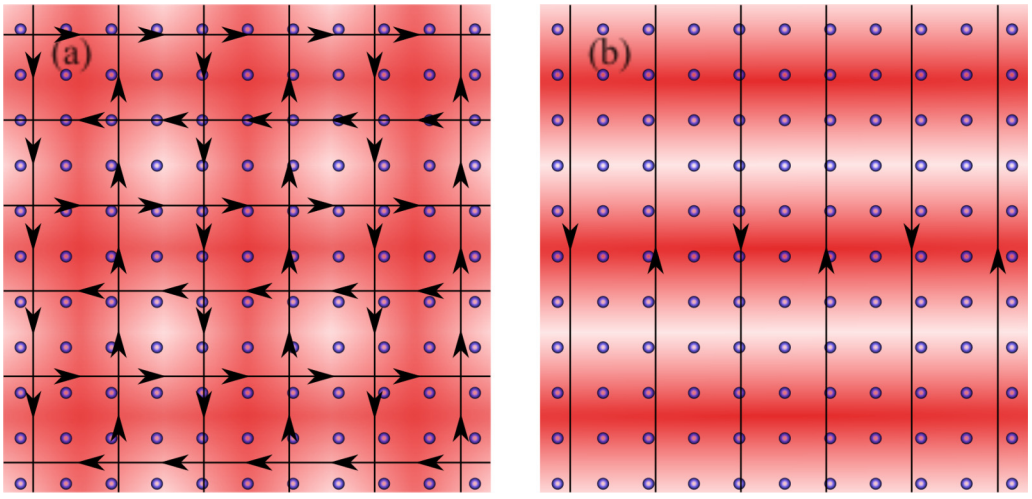

FIG. 12. (Color online) Two possible real-space structures of charge order in state II. (a) A checkerboard charge-density order together with oscillating currents along both x and y directions. (b) A stripe charge-density order together with an oscillating current along orthogonal direction.

components. This CDW order preserves C_4 lattice rotational symmetry but breaks time-reversal symmetry.

Plugging $\theta = \pi/4$, $\varphi_1 = \pi/4$, $\varphi_2 = \pi/4$ into Eq. (85) and again neglecting β compared to $\bar{\beta}_m$ and $\tilde{\beta}_m$, we find the effective action (82) in the form

$$S_{\text{eff}} = \alpha\Delta^2 - \frac{\bar{\beta}_m - \tilde{\beta}_m}{2}\Delta^4. \quad (107)$$

Because $\bar{\beta}_m - \tilde{\beta}_m > 0$, the transition is first order. It occurs at some T larger than mean field T_{CDW} at which α changes sign.

2. $\theta = \pi/4$, $\varphi_1 = \pi/2$, $\varphi_2 = 0$

In this case, Δ_1^Q develops along the y direction and Δ_2^Q develops along the x direction, i.e., $|\Delta_1^y| = |\Delta_2^x| \neq 0$ and $|\Delta_2^y| = |\Delta_1^x| = 0$. In real space, this order corresponds to incommensurate charge density modulations in the x direction and incommensurate current in the y direction. We show this in Fig. 12(b). Such an order breaks two $U(1)$ phase symmetries and breaks C_4 lattice symmetry down to C_2 such that the order parameter manifold is $U(1) \times U(1) \times Z_2$, where Z_2 corresponds to $C_4 \to C_2$. However, the order parameter manifold does not have an additional Z_2 component, which one would associate with time-reversal symmetry, because only Δ_1 or Δ_2 appear along a particular direction of $\mathbf{Q}$. Indeed, Δ_2 changes sign under time reversal, but this change is absorbed into $U(1)$ phase symmetry.

The effective action for nonzero Δ_1^y and Δ_2^x is obtained from (82):

$$S_{\text{eff}} = \alpha\left(|\Delta_1^y|^2 + |\Delta_2^x|^2\right) - 2(\bar{\beta}_m - \tilde{\beta}_m)|\Delta_1^y|^2|\Delta_2^x|^2. \quad (108)$$

Because $\bar{\beta}_m - \tilde{\beta}_m > 0$, the transition is again first order, into a state in which Δ_1^x and Δ_2^y have equal magnitudes.

VI. PREEMPTIVE COMPOSITE CDW ORDER

We now go beyond mean-field theory and discuss potential preemptive transitions, when a discrete Ising symmetry gets broken at a higher T than a continuous phase symmetry. We focus on the state I because in this state transitions are second order and the analysis of preemptive instabilities can be carried out within the GL expansion. This state is also more favorable for applications to hole-doped cuprates as phase transitions there are likely continuous ones. We will briefly discuss a potential preemptive order in the state II at the end of this section. We remind that the order parameter manifold in the state I is $U(1) \times Z_2 \times Z_2$, where one Z_2 is associated with the breaking of C_4 lattice rotational symmetry down to C_2 and another Z_2 is associated with Ising symmetry breaking associated with the relative phase between even and odd in k components of Δ_k^Q with a given Q. The lattice Z_2 symmetry is broken by strong interactions ($\tilde{\beta}_m$ and $\bar{\beta}_m$ terms in the action), while Z_2 associated with the relative phase is broken by weaker interactions, of order $\beta \ll \tilde{\beta}_m, \bar{\beta}_m$.

Following, we discuss two preemptive composite orders associated with the breaking of each of the two discrete Ising Z_2 symmetries without breaking of the $U(1)$ phase symmetry. We analyze composite orders within "stage II" HS formalism, by which we mean that we introduce HS fields associated with Z_2 composite orders, apply HS transformation to effective action written in terms of Δ fields to decouple Δ^4 terms, integrate over Δ fields, and analyze the effective action for composite fields in the saddle-point approximation. A similar procedure was applied in the study of a preemptive nematic order in Fe pnictides [66] and of a preemptive translational symmetry breaking in doped graphene [90].

The saddle-point approximation for the action in terms of composite order parameters is valid when fluctuations around the saddle-point solution are weak. This is the case when the number of components of the primary field Δ field is large. The HS approach assumes that the original model can be safely extended to a large number of field components $M \gg 1$ in the sense that the results obtained in the controlled analysis at large M are at least qualitatively correct for the original model with $M \sim 1$. We will perform a large-M calculation below and show that composite orders associated with the breaking of each of Z_2 symmetries in our case emerge at a higher T than the one at which the primary field orders. A caveat here is that in 2D a primary field with $M \geqslant 3$ does not order down to $T = 0$ (Ref. [95]), hence a breaking of a Z_2 symmetry at any nonzero T is a preemptive order. Whether the actual system shows the same behavior depends on the type of the problem. For Fe pnictides, the (magnetic) order parameter is a three-component unit vector, and it indeed does not order down to $T = 0$ in 2D, like in the large-M approximation. In quasi-2D systems, the primary field does order, but at a very low T, which for weak coupling along the third direction is certainly smaller than a finite critical T at which Z_2 symmetry gets broken. In our case, however, the primary field is a two-component unit vector [a $U(1)$ field], and the temperature at which the primary field orders in a quasi-2D system is finite and tends to Berezinskii-Kosterlitz-Thouless temperature in the 2D limit. Whether this temperature is still smaller than the one at which composite order develops is *a priori* unclear and cannot be addressed within HS-based, large-M analysis. Fortunately, the emergence of preemptive composite orders has been verified within the approach specifically designed for a $U(1)$ primary field [68]. We use the result of [68] as a verification that for the issue of a preemptive order, a model with a two-component primary field is not qualitatively different from models with a larger number of field components and proceed with the HS-based analysis.

A. A nematic transition

We first discuss whether the breaking of C_4 lattice rotational symmetry down to C_2 can occur before the continuous $U(1)$ phase symmetry gets broken. For this discussion, the presence of the two components of Δ_k^Q with a given Q does not play a role (the analysis of the truncated and full GL functional yield the same results with regard to C_4 breaking in the ordered state I). To simplify presentation, we then analyze the truncated GL functional with only the Δ_1 component present. Our analysis of a preemptive nematic order will closely follow that in Ref. [66], but we also discuss the stability of the nematic phase.

The effective action for coupled order parameters $\Delta_x = \Delta_1^{Q_x}$ and $\Delta_y = \Delta_1^{Q_y}$ is presented in Eq. (76). Adding gradient

terms and rescaling, we reexpress (76) as

$$S(\Delta_x,\Delta_y) = \alpha(|\Delta_x|^2+|\Delta_y|^2) + |\partial_\mu\Delta_x|^2 + |\partial_\mu\Delta_y|^2 + \frac{1}{2}(|\Delta_x|^2+|\Delta_y|^2)^2 - \frac{\beta^*}{2}(|\Delta_x|^2-|\Delta_y|^2)^2, \tag{109}$$

where, in comparison with (76), $\alpha^* = a^*(T-T_{\rm CDW})$ with $a^* = a/(\beta+\beta_m)$, and $\beta^* = (\beta_m-\beta)/(\beta_m+\beta)$. Because both β_m and β are positive and $\beta_m > \beta$, we have $0 < \beta^* < 1$. In principle, one should also include frequency dependence of the Δ fields and add the dynamical Landau damping $\gamma|\omega_m|$ term to α_q, but to analyze the transition at a finite T it is sufficient to consider only thermal fluctuations, i.e., those coming from $\omega_m = 0$.

We extend each Δ field to $M \gg 1$ components and rewrite $S(\Delta_x,\Delta_y)$ as

$$\begin{aligned} S(\Delta_x,\Delta_y) = &\sum_{i=1}^{M}[\alpha(|\Delta_{x,i}|^2+|\Delta_{y,i}|^2) + |\partial_\mu\Delta_{x,i}|^2 + |\partial_\mu\Delta_{y,i}|^2] \\ &+ \frac{1}{2M}\left(\sum_{i=1}^{M}\left(|\Delta_{x,i}|^2+|\Delta^2_{y,i}|^2\right)^2\right) - \frac{\beta^*}{2M}\left(\sum_{i=1}^{M}\left(|\Delta_{x,i}|^2-|\Delta^2_{y,i}|\right)\right)^2. \end{aligned} \tag{110}$$

We introduce two HS fields: ψ, conjugated to $i(|\Delta_{x,i}|^2+|\Delta_{y,i}|^2)$, and υ, conjugated to $|\Delta_{x,i}|^2-|\Delta_{y,i}|^2$, as

$$\begin{aligned} \exp\left(-\sum_{i=1}^{M}(|\Delta_{x,i}|^2+|\Delta_{y,i}|^2)^2/(2M)\right) &= \sqrt{\frac{M}{2\pi}}\int d\psi\, e^{\frac{-M\psi^2}{2}}\exp\left[i\psi\left(\sum_{i=1}^{M}\left(|\Delta_{x,i}|^2+|\Delta^2_{y,i}|^2\right)\right)\right], \\ \exp\left(\sum_{i=1}^{M}(|\Delta_{x,i}|^2-|\Delta_{y,i}|^2)^2/(2M)\right) &= \sqrt{\frac{M}{2\pi\beta^*}}\int d\upsilon\, e^{-\frac{M\upsilon^2}{2\beta^*}}\exp\left[\upsilon\left(\sum_{i=1}^{M}\left(|\Delta_{x,i}|^2-|\Delta^2_{y,i}|\right)\right)\right]. \end{aligned} \tag{111}$$

Substituting these integrals into the partition function $I = \int d\Delta_x d\Delta_y e^{-S(\Delta_x,\Delta_y)}$ and integrating over Δ_x and Δ_y, we obtain $I \propto \int d\psi\, d\upsilon\, e^{-MS_{\rm eff}(\psi,\upsilon)}$, where

$$S_{\rm eff}[\psi,\upsilon] = \frac{\psi^2}{2} + \frac{\upsilon^2}{2\beta^*} + \int\frac{d^2q}{4\pi^2}\ln[(\alpha+q^2-i\psi)^2-\upsilon^2]. \tag{112}$$

The extremum of $S_{\rm eff}$ is obtained from $\partial S_{\rm eff}/\partial\psi = 0$ and $\partial S_{\rm eff}/\partial\upsilon = 0$. This gives two equations

$$\frac{\partial S_{\rm eff}}{\partial\psi} = \psi - 2i\int\frac{d^2q}{4\pi^2}\frac{\alpha+q^2-i\psi}{(\alpha+q^2-i\psi)^2-\upsilon^2} = 0, \tag{113}$$

$$\frac{\partial S_{\rm eff}}{\partial\upsilon} = \frac{\upsilon}{\beta^*} - 2\int\frac{d^2q}{4\pi^2}\frac{\upsilon}{(\alpha+q^2-i\psi)^2-\upsilon^2} = 0. \tag{114}$$

The solution exists for an imaginary $\psi = i\psi_0$.

We follow Ref. [66] and introduce $r \equiv \alpha+\psi_0$ and $x \equiv q^2+r$. The primary fields get ordered when r changes sign and becomes negative. This does not happen in 2D, as long as $T > 0$. Replacing ψ_0 by $r-\alpha$, we obtain from Eq. (114)

$$\begin{aligned} r &= \alpha + \frac{1}{2\pi}\int_r^\Lambda\frac{dx\,x}{x^2-\upsilon^2} = \alpha + \frac{1}{2\pi}\ln\frac{\Lambda}{\sqrt{r^2-\upsilon^2}}, \\ \upsilon &= \upsilon\frac{\beta^*}{2\pi}\int_r^\infty\frac{dx}{x^2-\upsilon^2} = \upsilon\frac{\beta^*}{2\pi}\coth^{-1}\frac{r}{\upsilon}. \end{aligned} \tag{115}$$

1. The solution $\upsilon = 0$

The set of equations (115) obviously allows a "trivial" solution $\upsilon = 0$. We have then

$$r = \alpha + \frac{1}{2\pi}\ln\frac{\Lambda}{r}. \tag{116}$$

One can easily check the stability of this solution by verifying how the effective action changes when one moves along the trajectory which passes through a saddle point. For υ this implies shifting from $\upsilon = 0$ along the real axis, for ψ this implies shifting along the *real* axis from $\psi = i\psi_0 = i(r-\alpha)$, where r is the solution of (116). Introducing $\psi = i\psi_0+\delta\psi$ and $\upsilon \equiv \delta\upsilon$, substituting into the action, and expanding to second order in $\delta\psi$ and $\delta\upsilon$, we obtain

$$\begin{aligned} S_{\rm eff}(\psi,\upsilon) = S_{\rm eff}(i\psi_0,0) &+ \frac{(\delta\psi)^2}{2}\left(1+\frac{1}{2\pi r}\right) \\ &+ \frac{(\delta\upsilon)^2}{2\beta^*}\left(1-\frac{\beta^*}{2\pi r}\right). \end{aligned} \tag{117}$$

We see that the prefactor for $(\delta\psi)^2$ is definitely positive, i.e., $S_{\rm eff}$ definitely increases along the trajectory on Fig. 1. The prefactor for the $(\delta\upsilon)^2$ term is positive as long as $r > \beta^*/2\pi$. Combining this with Eq. (116), one finds that this holds when $\alpha > \alpha_{\rm cr}$, where

$$\alpha_{\rm cr} = \frac{\beta^*}{2\pi} - \frac{1}{2\pi}\ln\frac{2\pi\Lambda}{\beta^*}. \tag{118}$$

The condition $\alpha > \alpha_{\rm cr}$ implies that $T > T_{\rm cr}$, where $T_{\rm cr} = T_{\rm CDW} + \alpha_{\rm cr}/a$.

2. The solution with $\upsilon \neq 0$

Solving the set of saddle-point equations for $\upsilon \neq 0$, we obtain

$$r = \frac{\beta^*}{2\pi}\frac{\upsilon^*}{\tanh\upsilon^*}, \tag{119}$$

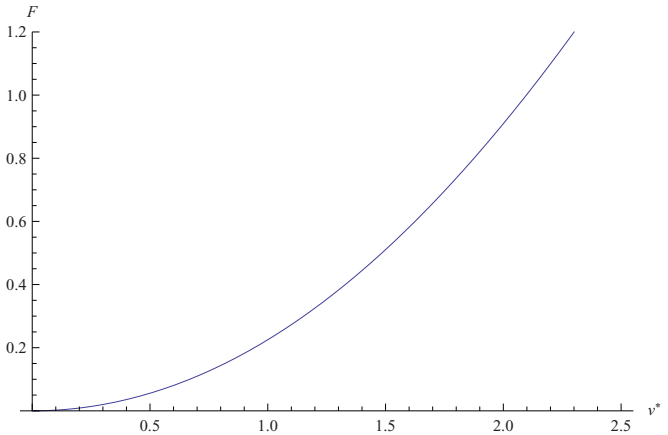

FIG. 13. (Color online) The plot of $F(\upsilon^*)$ from Eq. (120) as a function of υ^* with $\beta^* = 0.3$.

where $\upsilon^* \equiv \pi\upsilon/\beta^*$. The equation on υ^* takes the form

$$F(\upsilon^*) = \frac{2\pi}{\beta^*}(\alpha_{cr} - \alpha),$$
$$F(\upsilon^*) = 1 - \frac{\upsilon^*}{\tanh\upsilon^*} + \frac{1}{\beta^*}\ln\frac{\sinh\upsilon^*}{\upsilon^*}, \tag{120}$$

where, we remind, $\alpha = a(T - T_{CDW})$ Expanding the left-hand side of (120) at small υ^*, we obtain

$$\frac{(\upsilon^*)^2}{6}\left(\frac{1}{\beta^*} - 2\right) = \frac{2\pi}{\beta^*}(\alpha_{cr} - \alpha) \propto (T_{cr} - T). \tag{121}$$

We see that, if $2\beta^* < 1$, υ^* gradually increases when T becomes smaller than T_{cr}. To put it simply, the solution of the nonlinear saddle-point equation shows that the order in υ emerges below T_{cr}, as it is expected for a continuous, second-order transition. We see the same behavior from Fig. 13 where we plot $F(\upsilon^*)$ from (120) as a function of υ^*.

Let us now see what we get if we expand near the saddle-point solution. Introducing $\psi = i\psi_0 + \delta\psi$ and $\upsilon = (\beta^*/2\pi)\upsilon^* + \delta\upsilon$, where, for definiteness, υ^* is the positive solution of Eq. (120), and expanding to second order in $\delta\psi$ and $\delta\upsilon$, we obtain after a straightforward algebra

$$S_{\rm eff}(\psi,\upsilon) = S_{\rm eff}(i\psi_0,\beta^*\upsilon^*/\pi) + A\,(\delta\psi)^2 - B\,(\delta\upsilon)^2 - 2iC(\delta\psi)(\delta\upsilon), \tag{122}$$

where

$$A = \frac{1}{4\beta^*\upsilon^*}(2\beta^*\upsilon^* + \sinh 2\upsilon^*),$$
$$B = \frac{1}{4\beta^*\upsilon^*}(\sinh 2\upsilon^* - 2\upsilon^*), \tag{123}$$
$$C = \frac{1}{2\beta^*\upsilon^*}\sinh^2\upsilon^*.$$

Obviously, A, B, and C are positive for $\upsilon^* \neq 0$.

Equation (122) has the same form as Eq. (50) in the main text and Eq. (C78) in Appendix C. Like we did there, we reexpress $S_{\rm eff}(\psi,\upsilon)$ in (122) as

$$S_{\rm eff}(\psi,\upsilon) = S_{\rm eff}(i\psi_0,\beta^*\upsilon^*/\pi) + A\left((\delta\psi) - i\frac{C}{A}(\delta\upsilon)\right)^2 + \frac{C^2 - AB}{A}(\delta\upsilon)^2. \tag{124}$$

The contour has to be chosen such that the variable $(\delta\psi) - i\frac{C}{A}(\delta\upsilon)$ is real, i.e., we integrate over $\delta\psi$ parallel to the real axis.

As we already know, the condition that the saddle point is the minimum of the action along the integration contour is $C^2 - AB > 0$. Substituting the expressions from (123), we find

$$C^2 - AB = \frac{\sinh^2\upsilon^*}{4\beta^*(\upsilon^*)^2}I(\upsilon^*), \tag{125}$$

where

$$I(\upsilon^*) = \frac{1}{\beta^*}\left(\frac{\upsilon^*}{\tanh\upsilon^*} - 1\right) - \left[\frac{\upsilon^*}{\tanh\upsilon^*} - \left(\frac{\upsilon^*}{\sinh\upsilon^*}\right)^2\right]. \tag{126}$$

The condition that the saddle point is the minimum of the action along the integration contour is then $I(\upsilon^*) > 0$. Expanding at small υ^* we obtain

$$I(\upsilon^*) = \frac{(\upsilon^*)^2}{3}\left(\frac{1}{\beta^*} - 2\right). \tag{127}$$

We see that $I(\upsilon^*) > 0$ when $2\beta^* < 1$. This is the same condition as in Eq. (121). One can easily verify that when $0 < 2\beta^* < 1$, $I(\upsilon^*)$ is positive for all values of υ^*.

3. *First-order transition at* $\frac{1}{2} < \beta^* < 1$

For larger β^*, the prefactors in (127) and (121) are negative. The analysis of the full saddle-point solution [Eq. (120)] shows that, as α gets smaller, the saddle-point solution [i.e., the solution of (120)] first emerges at a finite υ^*_{cr}, i.e., the transition is first order [see Fig. 14, in which we plot $F(\upsilon^*)$ from (120) versus υ^* for $\frac{1}{2} < \beta^* < 1$].

As α gets smaller, two saddle-point solutions appear, one at $\upsilon^* > \upsilon^*_{cr}$, another at $\upsilon^* < \upsilon^*_{cr}$. By obvious reasons, the solution with $\upsilon^* > \upsilon^*_{cr}$ is expected to be stable, while the one at $\upsilon^* < \upsilon^*_{cr}$

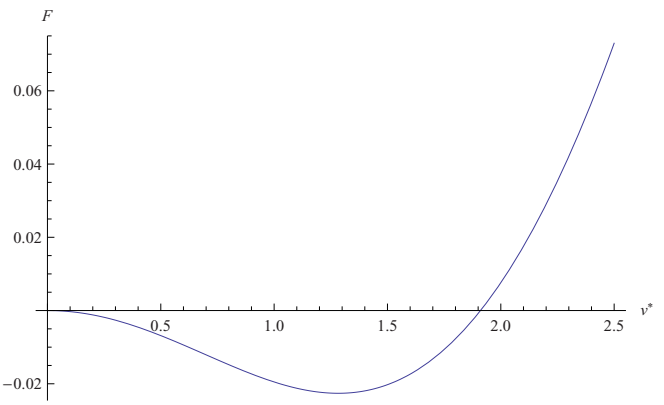

FIG. 14. (Color online) The plot of $F(\upsilon^*)$ from Eq. (120) as a function of υ^* with $\beta^* = 0.55$.

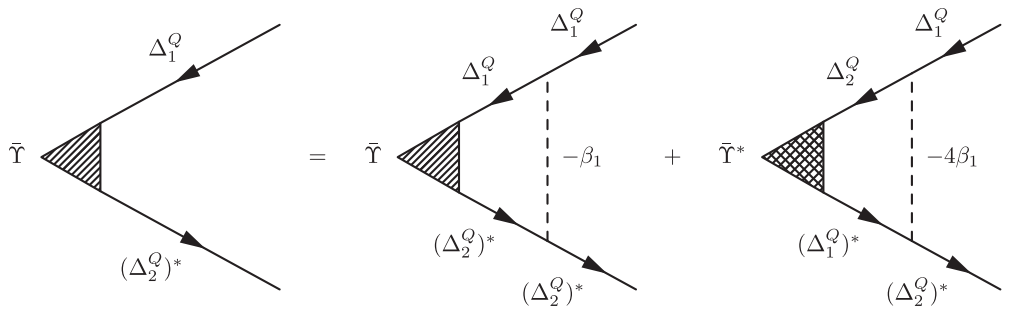

FIG. 15. Ladder equation for $\bar{\Upsilon} = \Delta_1^Q(\Delta_2^Q)^*$. Of the two terms in the right-hand side, one contains $\bar{\Upsilon}$, another $\bar{\Upsilon}^*$. For imaginary $\bar{\Upsilon}$, there is a sign change between these two terms.

is expected to be unstable. We see from Fig. 14 that the solution at $\upsilon^* > \upsilon^*_{\rm cr}$ corresponds to $dF(\upsilon^*)/d\upsilon^* > 0$, and the solution at $\upsilon^* < \upsilon^*_{\rm cr}$ corresponds to $dF(\upsilon^*)/d\upsilon^* < 0$. Now, evaluate

$$\frac{dF(\upsilon^*)}{d\upsilon^*} = \frac{\beta_1^*}{\beta^*}\left(\frac{\upsilon^*}{\tanh\upsilon^*} - 1\right) - \left[\frac{\upsilon^*}{\tanh\upsilon^*} - \left(\frac{\upsilon^*}{\sinh\upsilon^*}\right)^2\right]. \tag{128}$$

Comparing this with (126), we see that

$$\frac{dF(\upsilon^*)}{d\upsilon^*} \equiv I(\upsilon^*). \tag{129}$$

Hence, the solution with a positive $dF(\upsilon^*)/d\upsilon^*$ corresponds to $I(\upsilon^*) > 0$ and is stable, as expected.

B. Preemptive time-reversal symmetry breaking

We now return to the full GL model for Δ_1 and Δ_2 and consider a possibility of a preemptive breaking of Z_2 symmetry associated with the relative phase $\psi_1 - \psi_2 = \pm\pi/2$ between complex $\Delta_1^Q = |\Delta_1^Q|e^{i\psi_1}$ and $\Delta_2^Q = |\Delta_2^Q|e^{i\psi_2}$. We recall that a nematic order is selected already within the hot spot model, while the Z_2 part of the order parameter manifold associate with phase locking becomes relevant only once we go beyond the hot spot approximation and include the interaction between CDW order parameters Δ_k^Q and Δ_{-k}^Q. Accordingly, the coupling constant associated with the nematic Z_2 symmetry is larger than the one associated with the phase Z_2 symmetry, and, hence T_n, at which a nematic order sets in, is larger than a temperature T_t at which the other Z_2 symmetry gets broken. Still, it is essential to understand whether T_t is larger than $T_{\rm CDW}$, i.e., whether Z_2 symmetry associated with $\psi_1 - \psi_2 = \pi/2$ or $-\pi/2$ gets broken at a temperature higher than the one when $U(1)$ symmetry of the common phase $\psi_1 + \psi_2$ gets broken.

We assume that nematic order selects, say, $\mathbf{Q} = Q_x$ and consider GL model for Δ_1^x and Δ_2^x. A preemptive instability with respect to the relative phase of Δ_1^x and Δ_2^x would imply that at some $T = T_t > T_{\rm CDW}\Delta_1^x$ and Δ_2^x form a bound state with zero total momentum. In-between T_t and $T_{\rm CDW}$, $\delta\rho(r) = j_y(r) = 0$, but $\Upsilon \propto \langle\delta\rho(r)j_y(r)\rangle$ becomes nonzero. Under time reversal, Υ transforms into $-\Upsilon$, hence this order breaks Z_2 time-reversal symmetry.

1. Direct computation

One way to see that a preemptive transition is possible is to follow the same strategy as in the analysis of a spin-current order in anisotropic triangular antiferromagnets [96] and in the Heisenberg-Kitaev model on a hyperhoneycomb lattice [97,98], introduce a "two-particle" collective variable $\bar{\Upsilon} = \Delta_1^x(\Delta_2^x)^*$, and solve for the emergence of a two-particle bound state instability in the same way as it is done for superconductivity. For illustrative purposes, we consider the effective action (86), although the actual calculation has to be performed for the more generic action (89) as we will do below using the HS approach. We rewrite (86) as

$$\begin{aligned} S_{\rm eff} = {} & \alpha\left(\left|\Delta_1^x\right|^2 + \left|\Delta_2^x\right|^2\right) + \beta\left(\left|\Delta_1^x\right|^4 + \left|\Delta_2^x\right|^4\right) \\ & + \beta\left[\Delta_1^x\left(\Delta_2^x\right)^*\right]\left[\Delta_1^x\left(\Delta_2^x\right)^*\right] + \beta\left[\left(\Delta_1^x\right)^*\Delta_2^x\right]\left[\left(\Delta_1^x\right)^*\Delta_2^x\right] \\ & + 4\beta\left[\Delta_1^x\left(\Delta_2^x\right)^*\right]\left[\Delta_2^Q\left(\Delta_1^x\right)^*\right]. \end{aligned} \tag{130}$$

The ladder equation for $\bar{\Upsilon}$ is presented in Fig. 15. There are two terms in the right-hand side of this graphic equation: the first contains a "direct" $\bar{\Upsilon}\bar{\Upsilon}$ interaction from the first term in the second line of (130), and the second one contains the interaction between $\bar{\Upsilon}$ and $\bar{\Upsilon}^*$. Both interactions are repulsive, hence, no solution is possible if $\bar{\Upsilon}$ is real. However, if we search for a solution with a complex $\bar{\Upsilon}$, we obtain for infinitesimally small $\bar{\Upsilon}$

$$\bar{\Upsilon} = -\beta P(\bar{\Upsilon} + 4\bar{\Upsilon}^*), \tag{131}$$

where $P > 0$ stand for convolution of the propagators of Δ_1^Q and Δ_2^Q fields. The only information about P relevant to us at this stage is that it diverges at $T_{\rm CDW}$ when both propagators become massless. Hence, if Eq. (131) has a nontrivial solution, the corresponding T is larger than $T_{\rm CDW}$. A simple analysis of Eq. (131) shows that the solution does exist if we set $\bar{\Upsilon}$ to be purely imaginary, $\bar{\Upsilon} = i\Upsilon$, because then the combination $\bar{\Upsilon} + 4\bar{\Upsilon}^*$ becomes equal to $-3\bar{\Upsilon}$, and the minus sign compensates the overall minus sign in the right-hand side of (131). We emphasize that this is possible because the prefactor for $\bar{\Upsilon}\bar{\Upsilon}^*$ interaction term [the last term in (130)] is four times larger than the direct $\bar{\Upsilon}\bar{\Upsilon}$ interaction term. That $\bar{\Upsilon}$ is purely imaginary is entirely consistent with the fact that in the mean-field approximation Δ_1^Q is real and Δ_2^Q is imaginary, hence in below $T_{\rm CDW}$, $\bar{\Upsilon} = \Delta_1^x(\Delta_2^x)^*$ is also purely imaginary.

2. Hubbard-Stratonovich approach

Another way to see the emergence of a preemptive transition is to follow the same strategy as in the analysis of a preemptic nematic order and apply HS transformation to the effective action (89) by introducing collective variables conjugated to quartic terms in $S_{\rm eff}$. For this purpose, it is convenient to rescale Δ_2^x as $\Delta_2^x \to \Delta_2^x(\beta_1/\beta_2)^{1/4}$, add the gradient terms, and rewrite Eq. (89) as

$$S_{\rm eff} \propto (\alpha_1+q^2)\left|\Delta_1^x\right|^2+(\bar\alpha_2+q^2)\left|\Delta_2^x\right|^2+\frac{\gamma_1}{2}\left(\left|\Delta_1^x\right|^2+\left|\Delta_2^x\right|^2\right)^2 - \frac{\gamma_2}{2}\left(\left|\Delta_1^x\right|^2-\left|\Delta_2^x\right|^2\right)^2-\frac{\gamma_3}{2}\left\{i\left[\left(\Delta_1^x\right)^*\Delta_2^x-\Delta_1^x\left(\Delta_2^x\right)^*\right]\right\}^2, \tag{132}$$

where $\alpha_1 = a(T-T_e)$, $\bar\alpha_2 = \alpha_2(\beta_1/\beta_2)^{1/2} = a(T-T_o)$, where, we remind, T_e and T_o are (near identical) mean-field transition temperatures for even and odd in k components of Δ^x. Also,

$$\gamma_1 = \frac{1}{2}\beta_1+\frac{3}{2}\beta_3\left(\frac{\beta_1}{\beta_2}\right)^{1/2}, \quad \gamma_2 = \frac{3}{2}\beta_3\left(\frac{\beta_1}{\beta_2}\right)^{1/2}-\frac{1}{2}\beta_1, \quad \gamma_3 = \beta_3\left(\frac{\beta_1}{\beta_2}\right)^{1/2}. \tag{133}$$

The prefactors for the two q^2 terms in (132) as well as the prefactors a for α_1 and $\bar\alpha_2$ do not have to be equal, but this complication does not lead to new physics and we neglect it.

There are three quartic terms in (132). Accordingly, we introduce three HS bosonic fields Υ, conjugated to $i[\Delta_1^x(\Delta_2^x)^*-(\Delta_1^x)^*\Delta_2^x]$, Ψ, conjugated to $(|\Delta_1^x|^2+|\Delta_2^x|^2)$, and Ψ_1, conjugated to $(|\Delta_1^x|^2-|\Delta_2^x|^2)$. The expectation value of each HS field is proportional to the corresponding bilinear combination of Δ_1^x and Δ_2^x. The field Ψ describes Gaussian fluctuations of the modulus of a two-component order parameter and its expectation value is obviously nonzero at any T. The field Ψ_1 describes fluctuations of a relative magnitude of $|\Delta_1^x|^2$ and $|\Delta_2^x|^2$. For $\alpha_1 \neq \bar\alpha_2$, order parameters Δ_1^x and Δ_2^x are nonequal and $\langle|\Delta_1^x|^2-|\Delta_2^x|^2\rangle$ is nonzero at any T, hence the expectation value of Ψ_1 is also nonzero for all T. The field Υ is different from the other two because the expectation value of $\langle(\Delta_1^x)^*\Delta_2^x-\Delta_1^x(\Delta_2^x)^*\rangle$ and hence of Υ becomes nonzero only due to spontaneous symmetry breaking.

We assume, without going into details, that the model is extended to large M, as in the case of a nematic transition, and analyze the effective action for composite HS fields within the saddle-point approximation. A similar HS approach has been recently used to study TRS breaking in Fe pnictides [99–101]. We use, as before,

$$\begin{aligned}
&\exp\left[-\frac{\gamma_1\left(\left|\Delta_1^x\right|^2+\left|\Delta_2^x\right|^2\right)^2}{2}\right] \\
&= \int\frac{d\Psi}{\sqrt{2\pi\gamma_1}}\exp\left(\frac{-\Psi^2}{2\gamma_1}\right)\exp\left[i\Psi\left(\left|\Delta_1^x\right|^2+\left|\Delta_2^x\right|^2\right)\right], \\
&\exp\left[-\frac{\gamma_2\left(\left|\Delta_1^x\right|^2-\left|\Delta_2^x\right|^2\right)^2}{2}\right] \\
&= \int\frac{d\Psi_1}{\sqrt{2\pi\gamma_2}}\exp\left(-\frac{\Psi_1^2}{2\gamma_2}\right)\exp\left[\Psi_1\left(\left|\Delta_1^x\right|^2-\left|\Delta_2^x\right|^2\right)\right], \\
&\exp\left\{\frac{\gamma_3\left\{i\left[\Delta_1^x\left(\Delta_2^x\right)^*-\left(\Delta_1^x\right)^*\Delta_2^x\right]\right\}^2}{2}\right\} \\
&= \int\frac{d\Upsilon}{\sqrt{2\pi\gamma_3}}\exp\left(-\frac{\Upsilon^2}{2\gamma_3}\right) \\
&\quad\times\exp\left\{i\Upsilon\left[\Delta_1^x\left(\Delta_2^x\right)^*-\left(\Delta_1^x\right)^*\Delta_2^x\right]\right\}.
\end{aligned} \tag{134}$$

Substituting this transformation into (132) and performing Gaussian integration over the fields Δ_1^x and Δ_2^x we obtain the effective action in terms of collective variables Υ, Ψ, and Ψ_1 in the form

$$S_{\rm eff}(\Upsilon,\Psi,\Psi_1) = T\int_q\left\{\frac{\Upsilon^2}{2\gamma_3}+\frac{\Psi^2}{2\gamma_1}+\frac{\Psi_1^2}{2\gamma_2} + \ln\left[(\alpha_1+q^2-i\Psi)^2-\Psi_1^2-\Upsilon^2\right]\right\}, \tag{135}$$

where $\int_q = \int\frac{d^2q}{4\pi^2}$.

We analyze $S_{\rm eff}(\Upsilon,\Psi,\Psi_1)$ in the saddle-point approximation by solving the coupled set of saddle-point equations

$$\begin{aligned}
\Upsilon &= 2\gamma_3\int_q\frac{\Upsilon}{(\alpha_+-i\Psi+q^2)^2-(\alpha_-+\Psi_1)^2-\Upsilon^2}, \\
\Psi &= 2\gamma_1\int_q\frac{(\alpha_+-i\Psi+q^2)}{(\alpha_+-i\Psi+q^2)^2-(\alpha_-+\Psi_1)^2-\Upsilon^2}, \\
\Psi_1 &= 2\gamma_2\int_q\frac{(\alpha_-+\Psi_1)}{(\alpha_+-i\Psi+q^2)^2-(\alpha_-+\Psi_1)^2-\Upsilon^2},
\end{aligned} \tag{136}$$

where $\alpha_+ = (\alpha_1+\bar\alpha_2)/2 = a[T-(T_e+T_o)/2] \approx a(T-T_{\rm CDW})$, and $\alpha_- = (\bar\alpha_2-\alpha_1)/2 = (a/2)(T_e-T_o) > 0$.

Our goal is to verify whether a solution with $\Upsilon \neq 0$ emerges before the primary CDW order sets in. In our 2D case, the primary order sets in when $\alpha_+ \to -\infty$, hence, the emergence of $\Upsilon \neq 0$ at any finite α_+ will be a preemptive instability.

Introducing $\Psi = i\Psi_0$, $r_0 = \alpha_+ + \Psi_0$, and $r_1 = \alpha_- + \Psi_1$, we rewrite the last two equations in (136) as

$$\begin{aligned}
r_0 &= \alpha_+ + 2\gamma_1\int_q\frac{r_0}{r_0^2-r_1^2}, \\
r_1 &= \alpha_- + 2\gamma_2\int_q\frac{r_1}{r_0^2-r_1^2}.
\end{aligned} \tag{137}$$

Evaluating the integrals, we obtain

$$\begin{aligned}
r_0 &= \alpha_+ + \frac{\gamma_1}{2\pi}\ln\frac{\Lambda}{\sqrt{r_0^2-r_1^2}}, \\
r_1 &= \alpha_- + \frac{\gamma_2}{2\pi}\coth^{-1}\left(\frac{r_0}{r_1}\right)
\end{aligned} \tag{138}$$

($\coth^{-1}x$ is arc-hyperbolic-cotangent of x).

The primary fields Δ_1^x and Δ_2^x get ordered when $r_0^2-r_1^2$ becomes equal to zero. We see from (137) that this only happens at $\alpha_+ = -\infty$. This is specific to $d=2$ and to systems with $M \geqslant 3$ components, as we already discussed.

At high temperatures $T \gg T_{\rm CDW}$, $\alpha_1 \approx \alpha_2 > 0$, hence, $\alpha_+ \gg \alpha_- > 0$. In this range, the physically meaningful

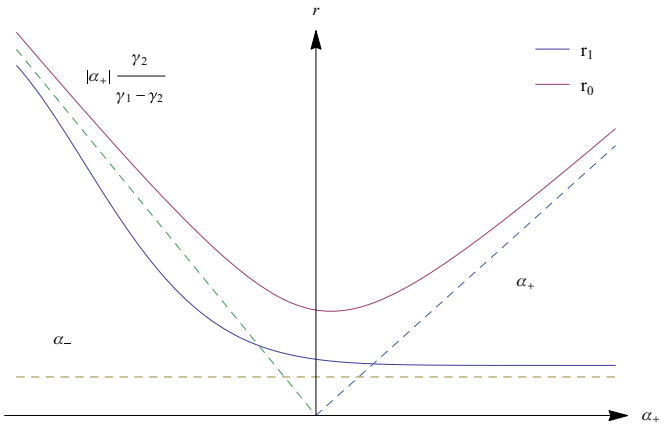

FIG. 16. (Color online) The behavior of r_1 and r_0 as a function of α_+.

solution of (138) is $r_0 \approx \alpha_+$, $r_1 \approx \alpha_-$. As temperature decreases, α_+ and r_0 decrease, while r_1 increases. Still, according to the first equation in (138), r_0 remains larger than r_1. Eventually, α_+ changes sign and becomes negative. The quantities r_0 and r_1 evolve as shown in Fig. 16. At finite but large negative α_+, r_0 and r_1 are both large and Eqs. (138) simplify to

$$r_0 = \alpha_+ + \frac{\gamma_1}{2\pi}\ln\frac{\Lambda}{\sqrt{r_0^2 - r_1^2}},$$
$$r_1 = \frac{\gamma_2}{2\pi}\coth^{-1}\left(\frac{r_0}{r_1}\right). \tag{139}$$

From the second equation, we obtain $r_0 = r_1\coth(2\pi r_1/\gamma_2)$. Plugging this back to both sides of the first equation and introducing $\bar{r}_1 = 2\pi r_1/\gamma_2$, we find, at $|\alpha_+| \gg \ln\Lambda$,

$$\bar{r}_1\coth\bar{r}_1 + \frac{\gamma_1}{\gamma_2}\ln\frac{\bar{r}_1}{\sinh\bar{r}_1} = \frac{2\pi}{\gamma_2}\alpha_+. \tag{140}$$

Solving this equation, we obtain

$$r_1 \approx |\alpha_+|\frac{\gamma_2}{\gamma_1-\gamma_2}. \tag{141}$$

Note that because r_0 and r_1 are close to each other at large $|\alpha_+|$, the susceptibility of the primary fields $\chi \propto 1/(r_0^2 - r_1^2)$ is strongly enhanced. Still, $r_0^2 > r_1^2$, i.e., the primary order does not develop.

We now look at the first equation in (136). Evaluating the integral, we find that the solution with infinitesimally small Υ emerges when

$$\frac{\gamma_3}{2\pi}\coth^{-1}\left(\frac{r_0}{r_1}\right) = r_1. \tag{142}$$

Using the second equation from (138), we rewrite this as the condition on a critical $r_{1,c}$,

$$r_{1,c} = \alpha_-\left(\frac{\gamma_3}{\gamma_3-\gamma_2}\right). \tag{143}$$

This critical $r_{1,c}$ is some positive number because $\alpha_- > 0$ and $\gamma_3 > \gamma_2$ [see Eq. (97), $\gamma_3 > \gamma_2$ is equivalent to $J_{\beta_1}J_{\beta_2} > J_{\beta_3}^2$]. We next use the fact that r_1 monotonically increases as the temperature decreases. Hence, r_1 must reach $r_{1,c}$ at some finite $T = T_t$, and below this temperature the expectation value of Υ becomes nonzero. A nonzero $\Upsilon = \pm\Upsilon_0$ in turn gives rise to a nonzero value of the composite order parameter $\langle\Delta_1^x(\Delta_2^x)^*\rangle \propto \pm i\Upsilon_0$.

In the consideration above, we used the fact that $\alpha_- > 0$, in which case the expectation value of Φ_1 is never zero [see Eq. (136)], and only Υ field acquires a nonzero value due to spontaneous symmetry breaking. In general, $\alpha_- \propto (T_e - T_o)$ is nonzero and positive. However, we found earlier that it is quite small because both T_e and T_o are very close to the original $T_{\rm CDW}$, which, we remind, is a mean-field CDW transition temperature in the "hot spot" approximation, when Δ_1^x and Δ_2^x are equivalent fields. If we set $T_e = T_o = T_{\rm CDW}$, i.e., set $\alpha_- = 0$, we immediately find from (136) that the field Φ_1 can also order only due to symmetry breaking. The self-consistent equations for Φ_1 and Υ now have equivalent kernels, and which of the two acquires a nonzero value depends on the ratio $\gamma_3\gamma_2$. Like we just said, in our case, $\gamma_3 > \gamma_2$, hence Υ field orders under proper conditions, but $\Phi_1 = 0$. In this situation, only the first two equations (136) matter, and solving them we obtain that Υ acquires a nonzero value when the two conditions are met:

$$r_0 = \alpha_+ + \frac{\gamma_3}{2\pi}\ln\frac{\Lambda}{r_0}, \quad 1 = \frac{\gamma_3}{2\pi}\frac{1}{r_0}. \tag{144}$$

Solving this set, we obtain that, like in a more general case, a nonzero Υ emerges at a negative but still finite

$$\alpha_+ = -\frac{\gamma_1}{2\pi}\left(\ln\frac{2\pi\Lambda}{\gamma_3} - \frac{\gamma_3}{\gamma_1}\right). \tag{145}$$

At larger negative α_+, i.e., at smaller T, a nonzero $\Upsilon = \pm\Upsilon_0$ gives rise to a nonzero value of the composite order parameter $\langle\Delta_1^x(\Delta_2^x)^*\rangle \propto \pm i\Upsilon_0$.

When $\gamma_3 = \gamma_2$ or, equivalently, $\beta_3 = \beta_1\beta_2$, the equations for Υ and Φ_1 are identical, and one can immediately make sure that Υ and Φ_1 in (136) can be cast as "real" and "imaginary" components of the "supervector" $\Theta = \sqrt{\Upsilon^2 + \Phi_1^2}e^{i\theta}$. In the HS analysis, the magnitude of Θ becomes nonzero at some finite T, however, neither Υ nor Φ_1 order at any finite T because of fluctuations between the directions of Υ and of Φ_1. In other words, in this situation, there will be no preemptive order which would break Z_2 TR symmetry. This is entirely consistent with the fact that without distinction between different α and β, the effective action decouples between Δ_k^Q and Δ_{-k}^Q, such that both orders appear simultaneously at $T = T_{\rm CDW}$. This last result shows that nonequivalence of β_i terms, namely, the inequality $\beta_1\beta_2 > \beta_3^2$, is the necessary condition for the existence of a preemptive state with composite order which breaks TRS.

3. *Preemptive order for state II*

Before we proceed with the phase diagram, we briefly discuss potential preemptive orders for state II. As we found in the previous section, the CDW transitions into both versions of state II are first order. In this situation, the analysis within the GL model is meaningless. One can still argue, though, that because order parameter manifold in the CDW-ordered state has additional Z_2 component (either Q_x/Q_y or $\pm\pi/2$

for the relative phase between Δ_1 and Δ_2, depending on the realization of state II), there may be a preemptive transition into a state with a composite order parameter. However, to investigate this possibility, one has to go beyond GL expansion in powers of Δ. We will not pursue this issue further.

VII. PHASE DIAGRAM

For the rest of the paper, we focus on state I, for which phase transitions are continuous ones. To construct the phase diagram for state I, we first consider how $T_{\rm CDW}(\xi)$ evolves when hole doping increases and magnetic correlation length decreases. We found that at a finite ξ, the scale $v_F^2\xi^{-2}/\bar{g} \sim \bar{g}/\lambda^2$ serves as the lower-energy cutoff for the logarithm, i.e., T in (16) gets replaced by, roughly, $(T^2 + \bar{g}^2/\lambda^4)^{1/2}$. As the consequence, $T_{\rm CDW}(\xi)$ decreases with increasing ξ and vanishes when $\xi_{\rm cr}^{-1} \sim \bar{g}/v_F$, i.e., when the dimensionless coupling constant $\lambda \sim 1$. We show this behavior in Fig. 17(b). The vanishing of $T_{\rm CDW}(\xi_{\rm cr})$ sets up a charge QCP at some distance away from a magnetic QCP. The temperature T_n at which composite nematic order sets in, and the temperature T_t at which the preemptive TRSB order sets in, also gets smaller as ξ increases. We analyzed the emergence of the composite and CDW orders at $T = 0$ using the same approach as in Ref. [71] [this requires one to include the dynamical term into α_q in Eq. (135)] and found that the three lines T_n, T_t, and $T_{\rm CDW}$ all terminate near the CDW quantum-critical point QCP 2, which actually becomes

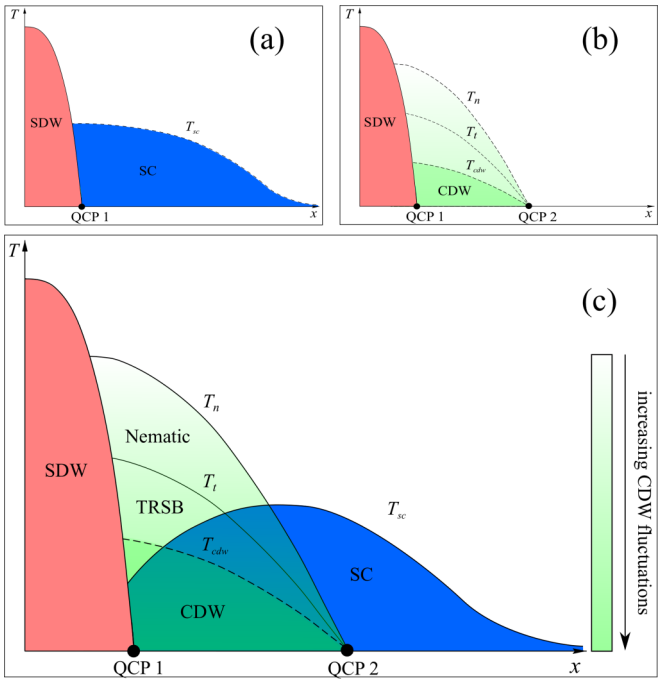

FIG. 17. (Color online) Phase diagram for state I. (a), (b) The behavior of superconducting $T_{\rm SC}$ (a) and the onset temperatures for charge order T_n, T_t, and $T_{\rm CDW}$ (b), when superconductivity and charge order are treated independent of each other. T_n is the preemptive nematic transition temperature, and T_t is the temperature below which a $q = 0$ order emerges, breaking time-reversal symmetry. (c) The full phase diagram, which includes the competition between superconductivity and charge order. $\rm QCP_1$ and $\rm QCP_2$ are quantum-critical points towards SDW and CDW order, respectively.

the point of weak first-order transition [71]. It is possible, although not proven yet, that a preemptive order survives down to $T = 0$, in which case QCP 2 splits into two or even three quantum-critical points. We show the behavior of $T_n(\xi)$, $T_t(\xi)$, and $T_{\rm CDW}(\xi)$ in Fig. 17(b).

The behavior of $T_{\rm CDW}(\xi)$ is different from that of superconducting $T_{\rm SC}(\xi)$. The latter does not vanish at a finite ξ and just interpolates between quantum-critical form $T_{\rm SC} \sim \omega_0$ at large ξ and BCS form $T_{\rm SC} \propto \omega_0 e^{-1/\lambda}$ at smaller ξ, when λ becomes a small parameter. This behavior of superconducting $T_{\rm SC}$ has been studied in Ref. [37] and we also discuss it in detail in Appendix F.

Figures 17(a) and 17(b) show the onset temperatures for superconducting order and for CDW and composite orders, when the CDW and SC are considered independent of each other. In reality, charge and superconducting orders compete for hot fermions on the FS, and the competition implies that the order, which sets up first, tends to suppress the other one. In the spin-fluctuation approach, the value of $T_{\rm SC}$ is larger than $T_{\rm CDW}$, but the two are of the same order and comparable in magnitude. The values of T_n and T_t are larger than $T_{\rm CDW}$, and we assume that at large ξ, we have $T_n, T_t > T_{\rm SC}$, i.e., the composite charge orders set up first upon the lowering of T. The composite order suppresses $T_{\rm SC}$ and gives rise to a nonmonotonic behavior of $T_{\rm SC}(\xi)$ already in the paramagnetic phase. At the same time, it increases the correlation length for the primary CDW order parameter [66], i.e., the composite order tends to increase $T_{\rm CDW}$. At larger ξ, $T_{\rm CDW}$ then well may become larger than the reduced $T_{\rm SC}$, in which case charge order develops prior to superconductivity. At the lowest T, our calculations in Sec. IV show that CDW and superconducting orders coexist. The phase diagram for state I is shown in Fig. 17(c). It has a number of features consistent with the experimental data on hole-doped cuprates. Namely, the theoretical phase diagram contains regions of SDW and d-wave superconductivity, and also a region with a nematic order, a region where time-reversal symmetry is broken, and a region of a true CDW order. The CDW order at $T = 0$ coexists with superconductivity and terminates at a CDW quantum-critical point QCP 2, distinct from the magnetic quantum-critical point QCP 1. It is tempting to associate the T_n line with the onset of nematic order seen in neutron scattering [1–3,5] and in Nernst experiments [102], associate T_t line with the onset temperature for the Kerr effect [6], intra-unit-cell magnetic order [7,8], the magnetoelectric birefringence [9], and associate $T_{\rm CDW}$ with the onset temperature of CDW order [10–13,16–18], perhaps pinned by impurities [14,15]. In our model calculations, the nematic transition temperature T_n is larger than the onset temperature T_t for time-reversal symmetry breaking. In general, the two temperatures are comparable, and the position of T_n and T_t lines on the phase diagram may depend on the type of material.

The association of T_t with these three experiments requires care because, as we said in the Introduction, Kerr effect does not change sign in a magnetic field over 10 T [6] and linear birefringence is often associated with the breaking of a mirror symmetry rather than with breaking of time reversal [9]. To address this issue in more detail, one needs to study 3D systems, particularly the arrangements of the charge currents between neighboring layers.

VIII. COMPARISON WITH ARPES DATA

In this section, we discuss in some detail the comparison between our theory and ARPES data. The data on the fermionic spectral function in the pseudogap region all show [21,77,103–106] that below a certain $T > T_{SC}$, the spectral weight in the antinodal regions transforms from the FS to high frequencies, and the FS looks like a set of four disconnected Fermi arcs. We show in the following that this is an expected behavior for a system with strong CDW fluctuations, but without a true CDW order.

A generic charge order with an ordering momentum Q introduces a new term $H' = \Delta_k^Q c_{k+Q}^\dagger c_{k-Q} + \text{H.c.}$ into the Hamiltonian. Then, fermions with momenta $k \pm Q, k \pm 3Q, k \pm 5Q, \ldots$ all become coupled. For commensurate $Q = \pi M/(N)$, where M and N are integers, the "chain" of coupled momenta gets closed when after N steps, for incommensurate Q it is not closed, but for practical purposes one can approximate Q by a close commensurate value. To diagonalize such a Hamiltonian, one has to solve an N-dimensional matrix equation [64]. The energy eigenstates with eigenvalues $E_1, E_2, \ldots, E_N$ are linear combinations of the original fermions

$$\begin{pmatrix} d_1 \\ d_2 \\ \vdots \\ d_N \end{pmatrix} = \begin{pmatrix} u_{11} & u_{12} & \ldots & u_{1N} \\ u_{21} & u_{22} & \ldots & u_{2N} \\ \vdots & \vdots & \ddots & \vdots \\ u_{N1} & u_{N2} & \ldots & u_{NN} \end{pmatrix} \begin{pmatrix} c_k \\ c_{k-2Q} \\ \vdots \\ c_{k-2(N-1)Q} \end{pmatrix}. \quad (146)$$

The ARPES spectral function measures the correlator of c fermions and contains contributions from all eigenstates, with different weights

$$\begin{aligned} I(\omega,k) &\propto \text{Im}[\langle c_k(\omega) c_k^\dagger(\omega)\rangle] \\ &= \text{Im}\left(\sum_i u_{i1}^2 \langle d_i(\omega) d_i^\dagger(\omega)\rangle\right) \\ &= \text{Im}\left(\sum_i \frac{u_{i1}^2}{\omega - E_i - i\Gamma}\right). \end{aligned} \quad (147)$$

We keep the damping term Γ finite to model the state in which CDW fluctuations are well developed but a true CDW order does not yet occur [107].

We use this procedure to obtain the spectral function $I(\omega,k)$ at $\omega = 0$, as a function of k for "damped" stripe CDW order with either $Q = Q_x$ or $Q = Q_y$. The position of the peak in this spectral function yields the location of the reconstructed FS in the CDW-ordered state, a Γ gives a finite width to the peak. In a macroscopic system, there exist domains with stripes in both directions, and we assume that the measured ARPES intensity is the sum of $I(\omega,k)$ for $Q = Q_x$ and Q_y.

We show our result for the photoemission intensity $I(0,k)$ in Fig. 18. The Fermi arcs, terminating at hot spots, are clearly visible. The actual FS's in the CDW-ordered state indeed cannot terminate inside the BZ, but other pieces of the FS have small spectral weights and are washed out by a finite Γ. In the calculations we used the dispersion from Ref. [21]: $\epsilon(k_x,k_y) = -2t(\cos k_x + \cos k_y) - 4t'(\cos k_x \cos k_y) - 2t''(\cos 2k_x + \cos 2k_y) - 4t'''(\cos 2k_x \cos k_y + \cos k_x \cos 2k_y) - \epsilon_0$, with

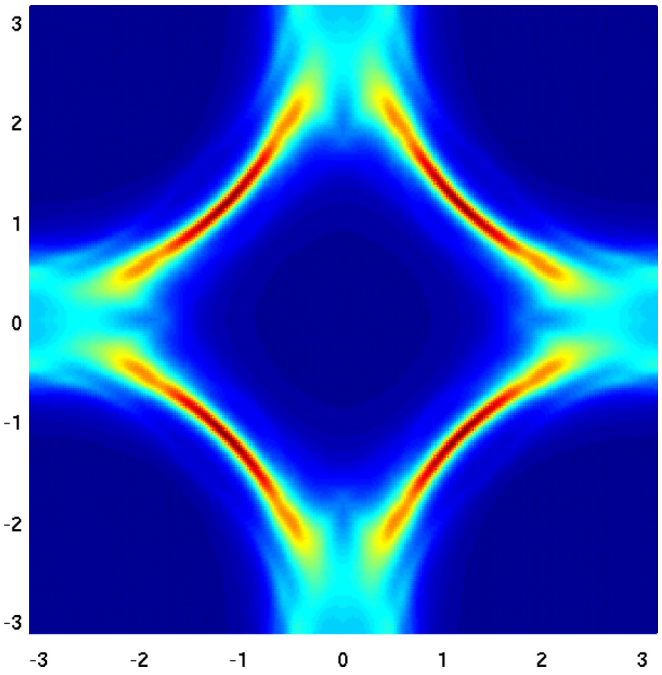

FIG. 18. (Color online) The theoretical spectral function at $\omega = 0$ for a state with strong CDW fluctuations, which we model by introducing CDW orders Δ_x and Δ_y, but keeping a finite lifetime of fermions on the FS. The Fermi arcs, terminating at hot spots, are clearly visible.

$t = 0.22$ eV, $t' = -0.034\,315$ eV, $t'' = 0.035\,977$ eV, $t''' = -0.007\,163\,7$ eV, and we took $\epsilon_0 = -0.243\,27$ eV, slightly different from $-0.240\,577$ eV in [21], to get a commensurate $2Q = 0.2\pi$ instead of $2Q \approx 0.19\pi$ in [21]. We then used $N = 10, M = 1$, and set $\Gamma = 50$ meV.

The appearance of the arcs can be understood analytically. Consider $Q = Q_y$ and focus on the region around hot spot 1 in Fig. 8, with momenta near $(\pi - Q, Q)$. One can easily verify that the most relevant momenta involved in CDW-induced mixing are $(\pi - Q, Q)$ and $(\pi - Q, -Q)$ since for the other momenta in (146), either the gap is smaller or the states are away from the FS. The effective 2×2 Hamiltonian $H = H_0 + H'$ can then be diagonalized by the standard Bogoliubov transformation. Defining $c_1 = c_k$, $c_2 = c_{k-2Q}$, $\epsilon_1 = \epsilon_k, \epsilon_2 = \epsilon_{k-2Q}$, and $\Delta = |\Delta_{k_0}^Q|$, with $k_0 = (\pi - Q, 0)$ we obtain

$$\begin{pmatrix} d_+ \\ d_- \end{pmatrix} = \begin{pmatrix} u & v \\ -v & u \end{pmatrix} \begin{pmatrix} c_1 \\ c_2 \end{pmatrix}, \quad (148)$$

where

$$\begin{aligned} u^2 &= \frac{1}{2}\left[1 + \frac{\epsilon_1 - \epsilon_2}{\sqrt{(\epsilon_1 - \epsilon_2)^2 + 4\Delta^2}}\right], \\ v^2 &= \frac{1}{2}\left[1 - \frac{\epsilon_1 - \epsilon_2}{\sqrt{(\epsilon_1 - \epsilon_2)^2 + 4\Delta^2}}\right]. \end{aligned} \quad (149)$$

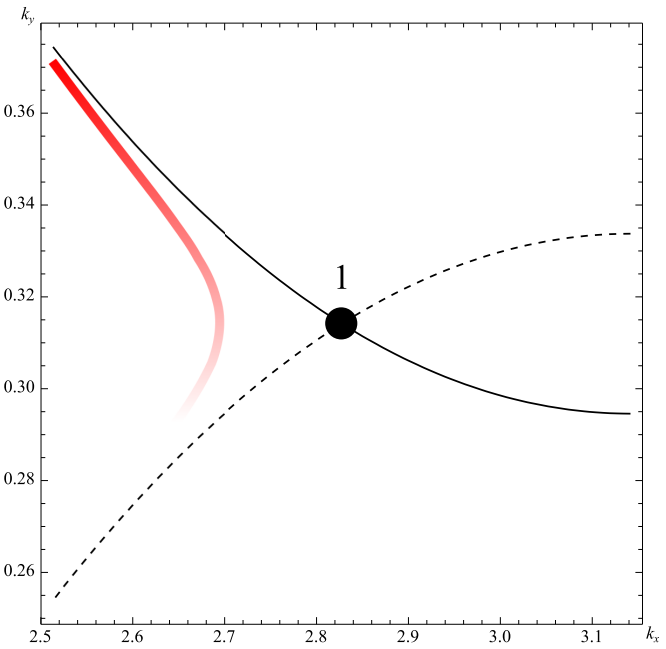

FIG. 19. (Color online) The position of the peak in spectral function at $\omega = 0$ around the hot spot 1 (red line). The saturation of color indicates the spectral weight of the peak. The spectrum to the right of the hot spot 1 is pushed out of BZ boundary by large enough CDW order parameter Δ used in the plot.

The energy eigenvalues are

$$E_{\pm} = \frac{\epsilon_1 + \epsilon_2}{2} \pm \sqrt{\left(\frac{\epsilon_1 - \epsilon_2}{2}\right)^2 + \Delta^2}. \tag{150}$$

The ARPES spectral function at $\omega = 0$ is

$$I(\omega = 0,k) \propto \mathrm{Im}(\langle c_1 c_1^{\dagger}\rangle) = \mathrm{Im}\left(\frac{u^2}{E_+ - i\Gamma} + \frac{v^2}{E_- - i\Gamma}\right). \tag{151}$$

The peaks in the momentum distribution curves are at $E_{\pm} = 0$, which correspond to $\epsilon_1\epsilon_2 = \Delta^2$. This condition defines a hyperbola in the momentum space around the hot spot 1, as shown in Fig. 19. The solid and dashed lines in this figure are the original FS $\epsilon_k = 0$ and the "shadow" FS $\epsilon_{k-2Q} = 0$. At small Δ, there is another part of the FS, to the right of point 1 in this figure, but for large enough Δ, used in the plot, this part is pushed out the BZ boundary. The spectral weight along the red line in Fig. 19 depends on coherence factors and is much larger for the part which is close to the original FS than for the part close to the shadow FS. As a result, the only visible spectral peak at $\omega = 0$ in the momentum space is along the former FS $\epsilon_k = 0$, and it effectively terminates at the hot spot, as in Fig. 19. The contribution from the domain with $Q = Q_x$ is obtained in a similar manner, and the full result is the spectral function with the largest intensity at four Fermi arcs, as in Fig. 18.

The Fermi arcs in the disordered CDW state and the Fermi pocket in the ordered CDW state, whose position and size are consistent with quantum oscillation measurements [19,108], have been recently obtained in the analysis [109], similar to the one we presented here, but extended to the full Brillouin zone (BZ).

We next consider the dispersion along the BZ boundary in the antinodal (AN) regions. Experiments [21] performed on $Pb_{0.55}Bi_{1.5}Sr_{1.6}La_{0.4}CuO_{6+\delta}$ (Pb-Bi2201) have detected two prominent features: (1) upon cooling below about the same temperature where arcs appear, the measured dispersion evolves into a band which comes towards a FS and then moves away from the FS, (2) the momentum, at which the reconstructed dispersion has a minimum, shifts from k_F to a larger value k_G, (3) once the system is further cooled down below T_{SC}, a weak, "shoulderlike" peak appears in the energy distribution curve at the binding energy $\omega \sim 25$ meV. We find that all these features can be accounted for within our theory.

Because the features are at finite energy, we can safely neglect Γ and compute ARPES dispersion assuming a true CDW order. However, we still need to consider two domains: domain I with CDW order with $\mathbf{Q} = Q_y$ and domain II with CDW order with $\mathbf{Q} = Q_x$. For simplicity, we will assume both CDW gaps can be approximated by constants, in which case $\Delta_x = \mu\Delta_y$, with $\mu > 1$. Because the typical energy scale for the fermionic dispersion in the AN region is much smaller than the bandwidth, we again can neglect high-energy electronic states. A simple analysis shows that for low-energy consideration it is sufficient to include three states with momenta $k, k + 2Q_{y,x}, k - 2Q_{y,x}$. We show this in Figs. 20(a) and 20(b).

In domain I, the two states with momenta k and $k + 2Q_y$ cross at a small positive energy $\delta\epsilon$ at $k_x = k_G = Q$, which is larger than the original k_F simply because the distance between the two neighboring hot spots (one on top of the other) is larger than the distance between the two points (k_F,π) and $(-k_F,\pi)$, at which the FS crosses the BZ boundary. The energy of the state with momentum $k - 2Q_y$ is much larger in this region, so we can further reduce the three-state system to a two-state system. The energy eigenvalues at the crossing point are $E_{1,2} = \delta\epsilon \pm \Delta_y$. Once Δ_y exceeds $\delta\epsilon$, one of the energies $E_1 = \delta\epsilon - \Delta_y$ becomes negative, and the corresponding state becomes visible by ARPES. Evaluating $E_1(k_x)$ at different k_x, we find that $E_1(k_x)$ initially follows the original dispersion and moves towards zero, but deviates from the bare dispersion as k_x approaches k_F, passes through a minimum at some finite negative energy, and then moves away from the Fermi level. We show this in Fig. 20(a). The minimum of the reconstructed dispersion is right at $k_G > k_F$, where the two unreconstructed states with momenta k and $k + 2Q_y$ cross. That the minimum of the reconstructed dispersion is at momentum larger than the original k_F is consistent with the experiment [21]. One can easily make sure that the shift of the minimum to $k_G > k_F$ is the consequence of the fact that the momentum of CDW order is along Q_y or Q_x. If the CDW order parameter was with $\mathbf{Q}$ along the zone diagonal, the result would be the opposite: the position of the local minimum would shift to a smaller momentum. This is yet another indication that CDW order does emerge with $\mathbf{Q} = (2Q,0)$ or $(0,2Q)$ rather than with the diagonal $(2Q, \pm 2Q)$. Note in this regard that k_G would remain equal to k_F if the reconstruction of the fermionic dispersion was due to precursors of superconductivity. We used the experimental value of $\delta\epsilon = 5$ meV, and set $\Delta_y = 35$ meV to match the energy of the local minima at k_G at $\omega = 30$ meV, as in [21].

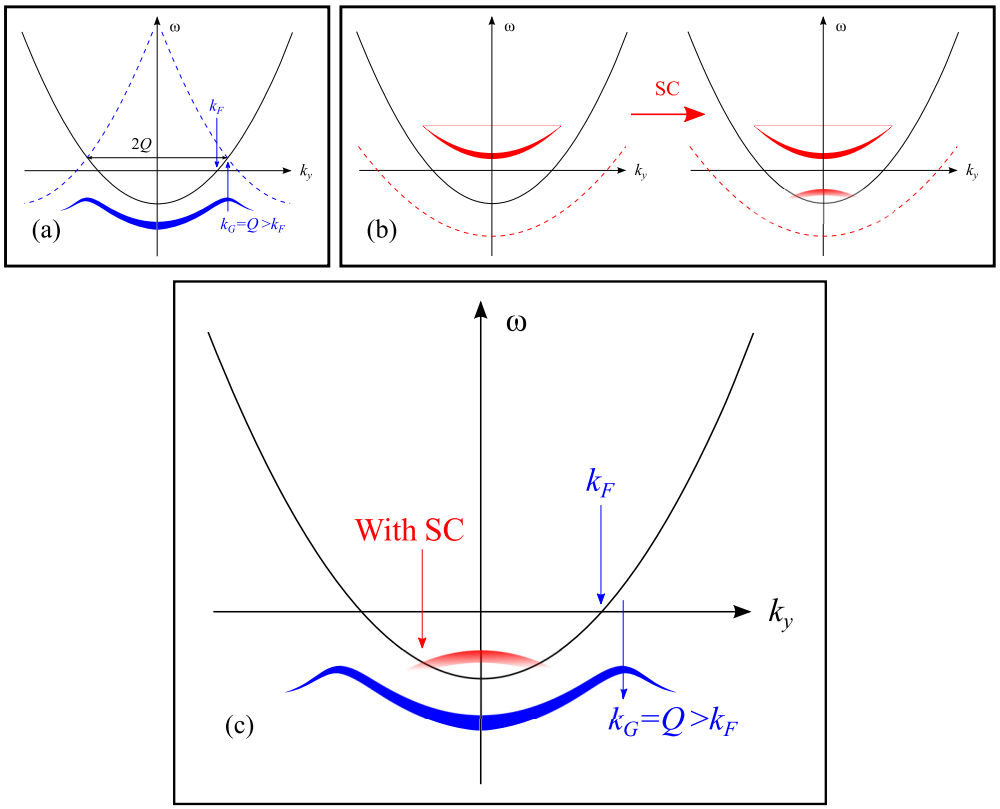

FIG. 20. (Color online) Interpretation of the ARPES data around antinodal areas. (a) Contribution from the domain I with $Q = Q_y$. (b) Contribution from the domain II with $Q = Q_x$. (c) The combined spectral peaks from both domains seen by ARPES.

In domain II, with CDW order with Q_x, two out of three states are degenerate, and we define $\epsilon_{\pi+2Q,k_y} = \epsilon_{\pi-2Q,k_y} \equiv \epsilon_b(k_y)$. We also define $\epsilon_a(k_y) = \epsilon_{\pi,k_y}$. Solving the 3×3 matrix equation on eigenvalues and eigenfunctions, we find that the dominant contribution to the spectral function comes from the peak at $E = E_{11} = (\epsilon_a + \epsilon_b)/2 + \sqrt{[(\epsilon_a - \epsilon_b)/2]^2 + 2\Delta_x^2} > \epsilon_a$. The value of E_{11} is positive for the set of parameters which we used. Because ARPES can only detect filled states, the peak at $E = E_{11} > 0$ is invisible to ARPES. In other words, in the normal state, the full dispersion, measured by ARPES, comes from domain I.

Once superconductivity sets in at T_{SC}, electron and hole states get mixed up, and the system develops a shadow image of E_1 at a negative energy, at $-\sqrt{E_{11}^2 + \Delta_{SC}^2}$. The superconducting gap Δ_{SC} is rather small in Pb-Bi2201, hence the image is approximately at $-E_{11}$. We show this in Fig. 20(b). The emergence of the new band below T_{SC} is again consistent with the experiment [21]. To match the measured position of the new band at around 25 meV, we use experimental values of $\epsilon_a(k_y = 0) = -38$ meV, $\epsilon_b(k_y = 0) = -59$ meV, and set $\Delta_x = 51$ meV, larger than $\Delta_y = 35$ meV. This is consistent with theoretical $\Delta_x = \mu\Delta_y$ and $\mu > 1$. In Fig. 20(c), we show the combined peaks from both domains. This is our theoretical result for the spectral function for comparison with ARPES. In our view, the theoretical spectral function is quite consistent with the data.

The above analysis is valid in the vicinity of hot spots. More efforts are needed to see whether our CDW order is compatible with ARPES along the cuts away from hot regions, particularly near zone diagonals. The data in these regions have been successfully fitted by the theory based on the pair-density-wave scenario [110]. To compare with the data within our CDW scenario, one needs to go beyond what we did so far and to solve for the CDW order parameter outside hot regions. This would require full model calculations on a lattice.

IX. CONCLUSIONS

The goal of this paper was twofold. First, to understand whether the spin-fluctuation approach, which describes d-wave superconductivity and non-Fermi-liquid physics in the normal state, also allows one to understand the development of charge order in hole-doped cuprates. Second, to study the structure of charge order parameter and potential preemptive instabilities which break discrete symmetries but leave a continuous $U(1)$ phase symmetry intact. We argued that a magnetically mediated interaction gives rise to charge order with momenta $Q_x = (2Q,0)$ and $Q_y = (0,2Q)$, as seen in the experiments. The critical temperature for the onset of the charge order T_{CDW} is comparable to superconducting T_{SC} at large values of magnetic correlation length ξ and the ratio T_{CDW}/T_{SC} tends to one at $\xi = \infty$. At the same time, as ξ decreases with increasing doping, the ratio T_{CDW}/T_{SC} decreases, and at some finite doping T_{CDW} vanishes, setting up the second quantum-critical point at some distance away from the magnetic one.

Our most significant observation is that the CDW order parameter Δ_k^Q with a given $\mathbf{Q}$, say Q_y, has two components,

one (Δ_1^Q) is an even function of the center-of-mass momentum k, another (Δ_2^Q), is an odd function of k. In real space, these two components describe, respectively, an incommensurate site and bond density variation $\delta\rho(r) \propto \cos 2Qy$, and an incommensurate current $j_x(r) \propto \sin 2Qy$. We derived and analyzed the full GL functional for four CDW components $\Delta_1^{Q_x}, \Delta_2^{Q_x}, \Delta_1^{Q_y}, \Delta_2^{Q_y}$ first in the mean-field approximation and then beyond mean field. Within mean field, we found two CDW states: state I and state II. Which of the two states is realized depends on the interplay between two system parameters, which are comparable to each other and which we only know approximately. The state I emerges via a continuous transition and is of stripe type: nonzero CDW components have either $\mathbf{Q} = Q_x$ or Q_y. Both Δ_1 and Δ_2 are nonzero, and the relative phase between these two $U(1)$ fields is locked at $\pm\pi/2$. The full order parameter manifold for state I is $U(1) \times Z_2 \times Z_2$ where one Z_2 is associated with the choice between Q_x and Q_y, another Z_2 with the choice between $\pi/2$ and $-\pi/2$ for phase locking, and $U(1)$ is the symmetry with respect to the common phase of Δ_1 and Δ_2. To obtain a phase with this order parameter manifold, it was essential to include the center-of-mass momentum dependence of Δ_k^Q for k near the midpoint between neighboring hot spots.

For state II, the CDW order emerges via a strong first-order transition, and in the ordered state $|\Delta_1^{Q_x}| = |\Delta_2^{Q_y}|$ and $|\Delta_1^{Q_y}| = |\Delta_2^{Q_x}|$. There are two realizations of state II and the choice is dictated by the interplay between parameters which become nonequal only due to k dependence of Δ_k^Q. One realization is the checkerboard order (all four Δ's are nonzero and equal by magnitude), another is a stripe state with only two nonzero components, say, $\Delta_1^{Q_x}$ and $\Delta_2^{Q_y}$. For both realizations, the order parameter manifold is $U(1) \times Z_2$, where in the first realization Z_2 is associated with the phase locking at $\pm\pi/2$ between Δ_1 and Δ_2 (same locking for Q_x and Q_y components), and in the second Z_2 is associated with the symmetry between choosing Δ_1 with Q_x or Q_y.

We focused on the state I because it emerges via a continuous transition and analyzed the GL action beyond mean field. Our goal was to understand whether the two Z_2 Ising symmetries can be broken at higher temperatures than T_{CDW} at which $U(1)$ symmetry gets broken. We used the HS approach, introduced composite fields conjugated to composite order parameters, which order if the corresponding Z_2 symmetry gets broken, integrated over the primary Δ fields, and analyzed the resulting effective action for the composite fields. We found that each of the Z_2 degrees of freedom gets broken before a true CDW order sets in. We found that at a highest T_n, a nematic order sets in, i.e., the system selects Q_x or Q_y, while $U(1)$ phase symmetry remains intact. Then, at $T_t \leqslant T_n$, another Z_2 symmetry gets broken, and the relative phase between Δ_1 and Δ_2 gets locked at $\pi/2$ or $-\pi/2$, while $U(1)$ symmetry of the common phase of Δ_1 and Δ_2 remains unbroken. In the real-space picture, below T_t both density and current components fluctuate, such that $\langle\delta\rho(r)\rangle = \langle j_x(r)\rangle = 0$, however, their fluctuations are correlated, and $\langle\delta\rho(r) j_x(r)\rangle$ is nonzero. Such an order breaks time-reversal symmetry. Finally, at $T_{\mathrm{CDW}} < T_t$, $U(1)$ symmetry gets broken and a true CDW order sets in.

The existence of the preemptive order is the crucial element in our scenario. Without it, CDW instability would be subleading to d-wave superconductivity and also to bond order with diagonal $\mathbf{Q}_d = (2Q, \pm 2Q)$ as in the mean-field approximation both have slightly larger onset temperatures than T_{CDW} ($T_{\mathrm{SC}} \geqslant T_{\mathrm{bo}} \geqslant T_{\mathrm{CDW}}$). However, the superconducting order parameter and order parameter for bond charge order do not break C_4 lattice rotational symmetry and have only one, even in k, component. Accordingly, there are no preemptive instabilities for these orders. Because T_{SC}, T_{bo}, and T_{CDW} are close to each other at large ξ and $T_n, T_t > T_{\mathrm{CDW}}$, it is likely that they also exceed T_{SC} and T_{bo}, in which case the first instability upon lowering of T is into a state with a composite CDW order. Once composite order forms, it reconstructs fermionic excitations and tends to reduce the onset temperatures for superconductivity/bond order because composite charge order and superconductivity/bond order compete for the FS. At the same time, a composite CDW order increases the susceptibility for the primary CDW fields and hence increases T_{CDW}, much like a spin-nematic order in Fe pnictides increases the Néel temperature of SDW order [66]. An increase of T_n and T_t compared to the onset of superconductivity/bond order becomes even stronger once we include into consideration 2D fluctuation effects because near-degenerate d-wave superconductivity and bond order form a weakly anisotropic $O(4)$ model, in which T_{SC} is strongly reduced by fluctuations from the $O(4)$ manifold.

The phase diagram resulting from our analysis is shown in Fig. 17(c). It has numerous features consistent with the experiments on hole-doped cuprates. We performed a more detailed comparison with ARPES studies and found good quantitative agreement with the data.

Overall, we believe that the most significant result of our theory is that it shows that pseudogap physics can be well understood within the same spin-fermion model which was earlier shown to yield d-wave superconductivity and non-Fermi-liquid physics. We believe that, with our result, the spin-fermion model reemerges as the strong candidate for the theoretical model for the cuprates.

Several issues are not covered by this analysis and are left for further study. One issue is the interplay between our spin-fluctuation scenario and the one based on microscopic analysis of charge fluctuations [28]. Another issue, specific to our model, is to what extent T_{CDW} for a true CDW order and T_n, T_t for preemptive transitions vary between different families of hole-doped cuprates. The third issue is the detailed analysis of the relation between our composite charge order which breaks time-reversal symmetry, and Kerr effect [6] and neutron scattering results from Refs. [7,8]. The fourth issue is the interplay between our incommensurate charge order and incommensurate pair-density-wave (PDW) order discussed in Refs. [75,76,110]. The two orders are "cousins" in the same way as SC and diagonal bond order are. Whether fluctuations between our CDW order and PDW order further complicate the phase diagram remains to be seen.

Note added. Recently, the phenomenological GL model for the PDW order parameter has been considered in a preprint by Agterberg and Kashuap [111]. They introduced two order parameters $\bar{\Delta}_p^{\bar{Q}} = c^\dagger_{p+\bar{Q},\alpha}(i\sigma^y_{\alpha\beta})c^\dagger_{-p+\bar{Q},\beta}$ with $\bar{Q}$ along

X and Y directions in momentum space, and argued that $\bar{\Delta}_p^{\bar{Q}}$ and $\bar{\Delta}_p^{-\bar{Q}}$ are not necessarily the same. The "cousins" CDW and PDW order parameters transform into each other by changing one c into $c^\dagger$ and replacing spin dependence $\delta_{\alpha\beta}$ for CDW into $i\sigma^y_{\alpha\beta}$ for PDW, but *without* changing the momentum. A cousin of our CDW order parameter $\Delta_k^Q = c^\dagger_{k+Q,\alpha}\delta_{\alpha\beta}c_{k-Q,\beta}$ with the center-of-mass momentum k is PDW order $c^\dagger_{k+Q,\alpha}(i\sigma^y_{\alpha\beta})c^\dagger_{k-Q,\beta} \equiv \bar{\Delta}_Q^{\bar{Q}}$ with the total momentum $2\bar{Q} = 2k$. The orders $\bar{\Delta}_p^{\bar{Q}}$ and $\bar{\Delta}_p^{-\bar{Q}}$ are then cousins of our Δ_k^Q and Δ_{-k}^Q, and the nonequivalence of $\bar{\Delta}_p^{\bar{Q}}$ and $\bar{\Delta}_p^{-\bar{Q}}$ explored in [111] is the PDW analog of the nonequivalence between Δ_k^Q and Δ_{-k}^Q, which we explored in this paper. Agterberg and Kashuap also identified an additional Z_2 component of the order parameter manifold, associated with time-reversal symmetry, and argued that Z_2 can be broken at a higher T than the one at which a true PDW order develops.

ACKNOWLEDGMENTS

We thank Ar. Abanov, E. Abrahams, D. Agterberg, H. Alloul, P. Armitage, W. A. Atkinson, D. Basov, E. Berg, G. Blumberg, Ph. Bourges, D. Chowdhury, C. Di Castro, P. Coleman, A. Finkelstein, K. Efetov, R. Fernandes, P. Goswami, M. Greven, M. Grilli, M.-H. Julien, A. Kapitulnik, B. Keimer, S. Kivelson, D. Le Boeuf, P. A. Lee, S. Lederer, D. Maslov, H. Meier, E. Mishchenko, M. Norman, A. Paramekanti, C. Pépin, N. Perkins, D. Pesin, D. Reznik, S. Sachdev, D. Scalapino, J. Schmalian, S. Sebastian, O. Starykh, L. Taillefer, A. Tsvelik, P. Wölfle, and V. Yakovenko for fruitful discussions. The work was supported by the DOE Grant No. DE-FG02-ER46900.

APPENDIX A: GAP EQUATIONS FOR MOMENTUM- AND FREQUENCY-DEPENDENT CDW ORDER PARAMETERS

In this appendix, we present the full linearized equations for the CDW order parameters as integral equations in momentum and frequency. We measure frequency and temperature in units of ω_0: $\Omega_m^* = \Omega_m/\omega_0$, $\Sigma^* = \Sigma/\omega_0$, $T^* = T/\omega_0$, and measure momentum in units of $(\gamma\omega_0)^{1/2} = 3\bar{g}/(2\pi v_F)$: $x^* = x/(\gamma\omega_0)^{1/2}, y^* = y/(\gamma\omega_0)^{1/2}$. We recall that $\omega_0 = 9\bar{g}/(16\pi)[(v_y^2 - v_x^2)/v_F^2]$, where $\bar{g}$ is the spin-fermion coupling. We keep the momentum dependence of $\Delta_k^Q(\Omega_m)$ along the FS and neglect the momentum dependence transverse to the FS. We consider the FS geometry as in Fig. 1 and, to avoid too lengthy formulas, consider the limit $v_x = 0$ when Fermi velocities at hot spots 1 and 2 are antiparallel and the ones at hot spots 3 and 4 are parallel. In this limit, the momentum dependence along the FS is along the x axis for $\Delta_{k_0}^Q$ and along the y axis for $\Delta_{k_\pi}^Q$. Integrating over momentum transverse to the FS, we obtain

$$\Delta^Q_{k_0}(\Omega^*_m,x^*) = -\frac{3T^*}{8}\sum_{|\Omega^*_{m'}|<1}\int_0^\infty dy^*\frac{\Delta^Q_{k_\pi}(\Omega^*_{m'},y^*)}{\sqrt{(y^*)^2+|\Omega^*_m-\Omega^*_{m'}|}}\frac{\left[x^*\mathrm{sgn}(\Omega^*_{m'})+i\left(\sqrt{(y^*)^2+|\Omega^*_m-\Omega^*_{m'}|}+\frac{3}{8}|\tilde{\Sigma}^*(\Omega^*_{m'},y^*)|\right)\right]^2}{\left[(x^*)^2+\left(\sqrt{(y^*)^2+|\Omega^*_m-\Omega^*_{m'}|}+\frac{3}{8}|\tilde{\Sigma}^*(\Omega^*_{m'},y^*)|\right)^2\right]^2}, \tag{A1}$$

$$\Delta^Q_{k_\pi}(\Omega^*_m,y^*) = -T^*\sum_{|\Omega^*_{m'}|<1}\int_0^\infty dx^*\frac{\Delta^Q_{k_0}(\Omega^*_{m'},x^*)}{\sqrt{(x^*)^2+|\Omega^*_m-\Omega^*_{m'}|}}\frac{\sqrt{(x^*)^2+|\Omega^*_m-\Omega^*_{m'}|}+\frac{3}{8}|\tilde{\Sigma}^*(\Omega^*_{m'},x^*)|}{|\tilde{\Sigma}^*(\Omega^*_{m'},x^*)|\left[(y^*)^2+\left(\sqrt{(x^*)^2+|\Omega^*_m-\Omega^*_{m'}|}+\frac{3}{8}|\tilde{\Sigma}^*(\Omega^*_{m'},x^*)|\right)^2\right]}, \tag{A2}$$

where $\tilde{\Sigma}^* = \Omega^*_m + \Sigma^*$ and $G^{-1}(k,\omega) = i\tilde{\Sigma}(k,\omega) - \epsilon_k$. For the self-energy, we obtain

$$\Sigma^*(\Omega^*_{m'},x^*) = T^*\sum_{|\Omega^*_{m'}|<\omega_0}\int_0^\infty dy^*\frac{1}{\sqrt{(y^*)^2+|\Omega_m-\Omega_{m'}|}}\frac{\mathrm{sgn}(\Omega^*_{m'})\left(\sqrt{(y^*)^2+|\Omega_m-\Omega_{m'}|}+\frac{3}{8}|\tilde{\Sigma}^*(\Omega_{m'},y^*)|\right)+ix}{(x^*)^2+\left(\sqrt{(y^*)^2+|\Omega_m-\Omega_{m'}|}+\frac{3}{8}|\tilde{\Sigma}^*(\Omega_{m'},y^*)|\right)^2}. \tag{A3}$$

The ix term numerator is even in $\Omega^*_{m'}$ and renormalizes the Fermi velocity. We follow the standard procedure and incorporate this term into the bare dispersion. The expression for $\Sigma^*(\Omega^*_{m'},y^*)$ is obtained from (A3) by interchanging x^* and y^*.

For large $\Sigma^*(\Omega^*_{m'},x^*) \propto (T\ \ln\xi)^{1/2}$, the dependence on momentum in the self-energy and in the CDW order parameters can be neglected, i.e., $\Delta^Q_{k_0}(\Omega^*_m,x^*) \approx \Delta^Q_{k_0}(\Omega^*_m)$, $\Delta^Q_{k_\pi}(\Omega^*_m,y^*) \approx \Delta^Q_{k_\pi}(\Omega^*_m)$, $\Sigma^*(\Omega^*_{m'},x^*) \approx \Sigma^*(\Omega^*_{m'})$. In this approximation, Eqs. (A1)–(A3) reduce to Eqs. (3)–(5) from the main text. In general, however, the gap equations are integral equations in both momentum and frequency. Moreover, at deviations from hot spots 1 and 2 along the FS, $\Delta^Q_{k_0,x^*}$ acquires an imaginary part, which is also odd in frequency: $\Delta^Q_{k_0}(\Omega^*_m,x^*) = \Delta_{0,a} + i\Delta_{0,b}x^*\mathrm{sgn}\omega$, where $\Delta_{0,a}$ and $\Delta_{0,b}$ are even functions of momentum and frequency. To match this behavior, $\Delta^Q_{k_\pi}$ also acquires an imaginary part, odd in frequency, but at deviations from hot spots 3 and 4 transverse to the FS: $\Delta^Q_{k_\pi}(\Omega^*_m,x^*,y^*) = \Delta_{\pi,a} + i\Delta_{\pi,b}x^*\mathrm{sgn}\omega$, where $\Delta_{\pi,a}$ and $\Delta_{\pi,b}$ are again even functions of momentum and frequency.

In the same approximation, the linearized equation for d-wave superconducting order parameter $\Delta_{\mathrm{SC}}(\Omega^*_m,y^*)$ is

$$\Delta_{\mathrm{SC}}(\Omega^*_m,y^*) = T^*\sum_{|\Omega^*_{m'}|<1}\int_0^\infty dx^*\frac{\Delta_{\mathrm{SC}}(\Omega^*_{m'},x^*)}{\sqrt{(x^*)^2+|\Omega^*_m-\Omega^*_{m'}|}}\frac{\sqrt{(x^*)^2+|\Omega^*_m-\Omega^*_{m'}|}+\frac{3}{8}|\tilde{\Sigma}^*(\Omega^*_{m'},x^*)|}{|\tilde{\Sigma}^*(\Omega^*_{m'},x^*)|\left[(y^*)^2+\left(\sqrt{(x^*)^2+|\Omega^*_m-\Omega^*_{m'}|}+\frac{3}{8}|\tilde{\Sigma}^*(\Omega^*_{m'},x^*)|\right)^2\right]}. \tag{A4}$$

The equation for rescaled gap function $\bar{\Delta}_{SC}(\Omega_m^*) = \Delta_{SC}(\Omega_m^*)/\Sigma^*(\Omega_m^*)$ for the most generic case, when (i) the gap depends on momentum along the FS and (ii) fermionic self-energy is not assumed to be larger than other terms in the pairing kernel, is

$$\bar{\Delta}(\Omega_m^*,x^*) = T^* \sum_{|\Omega_{m'}^*|<1} \int_0^\infty \frac{dy^*}{\sqrt{(y^*)^2+|\Omega_m^*-\Omega_{m'}^*|}} \left[\frac{\bar{\Delta}(\Omega_{m'}^*,y^*)}{|\Omega_{m'}|} - \frac{\bar{\Delta}(\Omega_m^*,x^*)}{\Omega_m}\frac{\Omega_{m'}^*}{|\Omega_{m'}|}\right] \times \frac{\sqrt{(y^*)^2+|\Omega_m^*-\Omega_{m'}^*|}+\frac{3}{8}|\tilde{\Sigma}^*(\Omega_{m'}^*,y^*)|}{\left[(x^*)^2+\left(\sqrt{(y^*)^2+|\Omega_m^*-\Omega_{m'}^*|}+\frac{3}{8}|\tilde{\Sigma}^*(\Omega_{m'}^*,y^*)|\right)^2\right]^2}. \tag{A5}$$

We see that the term with zero bosonic Matsubara does not cancel out completely. However, when $\tilde{\Sigma}^*$ is larger than other terms, the dependence of $\bar{\Delta}(\Omega_m^*,x^*)$ on x^* and of $\bar{\Delta}(\Omega_m^*,y^*)$ on y^* become weak, and Eq. (A5) reduces to Eq. (33) in the main text.

APPENDIX B: EVALUATION OF THE TERMS I_1–I_4

In this appendix, we evaluate the terms I_1–I_4, which we need to decide whether the system develops stripe or checkerboard order. Each I_i is a convolution of four fermionic propagators:

$$\begin{aligned} I_1 &\equiv -\frac{1}{2}\int G_1^2 G_2^2, \\ I_2 &\equiv -\frac{1}{2}\int G_1^2 G_5^2, \\ I_3 &\equiv -\int G_1 G_5^2 G_6, \\ I_4 &\equiv -\int G_1 G_2 G_5 G_6. \end{aligned} \tag{B1}$$

The abbreviations for the Green's function are $G_1 \equiv G[\omega_m,\mathbf{k_1}+(k_x,k_y)]$, etc., where 1,2 and 5,6 label hot spots in Fig. 1. The integrations are performed over running frequency ω_m and momenta k_x and k_y. We use Green's functions for free fermions and expand to linear order near hot spots. The Fermi velocities at relevant hot spots are $\mathbf{v}_{F,\mathbf{k}_1} = (v_x,v_y)$, $\mathbf{v}_{F,\mathbf{k}_2} = (v_x,-v_y)$, $\mathbf{v}_{F,\mathbf{k}_5} = (-v_x,v_y)$, and $\mathbf{v}_{F,\mathbf{k}_6} = (-v_x,-v_y)$.

For I_1 we obtain

$$I_1 = -\frac{T}{2}\sum_m \int_{-\Lambda}^{\Lambda} \frac{dk_x dk_y}{(2\pi)^2}\left[\frac{1}{i\omega_m-(v_x k_x+v_y k_y)}\right]^2 \times \left[\frac{1}{i\omega_m-(v_x k_x-v_y k_y)}\right]^2. \tag{B2}$$

We keep the upper cutoff Λ in the momentum integrals, i.e., integrate over a finite momentum range around hot spots. We will take the limits $v_x \ll v_y$ and $v_x\Lambda \gg T$. The ratio $v_x\Lambda/T$ can, in principle, be arbitrary for $T \sim T_{CDW}$, but is definitely large for $T \to 0$. We will keep $v_x\Lambda \geqslant T$ in our calculations.

Introducing the new parameters

$$x = v_x k_x, \quad y = v_y k_y, \quad \Lambda_x = v_x\Lambda, \quad \Lambda_y = v_y\Lambda \gg \Lambda_x, \tag{B3}$$

we rewrite I_1 as

$$I_1 = -\frac{T}{8\pi^2 v_x v_y}\sum_m \int_{-\Lambda_x}^{\Lambda_x} dx \int_{-\Lambda_y}^{\Lambda_y} dy \left(\frac{1}{y+x-i\omega_m}\right)^2 \times \left(\frac{1}{y-x+i\omega_m}\right)^2. \tag{B4}$$

We separate the y integral $\int_{-\Lambda_y}^{\Lambda_y} dy$ into $I_1 = \int_{-\infty}^{\infty} dy - \int_{|y|>\Lambda_y} dy \equiv I_{1a} - I_{1b}$. For I_{1a} we obtain

$$\begin{aligned} I_{1a} &= -\frac{T}{8\pi^2 v_x v_y}\sum_m \int_{-\Lambda_x}^{\Lambda_x} dx \int_{-\infty}^{\infty} dy \left(\frac{1}{y+x-i\omega_m}\right)^2 \times \left(\frac{1}{y-x+i\omega_m}\right)^2 \\ &= -\frac{iT}{16\pi v_x v_y}\sum_m \mathrm{sgn}(\omega_m)\int_{-\Lambda_x}^{\Lambda_x} dx \left(\frac{1}{x-i\omega_m}\right)^3 \\ &= -\frac{iT}{16\pi v_x v_y}\sum_m \int_{-\Lambda_x}^{\Lambda_x} dx \left(\frac{1}{x-i|\omega_m|}\right)^3 \\ &= -\frac{iT}{32\pi v_x v_y}\sum_m \left[\left(\frac{1}{|\omega_m|+i\Lambda_x}\right)^2 - \left(\frac{1}{|\omega_m|-i\Lambda_x}\right)^2\right] \\ &\approx -\frac{i}{64\pi^2 v_x v_y}\int d\omega \left[\left(\frac{1}{|\omega|+i\Lambda_x}\right)^2 - \left(\frac{1}{|\omega|-i\Lambda_x}\right)^2\right] \\ &= -\frac{1}{16\pi^2 v_x v_y}\frac{1}{\Lambda_x}. \end{aligned} \tag{B5}$$

Note that the original integrand is singular in the infrared, so it is important to keep the temperature *finite* as a regulator of the singularity and set $T \to 0$ only at the very end of calculations. We will use the same procedure for the other integrals.

The contribution to I_1 from $|y| > \Lambda_y$ is

$$\begin{aligned} I_{1b} &= -\frac{T}{8\pi^2 v_x v_y}\sum_m \int_{-\Lambda_x}^{\Lambda_x} dx \int_{|y|>\Lambda_y} dy \left(\frac{1}{y+x-i\omega_m}\right)^2 \times \left(\frac{1}{y-x+i\omega_m}\right)^2 \\ &= -\frac{T\Lambda_x}{2\pi^2 v_x v_y}\sum_m \int_{\Lambda_y}^{\infty} \frac{1}{\left(y^2+\omega_m^2\right)^2} \\ &= -\frac{1}{16\pi^2 v_x v_y}\frac{\Lambda_x}{\Lambda_y^2}. \end{aligned} \tag{B6}$$

In the first line, we used the fact that $\Lambda_y \gg \Lambda_x$. As we see, both contributions are small in $1/\Lambda$. The full result for I_1 is

$$I_1 = -\frac{1}{16\pi^2 v_x v_y}\left(\frac{1}{\Lambda_x} - \frac{\Lambda_x}{\Lambda_y^2}\right) \approx -\frac{1}{16\pi^2 v_x^2 v_y}\frac{1}{\Lambda}. \quad \text{(B7)}$$

For I_2 we have

$$I_2 = -\frac{T}{8\pi^2 v_x v_y}\sum_m \int_{-\Lambda_x}^{\Lambda_x} dx \int_{-\Lambda_y}^{\Lambda_y} dy \left(\frac{1}{x+y-i\omega_m}\right)^2 \times \left(\frac{1}{x-y+i\omega_m}\right)^2. \quad \text{(B8)}$$

We again separate the integral over y as $I_2 = \int_{-\infty}^{\infty} dy - \int_{|y|>\Lambda_y} dy \equiv I_{2a} - I_{2b}$. This time, the integral over y from $-\infty$ to ∞ vanishes because the poles are all located in the same half-plane. The integral I_{2b} also vanishes:

$$\begin{aligned} I_{2b} &= -\frac{T}{8\pi^2 v_x v_y}\sum_m \int_{-\Lambda_x}^{\Lambda_x} dx \int_{|y|>\Lambda_y} dy \left(\frac{1}{x+y-i\omega_m}\right)^2 \times \left(\frac{1}{x-y+i\omega_m}\right)^2 \\ &= -\frac{T\Lambda_x}{4\pi^2 v_x v_y}\sum_m \int_{\Lambda_y}^{\infty}\left[\left(\frac{1}{y-i\omega_m}\right)^4 + \left(\frac{1}{y+i\omega_m}\right)^4\right] \\ &\approx -\frac{\Lambda_x}{8\pi^3 v_x v_y}\int d\omega \int_{\Lambda_y}^{\infty}\left[\left(\frac{1}{y-i\omega}\right)^4 + \left(\frac{1}{y+i\omega}\right)^4\right] \\ &= 0. \end{aligned} \quad \text{(B9)}$$

As a result, $I_2 = 0$.

Now we turn to I_3. We explicitly write it as

$$I_3 = \frac{T}{4\pi^2 v_x v_y}\sum_m \int_{-\Lambda_x}^{\Lambda_x} dx \int_{-\Lambda_y}^{\Lambda_y} dy \left(\frac{1}{x+y-i\omega_m}\right)^2 \times \frac{1}{(x-y)^2+\omega_m^2}. \quad \text{(B10)}$$

As before, we write $I_3 = \int_{-\infty}^{\infty} dy - \int_{|y|>\Lambda_y} dy \equiv I_{3a} - I_{3b}$. We evaluate I_{3a} by extending the integral over y onto the half-plane where the integrand contains a single pole:

$$\begin{aligned} I_{3a} &= \frac{T}{4\pi^2 v_x v_y}\sum_m \int_{-\Lambda_x}^{\Lambda_x} dx \int_{-\infty}^{\infty} dy \left(\frac{1}{x+y-i\omega_m}\right)^2 \times \frac{1}{(x-y)^2+\omega_m^2} \\ &= \frac{T}{16\pi v_x v_y}\sum_m \mathrm{sgn}(\omega_m)\int_{-\Lambda_x}^{\Lambda_x} dx \left(\frac{1}{x-i\omega_m}\right)^2 \frac{1}{\omega_m} \\ &= -\frac{T}{16\pi v_x v_y}\sum_m \mathrm{sgn}(\omega_m)\frac{2\Lambda_x}{\Lambda_x^2+\omega_m^2}\frac{1}{\omega_m} \\ &\approx -\frac{1}{16\pi^2 v_x v_y}\frac{1}{\Lambda_x}\ln\frac{\omega_0}{T}. \end{aligned} \quad \text{(B11)}$$

We see that I_{3a} is logarithmically singular at $T \to 0$. The other part, I_{3b}, is regular at $T \to 0$. Therefore, to logarithmic accuracy,

$$I_3 \approx -\frac{1}{16\pi^2 v_x^2 v_y}\frac{1}{\Lambda}\ln\frac{\omega_0}{T}. \quad \text{(B12)}$$

Finally, for I_4 we have

$$I_4 = -\frac{T}{4\pi^2 v_x v_y}\sum_m \int_{-\Lambda_x}^{\Lambda_x} dx \int_{-\Lambda_y}^{\Lambda_y} dy \frac{1}{(x+y)^2+\omega_m^2} \times \frac{1}{(x-y)^2+\omega_m^2}. \quad \text{(B13)}$$

The most straightforward way to evaluate this integral is to first extend both x and y integrations to infinite limits and then check how the results change when we restore finite limits of integration. To evaluate the integral in infinite limits, we introduce new variables $a = x + y$ and $b = x - y$ and reexpress I_4 as

$$\begin{aligned} I_4 &\approx -\frac{T}{8\pi^2 v_x v_y}\sum_m \int_{-\infty}^{\infty} da \int_{-\infty}^{\infty} db \frac{1}{a^2+\omega_m^2}\frac{1}{b^2+\omega_m^2} \\ &= -\frac{1}{8 v_x v_y} T\sum_{\omega_m}\frac{1}{\omega_m^2} \\ &= -\frac{1}{32 v_x v_y}\frac{1}{T}. \end{aligned} \quad \text{(B14)}$$

We see that I_4 diverges as $1/T$. The divergence comes from momenta much smaller than Λ, hence, the prefactor for the $1/T$ term does not depend on whether the limits of momentum integration are infinite or finite. Integration in finite limits gives rise to corrections to (B14) of order $\{1 + O[T/(v_x\Lambda)]\}$.

APPENDIX C: ON THE STABILITY OF HS SADDLE POINT IN A COMPLEX PLANE

In the main text, we discussed the stability of the mean-field CDW solution. We used the HS transformation and obtained the effective action in terms of HS collective variables Δ_+ and Δ_-, proportional to the two CDW order parameters $\Delta^Q_{k_0}$ and $\Delta^Q_{k_\pi}$. We found that the saddle-point solution below T_{CDW} is such that one variable is real and another is imaginary. Expanding near the saddle-point solution, we obtained the effective action which contains bilinear combination of fluctuations of Δ_+ and Δ_- with imaginary prefactor. This form of the action persists also if we expand around $\Delta_+ = \Delta_- = 0$ at $T > T_{\mathrm{CDW}}$. The complex form of the action requires extra care when one analyzes the convergence of the Gaussian integrals over fluctuations of Δ_+ and Δ_-.

The same situation with two HS fields emerges in the analysis of a Z_2 spin-nematic order in Fe pnictides [66]. There, the solution of the saddle-point equations for collective nematic variables is again such that one variable is along the real axis and the other is along the imaginary axis. When one expands next the saddle-point solution, one faces the same issue of convergence of Gaussian integrals, taken by shifting one of the variables into a complex plane.

In this appendix, we discuss several generic issues, associated with the expansion near the saddle points in the complex plane and with the accuracy of using saddle-point approximation for HS fields. Specifically, we follow the

suggestion put forward in Ref. [88] and consider the model with no momentum dispersion (formally, in dimension $D = 0$). In this case, the partition function can, in certain limits, be evaluated explicitly with or without HS transformation. We use this fact to demonstrate that the computational procedure, which we used in the main text, yields the results identical to the one which one obtains in a direct integration over the primary fields.

We consider two extensions of the original bosonic model, which allow us to put the calculation of the partition function under control. One is the extension to large N. It is obtained by extending the underlying fermionic model to $N \gg 1$ fermionic flavors (for details see, e.g., Ref. [66]). The net result of such an extension is the appearance of the overall factor of N in the effective action for bosonic variables. Another is the extension to the number of components of the bosonic fields to large M. This gives rise to more complex form of the action as quadratic and quartic terms in bosons change differently. We argue below that the HS transformation is useful in the large-M limit, while at large N it is easier to evaluate the partition function by integrating directly over the original variables, without introducing HS collective variables. To put it differently, large-N and large-M limits are the two examples when one has to take care in choosing the variables whose fluctuations are weak. At large N, fluctuations of the original bosonic fields around the mean-field solution are weak and there is no need to perform the HS transformation. If one does transform to HS fields, one finds that fluctuations of HS fields around their mean-field solution are strong. On the contrary, at large M, fluctuations of the original Bose fields are strong, while fluctuations of the HS fields around their saddle-point values are weak. In this limit, HS transformation and the subsequent saddle-point analysis of the effective action in terms of the HS fields are fully justified.

Which extension better describes the original model is *a priori* unclear and requires complementary analyses [66,68], particularly in the cases when the analysis in terms of HS variables yields a preemptive transition into a state with a composite order. In principle, such a transition may exist only at large enough M and disappear when M is reduced to the original value of order one. At the same time, we are not aware of the examples when a composite order, detected in the model, extended to large M, does not exist in the original model with $M = O(1)$.

1. Model with one real field

We assume that the HS transformation from the original fermionic variables to collective bosonic variables is already performed and consider the action in terms of bosonic fields. As a warmup, consider the effective action for one real single-component bosonic field Δ:

$$S[\Delta] = \alpha\Delta^2 + \tfrac{1}{2}\Delta^4. \tag{C1}$$

The partition function is

$$I = \frac{1}{\sqrt{\pi}} \int e^{-S[\Delta]} d\Delta. \tag{C2}$$

At a mean-field level, $\langle\Delta\rangle = 0$ at $\alpha > 0$ and $\langle\Delta\rangle = \pm(-\alpha)^{1/2}$ at $\alpha < 0$.

a. Large N

Consider first the extension of the model to large N (large number of flavors of original fermions). This extension adds N as the overall factor to the action [66]

$$S[\Delta] = N\left[\alpha\Delta^2 + \tfrac{1}{2}\Delta^4\right]. \tag{C3}$$

We first compute the partition function directly and by using the HS transformation to composite Bose fields.

For $\alpha > 0$ and $\alpha^2 N \gg 1$, the quartic term can be neglected and we immediately obtain

$$I = \frac{1}{\sqrt{N\alpha}}, \quad \alpha > 0. \tag{C4}$$

For $\alpha < 0$ and $N\alpha^2 \gg 1$, we expand near $\Delta = \pm(-\alpha)^{1/2} = (|\alpha|)^{1/2}$ and after simple integration obtain

$$I = 2\frac{e^{\frac{N\alpha^2}{2}}}{\sqrt{2N|\alpha|}}, \quad \alpha < 0 \tag{C5}$$

(the overall factor 2 comes from summing up contributions from positive and negative Δ). The crossover between the two results for I occurs in the range $N\alpha^2 \leqslant 1$. In this range, more accurate analysis is needed to compute the partition function.

We now use the HS transformation

$$e^{-N\Delta^4/2} = \frac{1}{\sqrt{2\pi N}} \int d\psi\, e^{-\frac{\psi^2}{2N}} e^{i\psi\Delta^2}. \tag{C6}$$

Substituting this into (C2) and integrating over Δ, we obtain

$$I = \frac{1}{2\pi} \int d\psi\, e^{-S_{\rm eff}[\psi]},$$
$$S_{\rm eff}[\psi] = \frac{1}{2}\ln(\alpha + i\psi) + \frac{N\psi^2}{2}. \tag{C7}$$

So far, this is exact (the argument of the log is perfectly well defined for real ψ), and the integration over ψ indeed gives the correct I, as one can easily check. However, the reason we use the HS transformation is that we hope that the integration over the field ψ can be done by expanding around a saddle point. Let us see what we get if we do this.

First, let us obtain the saddle-point solution. Differentiating $S_{\rm eff}[\psi]$ from (C7) over ψ, we obtain

$$N\psi = \frac{i}{2}\frac{1}{\alpha - i\psi}. \tag{C8}$$

The solution is along the imaginary axis: $-i\psi = \psi_0$. Introducing $\alpha + \psi_0 = r_0$, we reexpress (C8) as

$$r_0 = \alpha + \frac{1}{2Nr_0}. \tag{C9}$$

There are two solutions of this equation. For one, $r_0 > 0$, for the other $r_0 < 0$. At large positive α, ψ_0 is obviously small and hence $r_0 \approx \alpha > 0$. Because r_0 never crosses zero [see (C9)], only the solution with a positive r_0 is physically relevant. We have

$$r_0 = \frac{\alpha}{2} + \sqrt{\frac{\alpha^2}{4} + \frac{1}{2N}}, \quad \psi_0 = -\frac{\alpha}{2} + \sqrt{\frac{\alpha^2}{4} + \frac{1}{2N}}. \tag{C10}$$

Now let us expand around this saddle point. Introducing $\tilde{\psi}$ via $\psi = i\psi_0 + \tilde{\psi}$ and substituting into (C7), we obtain, without

making any approximation,

$$S_{\rm eff}[\psi] = S_0 + N\frac{\tilde\psi^2}{2} + \frac{1}{2}\left[\ln\left(1-\frac{i\tilde\psi}{r_0}\right) + \frac{i\tilde\psi}{r_0}\right], \quad \text{(C11)}$$

where

$$S_0 = N\frac{\psi_0^2}{2} - \frac{1}{2}\ln r_0. \quad \text{(C12)}$$

Then,

$$I = \frac{e^{-\frac{N\psi_0^2}{2}}}{\sqrt{2\pi r_0}}\tilde I, \quad \text{(C13)}$$

where

$$\tilde I = \int_{-\infty}^{\infty} d\tilde\psi\, e^{-\{N\frac{\tilde\psi^2}{2} + \frac{1}{2}[\ln(1-\frac{i\tilde\psi}{r_0}) + \frac{i\tilde\psi}{r_0}]\}}. \quad \text{(C14)}$$

So far, all transformations were exact. Now let us see whether we can treat $\tilde\psi$ as small and expand near the saddle point. Let us start with positive α. At $\alpha > 0$ and $\alpha^2 N \gg 1$ we have $r_0 \approx \alpha$ and $\psi_0 \approx 1/(2\alpha N)$. Expanding in (C14) to second order in $\tilde\psi$, we obtain

$$S_{\rm eff}[\psi] = S_0 + N\frac{\tilde\psi^2}{2}\left(1 + \frac{1}{2N\alpha^2}\right). \quad \text{(C15)}$$

The integral over $\tilde\psi$ in (C14) is perfectly convergent, and evaluating it we obtain

$$I = \frac{1}{\sqrt{N\alpha}}, \quad \alpha > 0 \quad \text{(C16)}$$

which is the same result as in (C4).

For $\alpha < 0$ (and, still, $\alpha^2 N \gg 1$), the situation is more complex as now $\psi_0 \approx |\alpha|$ and $r_0 \approx 1/(2\alpha|N)$. Substituting these forms into (C13), (C14), and rescaling, we find

$$I = \sqrt{\frac{|\alpha|Ne}{\pi}}\, e^{\frac{N\alpha^2}{2}}\bar I, \quad \text{(C17)}$$

where in rescaled variables

$$\bar I = r_0\int_{-\infty}^{\infty} du\, e^{-\frac{u^2}{8\alpha^2 N}} e^{-\frac{1}{2}[\ln(1-iu)+iu]} \quad \text{(C18)}$$

and $u = \tilde\psi/r_0$. The exponent $e^{\frac{N\alpha^2}{2}}$ comes from the saddle point and is the same as in (C5). However, the prefactor cannot be obtained by expanding around the saddle point; we clearly see from (C18) that typical u are of order one, hence, one cannot approximate the logarithmical term in the exponent in (C18) by expanding to order u^2. Rather, one has to evaluate the full integral. This shows that the saddle-point approximation is only partially valid at large N: the exponent in I comes out right, but the prefactor cannot be obtained by expanding near the saddle point to order $\tilde\psi^2$.

The integrand in (C18) converges at $u \to \pm\infty$, and the integral can be easily evaluated by closing the integration contour in the lower half-plane ($u = a - ib, b > 0$). There is a branch cut along negative imaginary axis, at $b > 1$. Integrating over the boundaries of the branch cut we obtain after simple algebra

$$\bar I = -ir_0\int_1^{\infty} db\, e^{-b/2}\left[e^{-\frac{1}{2}(\ln b - 1 - i\pi)} - e^{-\frac{1}{2}(\ln b - 1 + i\pi)}\right]$$
$$= 2r_0\int_1^{\infty}\frac{db\, e^{-b/2}}{\sqrt{b-1}} = 2r_0\sqrt{\frac{2\pi}{e}}. \quad \text{(C19)}$$

Substituting this into (C17) we obtain

$$I = 2\frac{e^{\frac{N\alpha^2}{2}}}{\sqrt{2N|\alpha|}}, \quad \alpha < 0. \quad \text{(C20)}$$

This expression coincides with (C5), as it indeed should.

The message from this analysis is that, at large N, there is no advantage of using the HS transformation and expanding around a saddle point; it is more straightforward to compute I by directly integrating over Δ and expanding around its mean-field solution along the real axis. For $\alpha < 0$, one has to expand around the minimum of $S[\Delta]$ at a nonzero $\Delta = \pm|\alpha|^{1/2}$, and this expansion is controlled by $1/N$. Still, one can get the correct result for I even from HS analysis. The exponent at $\alpha < 0$ comes from the saddle point, but to get the prefactor right one has to do full integration, without expanding to quadratic order in the deviations from the saddle point.

b. Large M

Let us now consider a different extension of Eq. (C1). Suppose that the field Δ has M components, and $M \gg 1$. At large M, it is convenient to rescale the prefactor for the Δ^4 term to 1/M and analyze the action

$$S[\Delta] = \alpha\sum_{i=1}^{M}\Delta_i^2 + \frac{1}{2M}\left(\sum_{i=1}^{M}\Delta_i^2\right)^2. \quad \text{(C21)}$$

The partition function is

$$I = \frac{1}{\pi^{M/2}}\prod_{i=1}^{M}\int d\Delta_i e^{-S[\Delta]}. \quad \text{(C22)}$$

As in the previous section, we compute I in two ways: (i) by directly integrating over Δ_i and (ii) by using HS transformation

We begin with direct computation. Introducing M-dimensional spherical variables, one can rewrite (C22) as

$$I = (A_M/\pi^{M/2})\int_0^{\infty} r^{M-1}dr\, e^{-[\alpha r^2 + r^4/(2M)]}$$
$$= A_M M^{M/2}\int_0^{\infty}\frac{dx}{x}e^{M[\ln x - \alpha x^2 - (1/2)x^4]}, \quad \text{(C23)}$$

where $A_M = 2\pi^{M/2}/\Gamma(M/2)$ is the area of a M-dimensional sphere with unit radius. At large M, $\Gamma(M/2) \approx \sqrt{4\pi/M}(M/2)^{M/2}e^{-M/2}$.

Because of prefactor M in the exponent in (C23), the integral over x can be evaluated by expanding around the minimum of $\ln x - \alpha x^2 - (1/2)x^4$. The position of the minimum is at $x = x_0$, where

$$x_0 = \left[-\frac{\alpha}{2} + \sqrt{\frac{\alpha^2}{2} + 1/2}\right]^{1/2}. \quad \text{(C24)}$$

Introducing $x = x_0 + \tilde{x}$ and expanding around the saddle point, we obtain perfectly convergent integral over $\tilde{x}$ with M in the exponent, which justifies the expansion. Evaluating the integral over δx and adding the contribution from the saddle point, we obtain

$$I = e^{M(S_0+\frac{1+\ln 2}{2})}\frac{1}{(\alpha^2+2)^{1/4}(\sqrt{\alpha^2+2}-\alpha)^{1/2}}, \quad \text{(C25)}$$

where $S_0 = \ln x_0 - \alpha x_0^2 - (1/2)x_0^4$. Note that only a portion of the exponential prefactor in (C25) comes from the saddle point, another portion comes from A_M (the area of M-dimensional sphere).

We next evaluate the partition function using the HS transformation. Using a generic formula for $e^{-X^2/2M}$ for real x,

$$e^{-X^2/2M} = \sqrt{\frac{M}{2\pi}}\int d\psi\, e^{-M\frac{\psi^2}{2}} e^{i\psi X}, \quad \text{(C26)}$$

applying it to $X = \sum_{i=1}^{M}|\Delta_i|^2$ and integrating over the components of the Δ field, we obtain

$$I = \sqrt{\frac{M}{2\pi}}\int d\psi\, e^{-M[\frac{\psi^2}{2}+\frac{1}{2}\ln(\alpha - i\psi)]}. \quad \text{(C27)}$$

The saddle point is at $\psi = i\psi_0$, where

$$\psi_0 = -\frac{\alpha}{2} + \sqrt{\frac{\alpha^2}{4}+\frac{1}{2}}. \quad \text{(C28)}$$

As before, we can rewrite the equation for the saddle point as

$$r_0 = \alpha + \frac{1}{2r_0}, \quad \text{(C29)}$$

where $r_0 = \alpha + \psi_0$. This equation formally has two solutions, for one $r_0 > 0$, for the other $r_0 < 0$. However, only the solution with $r_0 > 0$ is meaningful because (i) at large positive α, ψ_0 is small and $r_0 \approx \alpha > 0$ and (ii) r_0 does not change sign as a function of α because $r_0 = 0$ is not a solution of (C29).

Introducing $\psi = i\psi_0 + \tilde{\psi}$ and expanding the exponent around the saddle point we obtain

$$I = \sqrt{\frac{M}{2\pi}}e^{M(\psi_0^2/2-\ln r_0)}\int d\tilde{\psi}\, e^{-M[\frac{\tilde{\psi}^2}{2}(1+1/(2r_0^2))]}. \quad \text{(C30)}$$

The integration is elementary and yields

$$I = \frac{1}{\sqrt{1+\frac{1}{2r_0^2}}}e^{M(\psi_0^2/2-\ln r_0)}. \quad \text{(C31)}$$

Using Eq. (C28) and the fact that $r_0 = \alpha + \psi_0 = \frac{\alpha}{2} + \sqrt{\frac{\alpha^2}{4}+\frac{1}{2}}$, one can easily verify that the expressions for the partition functions obtained directly and using the HS transformation, Eqs. (C25) and (C31), are identical.

The message here is that the partition function in the large-M limit can be computed directly by integrating over the Δ field, but it can also be obtained by using the HS transformation and expanding around the saddle point. This expansion is perfectly well justified at large M and, moreover, the exponent in I in (C31) contains the action taken right at the saddle point. In the direct integration, the exponent in I comes partly from the action at the minimum and partly from A_M.

Note that in both calculations we computed the partition function by expanding around the extremal value of the action (first derivative of the action vanishes). In the direct integration over Δ, the point for which $dS/d\Delta = 0$ is along the real axis, and the integration over fluctuations of Δ is also along the real axis. Within the HS approach, the extremum of the action is along the imaginary axis, and by writing $\psi = i\psi_0 + \tilde{\psi}$ we shift the integration contour into the complex plane. For the one-component model, this is not a dangerous procedure as the only requirement on the integration over $\tilde{\psi}$ in the HS approach is that the integration contour should merge with the real axis at infinite ψ. Still, the agreement between I obtained via the HS transformation and by direct integration over Δ along the real axis tells us that the shift into the complex plane, used in the HS calculation, is a perfectly legitimate procedure. For the one-field case, there is little doubt that this is true, but we will see below that the analogy between direct and HS calculations helps us to justify the integration over HS fields over the contour in the complex plane in a more involved case of two Bose fields.

2. Model with two order parameters

For definiteness, consider the two-field model discussed in Ref. [66] in connection with a preemptive spin-nematic order

$$S[\Delta_1,\Delta_2] = \alpha\left(\Delta_1^2+\Delta_2^2\right) + \frac{1}{2}\left(\Delta_1^2+\Delta_2^2\right)^2 - \frac{\beta}{2}\left(\Delta_1^2-\Delta_2^2\right)^2, \quad \text{(C32)}$$

where $0 < \beta < 1$. As before, we extend the model separately to large N and to large M.

a. Large N

The extension to large N is straightforward; one just has to multiply the effective action in Eq. (C32) by N. We have

$$I = \frac{1}{\pi}\int d\Delta_1\, d\Delta_2\, e^{-NS[\Delta_1,\Delta_2]}. \quad \text{(C33)}$$

We begin with a direct computation of I. Introducing $\Delta_1 = \Delta\cos\varphi, \Delta_2 = \Delta\sin\varphi$, and substituting into (C33), we obtain

$$I = \frac{2}{\pi}\int_0^\infty dx \int_{-\pi/4}^{\pi/4} d\varphi\, e^{[-N(\alpha x + \frac{x^2}{2}(1-\beta\cos^2 2\varphi))]}. \quad \text{(C34)}$$

For $\alpha > 0$ and $\alpha^2 N \gg 1$, the x^2 term in the exponent is irrelevant and we get

$$I = \frac{1}{N\alpha}. \quad \text{(C35)}$$

For negative α and, again, $\alpha^2 N \gg 1$, one can complete the square in the exponential term, introduce $y = x - |\alpha|/(1-\beta\cos^2 2\varphi)$ as a new variable, and integrate over y in infinite limits. This yields

$$I = \frac{4}{\sqrt{2\pi N}}\int_{-\pi/4}^{\pi/4}\frac{d\varphi}{\sqrt{1-\beta\cos^2 2\varphi}}e^{\frac{N\alpha^2}{2(1-\beta\cos^2 2\varphi)}}. \quad \text{(C36)}$$

The exponent has a maximum at $\varphi = 0$. Expanding near the maximum, we obtain

$$I = \frac{2\sqrt{2\pi}}{\sqrt{N(1-\beta)}} e^{\frac{N\alpha^2}{2(1-\beta)}} \int_{-\infty}^{\infty} dz\, e^{-\frac{2N\alpha^2\beta z^2}{(1-\beta)^2}}. \tag{C37}$$

Evaluating then the integral over z, we obtain

$$I = \frac{2}{N|\alpha|}\sqrt{\frac{1-\beta}{\beta}} e^{\frac{N\alpha^2}{2(1-\beta)}}. \tag{C38}$$

Now let us see whether we can reproduce this result using the HS analysis. We use

$$\begin{aligned} e^{-\frac{N\beta}{2}(\Delta_1^2+\Delta_2^2)^2} &= \sqrt{\frac{N}{2\pi\beta}} \int d\psi\, e^{(\frac{-N\psi^2}{2\beta})} e^{iN\psi(\Delta_1^2+\Delta_2^2)}, \\ e^{\frac{N}{2}(\Delta_1^2-\Delta_2^2)^2} &= \sqrt{\frac{N}{2\pi}} \int d\upsilon\, e^{(-\frac{N\upsilon^2}{2\beta})} e^{N\upsilon(\Delta_1^2-\Delta_2^2)}. \end{aligned} \tag{C39}$$

Substituting these integrals into (C33) and integrating over Δ_1 and Δ_2, we obtain

$$I = \frac{1}{2\pi\sqrt{\beta}} \int d\psi\, d\upsilon\, e^{-S_{\rm eff}[\psi,\upsilon]}, \tag{C40}$$

where

$$S_{\rm eff}[\psi,\upsilon] = N\left(\frac{\psi^2}{2} + \frac{\upsilon^2}{2\beta}\right) + \frac{1}{2}\ln\left[(\alpha - i\psi)^2 - \upsilon^2\right]. \tag{C41}$$

The equations on the extremum of the action are

$$\upsilon\left[1 - \frac{\beta}{N}\frac{1}{(\alpha - i\psi)^2 - \upsilon^2}\right] = 0, \quad -i\psi = \frac{1}{N}\frac{\alpha - i\psi}{(\alpha - i\psi)^2 - \upsilon^2}. \tag{C42}$$

One obvious solution is $\upsilon = 0$, $\psi = i\psi_0$, where, as in the previous case,

$$\psi_0 = -\frac{\alpha}{2} + \sqrt{\frac{\alpha^2}{4} + \frac{1}{N}} \tag{C43}$$

and

$$r_0 = \alpha + \psi_0 = \frac{\alpha}{2} + \sqrt{\frac{\alpha^2}{4} + \frac{1}{N}}. \tag{C44}$$

Introducing $\psi = i\psi_0 + \tilde{\psi}$ and expanding around this saddle point, we obtain

$$S_{\rm eff}[\psi,\upsilon] = S_0 + N\frac{\upsilon^2}{2\beta}\left(1 - \frac{\beta}{Nr_0^2}\right) + N\frac{\tilde{\psi}^2}{2}\left(1 + \frac{1}{Nr_0^2}\right), \tag{C45}$$

where

$$S_0 = -\frac{N}{2}\psi_0^2 + \ln r_0. \tag{C46}$$

For $\alpha > 0$ and $\alpha^2 N \gg 1$, $r_0 \approx \alpha$ and $\psi_0 \approx 1/(N\alpha)$. In this case, the saddle point is a minimum along real υ and real $\tilde{\psi}$. The effective action can be approximated by

$$S_{\rm eff}[\psi,\upsilon] \approx \ln\alpha + N\left(\frac{\upsilon^2}{2\beta} + \frac{\tilde{\psi}^2}{2}\right). \tag{C47}$$

Substituting this into the integral for I and integrating over υ and over $\tilde{\psi}$, we obtain

$$I = \frac{1}{N\alpha}, \tag{C48}$$

which coincides with (C36).

For $\alpha < 0$ and $\alpha^2 N \gg 1$, the situation is different. Now $r_0 \approx 1/(N|\alpha|)$ and the prefactor for the υ^2 term in (C45) becomes negative: $1 - \beta/(Nr_0^2) \approx -\beta N\alpha^2 < 0$. This obviously implies that the extremum at $\upsilon = 0$ is a maximum rather than a minimum, and one has to search for a solution of the saddle-point equations with $\upsilon \neq 0$. Such a solution is a "nematic" solution in the current nomenclature, although a true nematic order is indeed impossible in the zero-dimensional case.

The solution of (C42) for $\upsilon = \pm\upsilon_0 \neq 0$ is

$$\begin{aligned} \psi_0 &= \frac{|\alpha|}{1-\beta}, \quad \upsilon_0^2 = \left(\frac{\alpha\beta}{1-\beta}\right)^2 - \frac{\beta}{N}, \\ r_0 &= \alpha + \psi_0 = \frac{|\alpha|\beta}{1-\beta}, \quad r_0^2 - \upsilon_0^2 = \frac{\beta}{N}. \end{aligned} \tag{C49}$$

Such a solution is possible when $\alpha^2 N > (1-\beta)^2/\beta$.

Expanding near ψ_0 and $\pm\upsilon_0$, we obtain

$$I = \frac{1}{\pi\sqrt{\beta}} e^{\frac{N\alpha^2}{2(1-\beta)}} \left(\frac{Ne}{\beta}\right)^{1/2} \tilde{I}, \tag{C50}$$

where

$$\begin{aligned} \tilde{I} = \int_{-\infty}^{\infty} dx \int_{-\infty}^{\infty} dy\, e^{-\frac{N}{2}(\frac{x^2}{\beta}+y^2)} \\ \times e^{-\frac{1}{2}[\ln(1-\frac{2N}{\beta}(iyr_0+x\upsilon_0) - \frac{N(x^2+y^2)}{\beta}) + \frac{2N}{\beta}(iyr_0+x\upsilon_0)]}, \end{aligned} \tag{C51}$$

where $x = \upsilon - \upsilon_0$ and $|x|$ is assumed to be small. As in the case of one field, we cannot expand under the logarithm as typical x and y are such that the argument of the logarithm is of order one. The integrals over x and over y are, however, fully convergent, and the integration can be performed in any order. We notice that the integrand vanishes for all large y in the lower half-plane and integrate over y by closing the contour in the lower half-plane of y. There is again a branch but along the negative imaginary axis of y. Closing the contour such that it does not cross the imaginary axis of y in the range where the branch cut exists, and integrating over y, we obtain, after straightforward algebra,

$$\tilde{I} = 2\frac{(1-\beta)}{|\alpha|N}\left(\frac{2\pi}{e}\right)^{1/2} \int_{-\infty}^{\infty} dx\, e^{-\frac{x^2 N}{2\beta}(1-\beta)}. \tag{C52}$$

In writing (C52) we used the fact along the branch cut $iyr_0 + x\upsilon_0 = O(1/N)$ and $r_0 = \upsilon_0 + O(1/N)$. To leading order in $1/N$, we then have $y^2 \approx -x^2$, such that $x^2/\beta + y^2$ in the exponent in (C51) can be approximated by $x^2(1-\beta)/\beta$. Integrating finally over x in (C52) and substituting the result into (C50), we obtain

$$I = \frac{2}{N|\alpha|}\sqrt{\frac{1-\beta}{\beta}} e^{\frac{N\alpha^2}{2(1-\beta)}}. \tag{C53}$$

This is exactly the same result as Eq. (C38).

Furthermore, one can easily check that the direct calculation and the one using the HS transformation yield the same values of average quantities. In particular, the direct evaluation of

$$Q = \frac{\left|\Delta_1^2 - \Delta_2^2\right|}{\Delta_1^2 + \Delta_2^2} \tag{C54}$$

yields $Q = O(1/N)$ for $\alpha > 0$ and $Q \approx 1 - O(1/N)$ for $\alpha < 0$. In both cases, calculations are under control at $\alpha^2 N \gg 1$. The analysis based on the HS transformation yields the same result. The crossover from small Q to $Q \approx 1$ occurs in a narrow range $\alpha^2 N \leqslant 1$. In principle, one can compute I in this range and obtain the full crossover behavior of Q and related quantities. This, however, requires more computational efforts.

The conclusion of the large-N analysis is that we can reproduce the result for the partition function at large N by using the HS transformation. At $\alpha < 0$, to do so we need to expand near the "nematic" solution $\upsilon = \pm\upsilon_0$. Typical deviations from the saddle-point solution at nonzero υ_0 are small in $1/N$. We cannot expand under the logarithm in (C51) because typical values of the argument are of order one, but the integrand, viewed as a function of $y = \tilde{\psi} = \psi - i\psi_0$, is nicely convergent and can be evaluated using standard means. Once we integrate over y, the remaining integral over $x = \upsilon - \upsilon_0$ is a conventional Gaussian integral with large prefactor N in the exponent. Obviously, typical x^2 are of order $1/N$ and are small.

b. Large M

Let us now extend the original model of two scalar fields to the model of two M-component fields, and take the limit $M \gg 1$. We have

$$S[\Delta_1,\Delta_2] = \alpha \sum_{i=1}^{M} \left(\Delta_{1,i}^2 + \Delta_{2,i}^2\right) + \frac{1}{2M}\left(\sum_{i=1}^{M}\left(\Delta_{1,i}^2 + \Delta_{2,i}^2\right)\right)^2 - \frac{\beta}{2M}\left(\sum_{i=1}^{M}\left(\Delta_{1,i}^2 - \Delta_{2,i}^2\right)\right)^2 \tag{C55}$$

and

$$I = \frac{1}{\pi^M}\prod_{i=1}^{M}\int d\Delta_{1,i} d\Delta_{2,i} e^{-S[\Delta_1,\Delta_2]}. \tag{C56}$$

We again compute I in two ways: directly and via HS transformation. We will see that the HS approach is advantageous because the part of the action associated with the deviations from the saddle point contains large M in the prefactor. At the same time, the action written in terms of $\upsilon - \upsilon_0$ and $\varphi - i\varphi_0$ has a cross term with imaginary coefficient. The validity of the evaluation of the Gaussian integral over fluctuations in this situation has been questioned in Ref. [88]. We will see that the computation of I by direct integration over Δ_1 and Δ_2 is free from such complications as the integrals do not have to be shifted from the real axis. We argue that the way how the Gaussian integration has to be done in the HS approach is set by the necessity to obtain the same I as in the direct calculation. In this respect, the zero-dimensional case is a blessing, as for any $D > 0$ there is no way to check the HS calculation by directly integrating over Δ (the Δ^4 term contains components with four different momenta, subject to momentum conservation).

We begin with the direct calculation of I. Using m-dimensional spherical coordinates for each of the two M-component fields, we rewrite (C56) as

$$I = \frac{A_m^2}{\pi^M}\int_0^\infty d\Delta_1 \int_0^\infty d\Delta_2 \,(\Delta_1\Delta_2)^{M-1}\, e^{-S[\Delta_1,\Delta_2]}, \tag{C57}$$

where, as before, $A_M = 2\pi^{M/2}/\Gamma(M/2)$ is the area of a unit sphere in M dimensions. At large M, $\Gamma(M/2) \approx 2(M/2)^{M/2}e^{-M/2}\sqrt{\pi/M}$.

Introducing

$$\Delta_1 = \sqrt{z}\cos\varphi/2, \quad \Delta_2 = \sqrt{z}\sin\varphi/2, \quad 0 < \varphi < \pi \tag{C58}$$

we reexpress I as

$$I = \frac{A_M^2}{\pi^M 2^{M+1}}\int \frac{dz}{z}\int_0^\pi \frac{d\varphi}{\sin\varphi} e^{M\ln[z\sin\varphi] - \alpha z - \frac{z^2}{2M}(1-\beta\cos^2\varphi)}. \tag{C59}$$

Introducing $z = xM$ and $u = \cos\varphi$, we rewrite Eq. (C59) as

$$I = \frac{A_M^2 M^M}{\pi^M 2^{M+1}}\int \frac{dx}{x}\int_{-1}^{1}\frac{du}{1-u^2} e^{-MS[x,u]}, \tag{C60}$$

where

$$S[x,u] = -\ln x - \frac{1}{2}\ln(1-u^2) + \alpha x + \frac{x^2}{2}(1-\beta u^2). \tag{C61}$$

Because the exponent in (C60) contains an overall factor of M, we search for the extreme of $S[x,u]$ at $x = x_0$ and $u = u_0$. Differentiating over x and over u, we obtain

$$\frac{1}{x_0} - \alpha - x_0\left(1 - \beta u_0^2\right) = 0, \quad u_0\left[\beta x_0^2 - \frac{1}{1-u_0^2}\right] = 0. \tag{C62}$$

The second equation in (C62) has two solutions: $u_{0,1} = 0$ and $u_{0,2}^2 = 1 - 1/(\beta x_0^2)$. For the first solution, we have from the first equation in (C62) $x = x_{0,1}$, where

$$x_{0,1} = -\frac{\alpha}{2} + \sqrt{\frac{\alpha^2}{4} + 1} \tag{C63}$$

(we recall that, by construction, $x > 0$). For the second solution, we have

$$x_{0,2} = -\alpha/(1-\beta) \quad \text{and} \quad u_{0,2}^2 = 1 - \alpha_c^2/\alpha^2, \tag{C64}$$

where $\alpha_c = (1-\beta)/\sqrt{\beta}$. Obviously, the solution with a nonzero $u_{0,2}$ exists only for $\alpha < 0$, when $|\alpha| > \alpha_c$. At the critical value $\alpha = -\alpha_c$, $x_{0,1} = x_{0,2} = 1/\sqrt{\beta}$.

We now expand the action near each of the solutions. Expanding near $u_0 = 0$, $x = x_{0,1}$ we obtain

$$S[x,u] = S[x_{0,1},0] + \frac{u^2}{2}\left(1 - \beta x_{0,1}^2\right) + \frac{1}{2}(x - x_{0,1})^2\left(1 + \frac{1}{x_{0,1}^2}\right). \tag{C65}$$

We see that the prefactor for the $(x - x_{0,1})^2$ term is definitely positive, but the one for the u^2 term may have either sign. The

solution with $u_0 = 0$ is the minimum of the effective action in the region where $\beta x_{0,1}^2 < 1$. An elementary calculation shows that this holds when $\alpha > -\alpha_c$. We checked the second solution for these α and found that it corresponds to the maximum of the action and is therefore irrelevant. Evaluating the Gaussian integrals over u and over $x - x_{0,1}$, we obtain

$$I = \frac{A_M^2 M^{M-1}}{\pi^{M-1} 2^M} \frac{1}{\sqrt{1-\beta x_{0,1}^2}} \frac{1}{\sqrt{1+x_{0,1}^2}}. \tag{C66}$$

The case $\alpha > \alpha_c$ is more interesting for our purposes. Now, the solution with $u_{0,1} = 0$ becomes a maximum with respect to variations of u, and we need to look at another extremal solution $u = \pm u_{0,2} = \pm(1 - \alpha_c^2/\alpha^2)^{1/2}$ and $x = x_{0,2}$. Expanding in $\tilde{u} = u - u_{0,2}$ and $\tilde{x} = x - x_{0,2}$, we obtain

$$S[x,u] = S[x_{0,2},u_{0,2}] + A\tilde{x}^2 + B\tilde{u}^2 - 2C\tilde{x}\tilde{u}, \tag{C67}$$

where

$$\begin{aligned} A &= \frac{1}{2}(1-\beta) + \beta\left(1 - u_{0,2}^2\right), \\ B &= \frac{u_{0,2}^2}{\left(1-u_{0,2}^2\right)^2}, \\ C^2 &= \frac{\beta u_{0,2}^2}{1-u_{0,2}^2}. \end{aligned} \tag{C68}$$

One can immediately make sure that

$$AB - C^2 = \frac{1-\beta}{2} \frac{u_{0,2}^2}{\left(1-u_{0,2}^2\right)^2} > 0. \tag{C69}$$

The integral

$$J = \int d\tilde{x}\, d\tilde{u}\, e^{-M[A\tilde{x}^2 + B\tilde{u}^2 - 2C\tilde{x}\tilde{u}]} \tag{C70}$$

then perfectly converges, no matter in what order we integrate. There is indeed no need to shift the integration contour from the real axis. Integrating in (C70), we obtain

$$J = \frac{\pi}{M} \frac{1}{\sqrt{AB - C^2}}. \tag{C71}$$

Substituting this result into the expression for I and multiplying the result by 2 because there are two extremal points $+u_{0,2}$ and $-u_{0,2}$ and one has to expand near both, we obtain

$$I = \frac{\sqrt{2}}{\beta^{M/2}} e^{\frac{M}{2}\left[\frac{\alpha^2}{1-\beta}+1\right]} \frac{\sqrt{(1-\beta)}}{\sqrt{\alpha^2 - \alpha_c^2}}. \tag{C72}$$

This result is valid as long as $u_{2,0}$ exceed typical $|\tilde{u}|$. The corresponding condition is $\alpha^2 - \alpha_c^2 \geqslant 1/\sqrt{M}$.

We next compute I by applying the HS transformation. The computational steps are the same as at large N, and the expression for I is

$$I = \frac{M}{2\sqrt{\beta}} \int d\psi\, d\upsilon\, e^{-M S_{\rm eff}[\psi,\upsilon]}, \tag{C73}$$

where

$$S_{\rm eff}[\psi,\upsilon] = \frac{\psi^2}{2\beta} + \frac{\upsilon^2}{2} + \frac{1}{2}\ln[(\alpha - i\psi)^2 - \upsilon^2]. \tag{C74}$$

The saddle-point equations have the same form as at large N: $\psi = i\psi_0$ and $\upsilon = \upsilon_0$, where

$$\psi_0 = \frac{\alpha + \psi_0}{(\alpha+\psi_0)^2 - \upsilon_0^2}, \quad \upsilon_0 \left(1 - \frac{\beta}{(\alpha+\psi_0)^2 - \upsilon_0^2}\right) = 0. \tag{C75}$$

One solution is obviously

$$\upsilon_{0,1} = 0, \quad \psi_{0,1} = -\frac{\alpha}{2} + \sqrt{\frac{\alpha^2}{4} + 1}. \tag{C76}$$

The other solution is

$$\upsilon_{0,2}^2 = \frac{\beta^2}{(1-\beta)^2}\left(\alpha^2 - \alpha_c^2\right), \quad \psi_{0,2} = -\frac{\alpha}{1-\beta}, \tag{C77}$$

where $\alpha_c = (1-\beta)/\sqrt{\beta}$ is the same as the one introduced after Eq. (C65). For $\alpha > -\alpha_c$, one can easily show that the solution with $\upsilon_{0,1} = 0$ corresponds to the minimum of $S_{\rm eff}[\psi,\upsilon]$. Expanding near this point and evaluating the (fully convergent) Gaussian integrals over υ and over $\tilde{\psi} = \psi - i\psi_0$, we immediately reproduce Eq. (C66).

For $\alpha < -\alpha_c$, we need to consider the second solution and expand around a nonzero $\upsilon_{0,2}$ and $\psi_{0,2}$. There are two solutions: $+\upsilon_{0,2} = \pm[\beta/(1-\beta)](\alpha^2 - \alpha_c^2)^{1/2}$ and $-\upsilon_{0,2}$. We expand near one of them, say, $+\upsilon_{0,2}$, assume that we are in the region where $(\upsilon - \upsilon_{0,2})^2 \ll \upsilon_{0,2}^2$, and multiply the result by 2. Expanding near $\upsilon_{0,2}$ and $\psi_{0,2}$, we obtain

$$S[\psi,\upsilon] = S[\psi_{0,2},\upsilon_{0,2}] + \bar{A}\tilde{\psi}^2 - \bar{B}\tilde{\upsilon}^2 + 2iC\tilde{\psi}\tilde{\upsilon}, \tag{C78}$$

where

$$\begin{aligned} \bar{A} &= \frac{1}{2}\left(1 + \frac{\beta + 2\upsilon_{0,2}^2}{\beta^2}\right), \quad \bar{B} = \frac{\upsilon_{0,2}^2}{\beta^2}, \\ \bar{C}^2 &= \frac{\upsilon_{0,2}\sqrt{\upsilon_{0,2}^2 + \beta}}{\beta^2}. \end{aligned} \tag{C79}$$

One can immediately make sure that all three prefactors are positive, but now

$$\bar{A}\bar{B} - \bar{C}^2 = -2\frac{(1-\beta)\upsilon_{0,2}^2}{\beta^3} < 0. \tag{C80}$$

The quadratic form (C78) has exactly the same form as the one in our analysis of the stability of the CDW solution [see Eq. (50) in the main text]. Here, however, we have a benchmark: the result for I must agree with Eq. (C72).

We first follow the analysis in the main text and combine the last three terms in the right-hand side of (C78) in the same way as we did there, into

$$\bar{A}\left(\tilde{\psi} + i\frac{\bar{C}}{\bar{A}}\tilde{\upsilon}\right)^2 + \frac{\bar{C}^2 - \bar{A}\bar{B}}{\bar{A}}\tilde{\upsilon}^2. \tag{C81}$$

We then integrate first over $\tilde{\psi}$ by shifting the integration variable by adding an imaginary constant, and then over $\tilde{\upsilon}$. Both integrals are fully convergent, and integrating over $\tilde{\psi}$ and $\tilde{\upsilon}$ and assembling the prefactors, we obtain

$$I = \frac{\sqrt{2}}{\beta^{M/2}} e^{\frac{M}{2}\left[\frac{\alpha^2}{1-\beta}+1\right]} \frac{\sqrt{(1-\beta)}}{\sqrt{\alpha^2 - \alpha_c^2}}. \tag{C82}$$

This is exactly the same result as Eq. (C72). The agreement justifies the integration procedure we used in the main text. Like we said there, we could alternatively integrate over $\tilde{v}$ first by combining the last three terms in the right-hand side of (C78) into

$$-\bar{B}\left(\tilde{v}-i\frac{\bar{C}}{\bar{B}}\tilde{\psi}\right)^2-\frac{\bar{C}^2-\bar{A}\bar{B}}{\bar{B}}\tilde{\psi}^2, \tag{C83}$$

and then integrate over $\tilde{\psi}$. In this integration procedure, both integrals are formally divergent if we integrate in infinite limits. However, as we said in the main text, if we integrate in finite limits and set the limit of integration to infinity only after the integration, we do reproduce the same result as in Eqs. (C72) and (C82).

The conclusion of the large-M analysis is that it is perfectly legitimate to expand near the saddle point in which one variable is along the real axis and the other is along the imaginary axis, and the way to obtain the correct result is to combine variables such that we get two convergent integrals. Here, we explicitly verified this by comparing the answer [Eq. (C82)] with the one obtained by integrating over the real axis, without shifting the contour [Eq. (C72)].

Another way to see that the integration around the saddle point in the HS scheme is noncontroversial is to consider the last three terms in the right-hand side of (C78) as a matrix and evaluate its two eigenvalues. This is a simple exercise, and the result is that both eigenvalues have positive real parts when $\bar{C}^2>\bar{A}\bar{B}$, which implies that Gaussian integrals over fluctuations are convergent.

Indeed, in the zero-dimensional case there is no true nematic order. Still, the analysis in this appendix shows that one can successfully apply the HS procedure and reproduce the exact results for the partition function by integrating in the near vicinity of the saddle point. The key message is that the need to integrate over fluctuations along the contour in the complex plane is not an obstacle; Gaussian integrals over fluctuations near the saddle point nicely converge.

APPENDIX D: AN ALTERNATIVE HS ANALYSIS, WITH SADDLE POINTS ALONG THE REAL AXIS

In Sec. IV B of the main text, we represented the four-fermion interaction in the CDW channel as in Eq. (47), i.e., as

$$H'=\bar{\chi}\left(\bar{\rho}_{k_0}\rho_{k_\pi}+\bar{\rho}_{k_\pi}\rho_{k_0}\right)=\frac{\bar{\chi}}{2}\left(\bar{\rho}_{k_0}+\bar{\rho}_{k_\pi}\right)\left(\rho_{k_0}+\rho_{k_\pi}\right)-\frac{\bar{\chi}}{2}\left(\bar{\rho}_{k_0}-\bar{\rho}_{k_\pi}\right)\left(\rho_{k_0}-\rho_{k_\pi}\right). \tag{D1}$$

In this appendix, we consider a more general representation

$$H'=\bar{\chi}\left(\bar{\rho}_{k_0}\rho_{k_\pi}+\bar{\rho}_{k_\pi}\rho_{k_0}\right)=\frac{\bar{\chi}}{2\sqrt{a_1a_2}}\left(\sqrt{a_2}\bar{\rho}_{k_0}+\sqrt{a_1}\bar{\rho}_{k_\pi}\right)\left(\sqrt{a_2}\rho_{k_0}+\sqrt{a_1}\rho_{k_\pi}\right)-\frac{\bar{\chi}}{2\sqrt{a_1a_2}}\left(\sqrt{a_2}\bar{\rho}_{k_0}-\sqrt{a_1}\bar{\rho}_{k_\pi}\right)\left(\sqrt{a_2}\rho_{k_0}-\sqrt{a_1}\rho_{k_\pi}\right), \tag{D2}$$

in which we initially treat a_1 and a_2 as arbitrary positive parameters. We see that we have two Hermitian interactions: the first one is repulsive and the second is attractive. We now introduce two HS fields Δ' and Δ for these interactions and perform HS transformation. We introduce $\tilde{\chi}\equiv\bar{\chi}/\sqrt{a_1a_2}$, and we use the same identities as Eq. (48):

$$\exp\left(\frac{\tilde{\chi}}{2}\bar{z}_+z_-\right)=\int\frac{d\Delta' d\bar{\Delta}'}{2\pi\tilde{\chi}}\exp\left[-\frac{|\Delta'|^2}{2\tilde{\chi}}+\frac{i}{2}(\Delta' z_+ +\bar{\Delta}'\bar{z}_+)\right],$$
$$\exp\left(\frac{\tilde{\chi}}{2}\bar{z}_-z_-\right)=\int\frac{d\Delta\, d\bar{\Delta}}{2\pi\tilde{\chi}}\exp\left[-\frac{|\Delta|^2}{2\tilde{\chi}}+\frac{1}{2}(\Delta z_- +\bar{\Delta}\bar{z}_-)\right]. \tag{D3}$$

All integrals converge along the real axis. We apply these identities to $z_+=\sqrt{a}_2\rho_{k_0}+\sqrt{a}_1\rho_{k_\pi}$ and $z_-=\sqrt{a}_2\rho_{k_0}-\sqrt{a}_1\rho_{k_\pi}$ and obtain the effective action

$$\begin{aligned}S_{\rm eff}=S_0&+\frac{1}{2\tilde{\chi}}\bar{\Delta}'\Delta'-\frac{i}{2}\bar{\Delta}'\left(\sqrt{a_1}\rho_{k_\pi}+\sqrt{a_2}\rho_{k_0}\right)\\&-\frac{i}{2}\left(\sqrt{a_1}\bar{\rho}_{k_\pi}+\sqrt{a_2}\bar{\rho}_{k_0}\right)\Delta'\\&+\frac{1}{2\tilde{\chi}}\bar{\Delta}\Delta-\frac{1}{2}\bar{\Delta}\left(\sqrt{a_2}\rho_{k_0}-\sqrt{a_1}\rho_{k_\pi}\right)\\&-\frac{1}{2}\left(\sqrt{a_2}\bar{\rho}_{k_0}-\sqrt{a_1}\bar{\rho}_{k_\pi}\right)\Delta,\end{aligned} \tag{D4}$$

where S_0 contains the fermionic part of the action.

1. Fluctuations at $T > T_{\rm CDW}$

Now, let us integrate out the fermions and expand the effective action in powers of Δ and Δ'. To quadratic order in the HS fields we obtain

$$\begin{aligned}S_{\rm eff}[\bar{\Delta}',\Delta',\bar{\Delta},\Delta]=&\frac{1}{2\tilde{\chi}}|\Delta'|^2+\frac{1}{2\tilde{\chi}}|\Delta|^2\\&+\frac{1}{4}(a_1A_2+a_2A_1)(|\Delta'|^2-|\Delta|^2)\\&-\frac{i}{4}(a_2A_1-a_1A_2)(\bar{\Delta}'\Delta+\bar{\Delta}\Delta'),\end{aligned} \tag{D5}$$

where A_1 and A_2 are defined in Eq. (52). We now choose

$$a_1=A_1\quad\text{and}\quad a_2=A_2. \tag{D6}$$

With this choice, the effective action becomes Hermitian and the HS fields Δ and Δ' decouple:

$$\begin{aligned}S_{\rm eff}[\bar{\Delta}',\Delta',\bar{\Delta},\Delta]=&\left(\frac{1}{2\tilde{\chi}}+\frac{A_1A_2}{2}\right)|\Delta'|^2\\&+\left(\frac{1}{2\tilde{\chi}}-\frac{A_1A_2}{2}\right)|\Delta|^2.\end{aligned} \tag{D7}$$

We see that the prefactor for $|\Delta'|^2$ is always positive, i.e., $(\langle\Delta'\rangle)=\langle\tilde{\chi}(\sqrt{A_1}\rho_{k_\pi}+\sqrt{A_2}\rho_{k_0})\rangle=0$. Using this condition,

we find the relation between the average values of ρ_{k_π} and ρ_{k_0}:

$$\mu \equiv -\frac{\langle \Delta_{k_\pi^Q}\rangle}{\langle \Delta^Q_{k_0}\rangle} = -\frac{\langle \chi\rho_{k_\pi}\rangle}{\langle \chi\rho_{k_0}\rangle} = \sqrt{\frac{A_2}{A_1}}. \tag{D8}$$

The prefactor for the $|\Delta|^2$ term becomes negative at $T_{\rm CDW}$, for which, in original parameters,

$$\bar\chi\sqrt{A_1A_2} = 1. \tag{D9}$$

Restoring the frequency and momentum dependence of $\bar\chi$, we find the same CDW instability condition as in Eq. (60). One can easily make sure that Eq. (D8) is also equivalent to the condition on $\langle\Delta_{k_\pi^Q}\rangle/\langle\Delta^Q_{k_0}\rangle$, which we obtained by solving the linearized gap equations (16).

2. Fluctuations at $T < T_{\rm CDW}$

a. Near $T_{\rm CDW}$

Next, suppose that we are at a temperature $T = T_{\rm CDW} - \delta$ and δ is small. In this range, the order parameter $|\Delta|^2 \sim \delta$ is also small, and one can restrict with only fourth-order terms in the expansion in powers of $|\Delta|$. Expanding in $S_{\rm eff}$ we obtain

$$\begin{aligned} &S_{\rm eff}[\bar\Delta',\Delta',\bar\Delta,\Delta] \\ &= \frac{1}{2\tilde\chi}(|\Delta'|^2+|\Delta|^2) + \frac{1}{4}(a_1A_2+a_2A_1)(|\Delta'|^2-|\Delta|^2) \\ &\quad - \frac{1}{16}\big(a_1^2I_2+a_2^2I_1\big)[(\bar\Delta^2-\bar\Delta'^2)(\Delta^2-\Delta'^2) - 4|\Delta|^2|\Delta'|^2] \\ &\quad - \frac{i}{4}(a_2A_1-a_1A_2)(\bar\Delta'\Delta+\bar\Delta\Delta') \\ &\quad + \frac{i}{8}\big(a_2^2I_1-a_1^2I_2\big)[\bar\Delta\bar\Delta'(\Delta^2-\Delta'^2)+(\bar\Delta^2-\bar\Delta'^2)\Delta\Delta']. \end{aligned} \tag{D10}$$

We first find the modified relation between parameters a_1 and a_2, which will keep $\Delta' = 0$ as an extremum of the action and then show that this extremum is a local minimum. The need to modify the a_1/a_2 ratio comes from the fact that in the CDW-ordered state, fourth-order terms bring $O(|\Delta|^2) = O(\delta)$ Gaussian corrections to quadratic terms in Δ' and $\bar\Delta'$. A simple experimentation shows that we need to keep $\Delta' = 0$ as an extremum and we need to choose

$$\frac{a_2}{a_1} = \frac{A_2}{A_1} + \frac{1}{2}\left(|I_2| - \frac{A_2^2}{A_1^2}|I_1|\right)|\Delta|^2. \tag{D11}$$

From the fact that $(\langle\Delta'\rangle) = \langle\tilde\chi(\sqrt{a_1}\rho_{k_\pi} + \sqrt{a_2}\rho_{k_0})\rangle = 0$ we find that

$$\mu^2 \equiv \frac{\langle\tilde\chi\,\rho_{k_\pi}\rangle^2}{\langle\tilde\chi\,\rho_{k_0}\rangle^2} = \frac{A_2}{A_1} + \frac{1}{2}\left(|I_2| - \frac{A_2^2}{A_1^2}|I_1|\right)|\Delta|^2. \tag{D12}$$

One can straightforwardly check that this equation is consistent with Eq. (67).

Next, we verify that $\Delta' = 0$ and $\Delta = O(\sqrt{\delta})$ correspond to a local minimum of the effective action. We write the effective action as

$$\begin{aligned} &S_{\rm eff}[\bar\Delta',\Delta',\bar\Delta,\Delta] \\ &= \left(\frac{1}{\tilde\chi}+a\delta\right)|\Delta'|^2 - a\delta|\Delta|^2 \\ &\quad + \frac{1}{16}\big(A_1^2|I_2| + A_2^2|I_1|\big)[|\Delta'|^4 + |\Delta|^4 \\ &\quad - (\bar\Delta^2\Delta'^2 + \bar\Delta'^2\Delta^2) - 4|\Delta|^2|\Delta'|^2], \end{aligned} \tag{D13}$$

where $a > 0$ is a number of order one. Expanding around

$$\begin{aligned} |\Delta'| &= 0, \\ |\Delta| &= \sqrt{\frac{8\delta}{A_1^2|I_2| + A_2^2|I_1|}}, \end{aligned} \tag{D14}$$

we immediately find that this solution is the local minimum of $S_{\rm eff}$.

If we now neglect the noncritical fields $\bar\Delta'$ and Δ', we obtain the effective action in terms of the order parameter Δ *along the real axis*. The action has the form

$$S_{\rm eff} = \alpha|\Delta|^2 + \beta|\Delta|^4 + \cdots, \tag{D15}$$

where $\alpha = -a\delta = a(T - T_{\rm CDW})$ and $\beta = (1/16)(A_1^2|I_2| + A_2^2|I_1|) > 0$. This agrees with Eq. (69) [we recall that $(1+\lambda)/(1-\lambda) = \sqrt{A_1/A_2}$ in (69)]. If we would not neglect Δ' but rather integrated over it (assuming that fourth-order term $|\Delta'|^4$ is irrelevant), we obtained the same effective action as in (D15) but with slightly modified prefactors.

b. Smaller temperatures, full nonlinear analysis

When δ is not small we can no longer expand in Δ. We go back to the original effective action (D4):

$$S_{\rm eff} = \frac{1}{2\tilde\chi}(|\Delta'|^2+|\Delta|^2) + \Psi_\pi^\dagger\mathcal{G}_\pi^{-1}\Psi_\pi + \Psi_0^\dagger\mathcal{G}_0^{-1}\Psi_0, \tag{D16}$$

where we defined $\Psi_\pi^\dagger = (c^\dagger_{k_\pi+Q}, c^\dagger_{k_\pi-Q})$, $\Psi_0^\dagger = (c^\dagger_{k_0+Q}, c^\dagger_{k_0-Q})$, and

$$\begin{aligned} \mathcal{G}_\pi^{-1} &= \begin{pmatrix} G^{-1}_{k_\pi+Q} & \frac{\sqrt{a_1}}{2}(\bar\Delta + i\bar\Delta') \\ -\frac{\sqrt{a_1}}{2}(\Delta + i\Delta') & G^{-1}_{k_\pi-Q}\end{pmatrix}, \\ \mathcal{G}_0^{-1} &= \begin{pmatrix} G^{-1}_{k_0+Q} & \frac{\sqrt{a_2}}{2}(\bar\Delta - i\bar\Delta') \\ -\frac{\sqrt{a_2}}{2}(\Delta - i\Delta') & G^{-1}_{k_0-Q}\end{pmatrix}. \end{aligned} \tag{D17}$$

Explicitly integrating out fermionic degrees of freedom we obtain

$$\begin{aligned} S_{\rm eff}[\bar\Delta',\Delta',\bar\Delta,\Delta] &= \frac{1}{2\tilde\chi}(|\Delta'|^2+|\Delta|^2) - \ln\left\{G^{-1}_{k_\pi+Q}G^{-1}_{k_\pi-Q}\right. \\ &\quad \left. - \frac{a_1}{4}[|\Delta|^2 - |\Delta'|^2 + i(\bar\Delta\Delta' + \bar\Delta'\Delta)]\right\} \\ &\quad - \ln\left\{G^{-1}_{k_0+Q}G^{-1}_{k_0-Q} - \frac{a_2}{4}[|\Delta|^2 - |\Delta'|^2\right. \\ &\quad \left. - i(\bar\Delta\Delta' + \bar\Delta'\Delta)]\right\}. \end{aligned} \tag{D18}$$

The summations over frequency and momentum are assumed.

As before, we must tune a_1 and a_2 such that $\Delta' = 0$ remains an extremum of the action, and then to show that this extremum is actually a local minimum. First, we differentiate the effective action with respect to $\bar{\Delta}'$, and we find

$$\left.\frac{\partial S_{\rm eff}}{\partial \bar{\Delta}'}\right|_{\Delta'=0} = \frac{ia_1}{4}\sum_{k,\omega}\frac{\Delta}{G^{-1}_{k_\pi+Q}G^{-1}_{k_\pi-Q}-\frac{a_1}{4}|\Delta|^2} - \frac{ia_2}{4}\sum_{k,\omega}\frac{\Delta}{G^{-1}_{k_0+Q}G^{-1}_{k_0-Q}-\frac{a_2}{4}|\Delta|^2} = -\frac{i}{4}(a_1\bar{A}_2 - a_2\bar{A}_1)\Delta, \tag{D19}$$

where in the last line we have defined

$$\bar{A}_2 = \sum_{k,\omega}\frac{1}{-G^{-1}_{k_\pi+Q}G^{-1}_{k_\pi-Q}+\frac{a_1}{4}|\Delta|^2}, \qquad \bar{A}_1 = \sum_{k,\omega}\frac{1}{-G^{-1}_{k_0+Q}G^{-1}_{k_0-Q}+\frac{a_2}{4}|\Delta|^2}. \tag{D20}$$

Diagrammatically, $\bar{A}_1$ and $\bar{A}_2$ are nothing but the polarization bubbles with fully dressed normal and anomalous propagators. Imposing the condition on the extremum of the action, we obtain

$$a_1 = \bar{A}_1 \quad \text{and} \quad a_2 = \bar{A}_2, \tag{D21}$$

which is to be compared with Eq. (C13). Taking the derivative with respect to Δ, we find that the CDW instability sets in when

$$\tilde{\chi}\bar{A}_1\bar{A}_2 = 1. \tag{D22}$$

Next, we show that $\Delta' = 0$ is a local minimum. We define the real and imaginary parts of Δ and Δ' as

$$\Delta = x + iy, \qquad \Delta' = x' + iy'. \tag{D23}$$

Substituting this into the action, we obtain

$$S_{\rm eff}[x,y,x',y'] = \frac{1}{2\tilde{\chi}}(x^2+y^2+x'^2+y'^2) - \ln\left\{G^{-1}_{k_\pi+Q}G^{-1}_{k_\pi-Q} - \frac{\bar{A}_1}{4}[x^2+y^2-x'^2 - y'^2+i(xx'+yy')]\right\} - \ln\left\{G^{-1}_{k_0+Q}G^{-1}_{k_0-Q} - \frac{\bar{A}_2}{4}[x^2+y^2-x'^2 - y'^2+i(xx'+yy')]\right\}. \tag{D24}$$

Differentiating $\mathcal{S}_{\rm eff}$ twice with respect to x' and using Eq. (D22), we obtain

$$\left.\frac{\partial^2 S_{\rm eff}}{\partial x'^2}\right|_{x'=0,\ y'=0} = 2\bar{A}_1\bar{A}_2 - \frac{x^2}{16}\left(\bar{A}_2^2|\bar{I}_1| + \bar{A}_1^2|\bar{I}_2|\right), \tag{D25}$$

where

$$\bar{I}_2 = -\frac{1}{2}\sum_{k,\omega}\frac{1}{\left[-G^{-1}_{k_\pi+Q}G^{-1}_{k_\pi-Q}+\frac{1}{4}\bar{A}_1(x^2+y^2)\right]^2}, \qquad \bar{I}_1 = -\frac{1}{2}\sum_{k,\omega}\frac{1}{\left[-G^{-1}_{k_0+Q}G^{-1}_{k_0-Q}+\frac{1}{4}\bar{A}_2(x^2+y^2)\right]^2}. \tag{D26}$$

These two are given by the same square diagrams from Fig. 7, which we used before, but for the case when CDW order is already developed Evaluating the integrals, we find that $\partial^2 S_{\rm eff}/\partial x'^2$ is positive no matter what x is. The same holds for differentiation over y'. Hence, $\Delta' = 0$ is a local minimum.

The rest of the analysis proceeds the same way as near $T = T_{\rm CDW}$. Namely, if we neglect Δ', the effective action in terms of Δ has a conventional form, and $|\Delta|^2$ increases as T decreases. This still holds even if we perform the Gaussian integration over fluctuations of Δ'.

APPENDIX E: AN ALTERNATIVE METHOD TO GO BEYOND HOT SPOT TREATMENT

In this appendix, we present a complementary approach to go beyond hot spot treatment of the CDW order parameters Δ_1^Q and Δ_2^Q. The conclusion we reach here is the same: Δ_1^Q has a stronger instability. For GL coefficients in Eq. (89), this corresponds to $\alpha_2 > \alpha_1$. In the main text, we assumed that even and odd components of Δ_k^Q behave as $\cos k$ and $\sin k$, respectively, along the direction of the center-of-mass momentum $\mathbf{k}$. Here, we assume a more simple momentum dependence of $\Delta_1^Q(k)$ and $\Delta_2^Q(k)$, namely, assume that the CDW gap is concentrated around antinodal regions, and the even component is a constant and the odd component is a linear dependence on momentum in a hot region:

$$\Delta_1^Q(k) \approx \text{const} = \Delta_1^Q(k_0), \qquad \Delta_2^Q(k) \approx \left|\Delta_2^Q(k_0)\right|\frac{\pi - k_x - k_y}{\pi - k_0}, \tag{E1}$$

where k_0 is the center-of-mass momenta when Δ_k^Q connects two fermions right at hot spots. Obviously, Δ_1^Q and Δ_2^Q are symmetric and antisymmetric about the $(\pi,0)$ point, respectively. We approximate the interaction $\bar{\chi}(\mathbf{k},\mathbf{k}')$ by a constant within some momentum window $\pi - \delta < k'_x - k_x < \pi + \delta$ and $\pi - \delta < k'_y - k_y < \pi + \delta$ and set it to zero outside this window. We then explicitly compute the eigenvalues for even and odd in k solutions and compare them. The two eigenvalues are given by (λ_1 is for even solution)

$$\lambda_1 = \bar{\chi}^2\int_{-\delta}^{\delta}\frac{dp f\left(\epsilon_{k_\pi+p+Q}\right) - f\left(\epsilon_{k_\pi+p-Q}\right)}{\epsilon_{k_\pi+p-Q} - \epsilon_{k_\pi+p+Q}} \times \int_{-\delta}^{\delta}\frac{dq f\left(\epsilon_{k_0+p+q+Q}\right) - f\left(\epsilon_{k_0+p+q-Q}\right)}{\epsilon_{k_0+p+q-Q} - \epsilon_{k_0+p+q+Q}}\frac{\Delta_1^Q(k_0+p+q)}{\Delta_1^Q(k_0)},$$
$$\lambda_2 = \bar{\chi}^2\int_{-\delta}^{\delta}\frac{dp f\left(\epsilon_{k_\pi+p+Q}\right) - f\left(\epsilon_{k_\pi+p-Q}\right)}{\epsilon_{k_\pi+p-Q} - \epsilon_{k_\pi+p+Q}} \times \int_{-\delta}^{\delta}\frac{dq f\left(\epsilon_{k_0+p+q+Q}\right) - f\left(\epsilon_{k_0+p+q-Q}\right)}{\epsilon_{k_0+p+q-Q} - \epsilon_{k_0+p+q+Q}}\frac{\Delta_2^Q(k_0+p+q)}{\Delta_2^Q(k_0)}, \tag{E2}$$

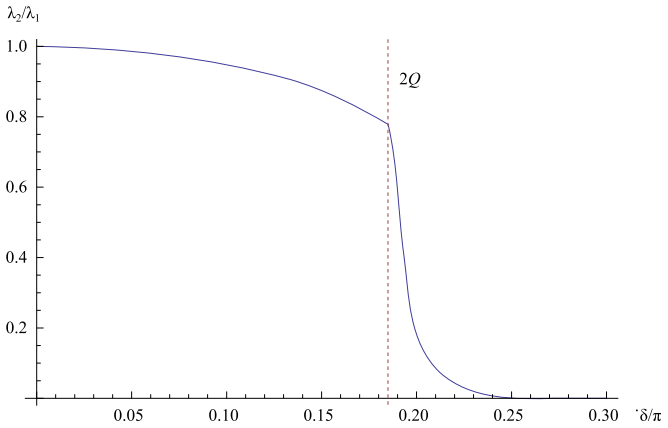

FIG. 21. (Color online) The ratio of the eigenvalues λ_1 and λ_2 for even and odd in k CDW order parameters Δ_1^Q and Δ_2^Q, respectively, as a function as the momentum integration range δ of integration around the hot spots. Note the change of the behavior at $\delta = 2Q$. We set $T = 1$ meV.

where $f(\epsilon)$ is the Fermi function. We set $\mathbf{Q} = Q_y$ and $\mathbf{k}_0 = (\pi - Q,0)$ and evaluated the two integrals numerically using the dispersion relation ϵ_k for $Pb_{0.55}Bi_{1.5}Sr_{1.6}La_{0.4}CuO_{6+\delta}$ (see Ref. [21]). In Fig. 21, we show our results for λ_2/λ_1 as a function of the size of the momentum window δ.

We see from the plot that, as expected, $\lambda_2 < \lambda_1$, i.e., the even solution emerges at a higher T. At the same time, the values of λ_2 and λ_1 are quite close as long as $\delta < 2Q$. That λ_1 is larger, but λ_2 is a close second is consistent with the analysis in the main text and with Refs. [64,65].

APPENDIX F: BOND ORDER WITH DIAGONAL MOMENTA ($\pm 2Q$,$\pm 2Q$)

For completeness and for comparison with our results on CDW order with Q_x or Q_y, we also consider charge order with momenta $\bar{\mathbf{Q}} = (2Q,\pm 2Q)$, as depicted in Fig. 22. A charge order with diagonal momentum has been studied in Refs. [57,58]. The critical temperature for the instability

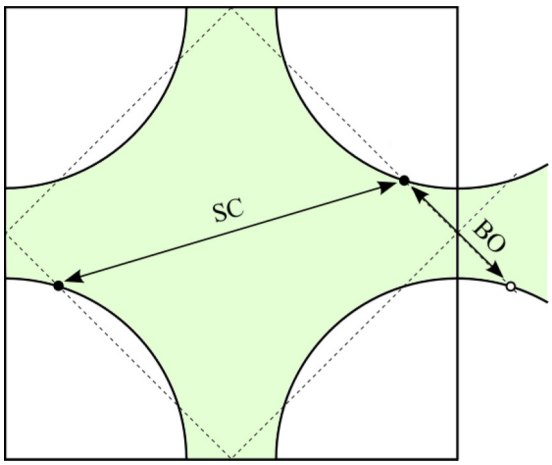

FIG. 22. (Color online) Fermions which contribute to diagonal bond order and d-wave superconducting order. Filled and empty circles denote particle and hole states, respectively.

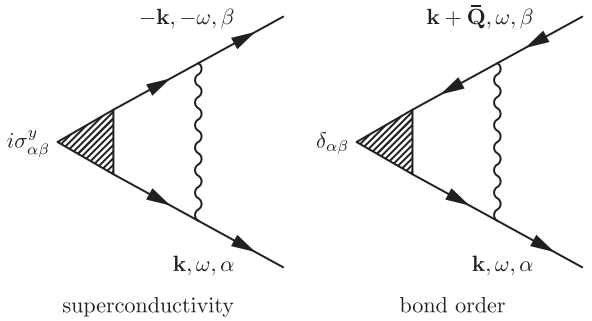

FIG. 23. The diagrammatic expressions for the fully renormalized vertices in superconducting and bond order channels.

towards such order is exactly the same as superconducting T_{SC} if one neglects the curvature of the FS near the hot spots. The gap function for a diagonal charge order has a d-wave structure $\langle c^\dagger(k+\bar{Q})c(k-\bar{Q})\rangle = \Delta(\cos k_x - \cos k_y)$, the same as a d-wave superconducting order parameter. A d-wave charge order does not create a charge-density modulation $\langle c^\dagger(r)c(r)\rangle$, but it introduces modulations of the correlation function between neighboring sites:

$$\langle c^\dagger(\mathbf{r})c(\mathbf{r}+\mathbf{a})\rangle = 2\Delta\cos\bar{\mathbf{Q}}\cdot\left(\mathbf{r}+\frac{\mathbf{a}}{2}\right)(\delta_{\mathbf{a},\mathbf{x}} - \delta_{\mathbf{a},\mathbf{y}}), \quad \text{(F1)}$$

where $\mathbf{x}$ and $\mathbf{y}$ are vectors along x and y directions, in units of interatomic spacing $\mathbf{a}$. A charge order of this kind is called bond order (BO).

To obtain the onset temperature for BO, T_{BO}, and compare it with SC T_{SC} in the presence of FS curvature, we add to the spin-fermion action two infinitesimal vertices $\Phi_0(k)c_{k,\alpha}(i\sigma^y_{\alpha\beta})c_{-k,\beta}$ and $\Psi_0(k)c_{k,\alpha}\delta_{\alpha\beta}c^\dagger_{k+\bar{Q},\beta}$, where k stands for 2+1 momentum $(\omega_m,\mathbf{k})$. These vertices get renormalized by spin-fermion interaction, and the critical temperature (T_{BO} or T_{SC}) is obtained when the corresponding susceptibility diverges, i.e., the solution for fully renormalized $\Phi(k)$ or $\Psi(k)$ exists even when the bare vertices are set to zero.

The authors of [57,58] have demonstrated that a superconducting instability and an instability towards bond order come from the fermions located in the same hot regions, only for bond order one of the regions is shifted by $(2\pi,0)$. The ladder renormalizations of $\Phi_0(k)$ and $\Psi_0(k)$ are shown in in Fig. 23, where the wavy line is the spin-fermion interaction. In analytical form we have, at the corresponding critical temperatures,

$$\Phi(k) = -3\bar{g}\int G(k')G(-k')\chi(k-k')\Phi(k'+\pi),$$
$$\Psi(k) = 3\bar{g}\int G(k')G(k+\bar{Q})\chi(k-k')\Psi(k'+\pi), \quad \text{(F2)}$$

where the spin-fermion coupling $\bar{g}$ and the dynamical spin susceptibility $\chi(k-k')$ are defined in Eqs. (1) and (2) in the main text. The difference in the overall sign in the right-hand side is due to different Pauli algebra: for superconducting vertex $\sigma^i_{\alpha'\alpha}(i\sigma^y_{\alpha\beta})\sigma^i_{\beta\beta'} = -3i\sigma^y_{\alpha'\beta'}$, while for bond vertex $\sigma^i_{\alpha'\alpha}(\delta_{\alpha\beta})\sigma^i_{\beta\beta'} = 3\delta_{\alpha'\beta'}$. One can easily verify [57] that, if one neglects the curvature of the FS, one finds $\epsilon_{k+\bar{Q}} = -\epsilon_k$, and hence $G(-k) = -G(k+\bar{Q})$. In this approximation, the

kernels in the two equations (F2) become identical, hence, $T_{SC} = T_{BO}$. Once the curvature of the FS is included, the degeneracy is lifted and $T_{SC} > T_{BO}$. The reasoning is that superconductivity involves fermions with strictly opposite k, and the momentum integration can still be replaced by the integration over ϵ_k, with a constant prefactor, even in the presence of the FS curvature. For BO, the relation $\epsilon_{k+\bar{Q}} = -\epsilon_k$ no longer holds in the presence of the FS curvature, and this reduces the kernel in the Eq. (F2) for Ψ.

Explicitly, expanding near a hot spot, we obtain

$$\epsilon(k) = -v_F(k_\perp + \tilde{\kappa} k_\parallel^2/k_F), \qquad \epsilon(k+\pi) = v_F(k_\perp - \tilde{\kappa} k_\parallel^2/k_F), \tag{F3}$$

where $k_\parallel$ and $k_\perp$ are momenta parallel and perpendicular to the FS, respectively, and $\tilde{\kappa}$ is a dimensionless parameter characterizing the curvature of the FS. We will use dimensionless parameters

$$\tilde{g} \equiv \frac{\bar{g}}{v_F k_F}, \qquad \tilde{\xi} \equiv \xi k_F, \tag{F4}$$

where ξ is the magnetic correlation length, present in $\chi(k-k')$. The dimensionless coupling $\tilde{g}$, dimensionless correlation length $\tilde{\xi}$, and dimensionless FS curvature $\tilde{\kappa}$ are three input parameters for the consideration in this section. An additional parameter, set by the FS geometry, is the angle between Fermi velocities at hot spots separated by (π,π). To simplify the presentation, we assume that these two velocities are orthogonal to each other.

In this Appendix, we follow earlier works [37,38,57,58,82,85] and assume that the spin-fermion interaction can be well approximated by its value between fermions on the FS. Integrating over momenta transverse to the FS in the fermionic propagators, we obtain integral equations for $\Phi(\omega_m,k_\parallel)$ and $\Psi(\omega_m,k_\parallel)$, which depend on frequency and on momenta along the FS. The equations are

$$\Phi(\omega_m,k_\parallel) = \frac{3\tilde{g}k_F}{2}\int_{m'k'_\parallel} K(\omega_m,k_\parallel,\omega'_m,k'_\parallel;0)\Phi(\omega'_m,k'_\parallel), \tag{F5}$$

$$\Psi(\omega_m,k_\parallel) = \frac{3\tilde{g}k_F}{2}\int_{m'k'_\parallel} K(\omega_m,k_\parallel,\omega'_m,k'_\parallel;\tilde{\kappa})\Psi(\omega'_m,k'_\parallel), \tag{F6}$$

where $\int_{m'k'_\parallel}$ stands for $T\sum_{m'}\int dk'_\parallel/2\pi$ and

$$K(\omega_m,k_\parallel,\omega'_m,k'_\parallel;\tilde{\kappa}) = \frac{|\omega'_m + \Sigma(\omega'_m,k'_\parallel)|}{[\omega'_m + \Sigma(\omega'_m,k'_\parallel)]^2 + v_F^2\tilde{\kappa}^2 k_\parallel'^4/k_F^2}\,\frac{1}{k_\parallel^2 + k_\parallel'^2 + \gamma|\omega_m - \omega'_m| + \tilde{\xi}^{-2}k_F^2}. \tag{F7}$$

1. T_{SC} and T_{BO} at the onset of SDW order $\xi^{-1} = 0$

It is convenient to introduce the set of rescaled variables

$$\bar{T} = \frac{\pi T}{\omega_0}, \quad \bar{\omega}_m = \frac{\omega_m}{\omega_0}, \quad \bar{k}_\parallel = \frac{k_\parallel}{\sqrt{\gamma\omega_0}} \tag{F8}$$

where $\omega_0 = 9\bar{g}/(16\pi) \times [(v_y^2 - v_x^2)/v_F^2]$ was introduced in the main text. In these notations, the linearized gap equation for BO becomes

$$\Psi(\bar{\omega}_m,\bar{k}_\parallel) = \frac{1}{4\pi}\int_{\bar{T}} \frac{d\bar{\omega}_m d\bar{k}'_\parallel}{\bar{k}_\parallel^2 + \bar{k}_\parallel'^2 + |\bar{\omega}_m - \bar{\omega}'_m|} \times \frac{|\bar{\omega}'_m + \bar{\Sigma}(\bar{\omega}'_m,\bar{k}'_\parallel)|}{|\bar{\omega}'_m + \bar{\Sigma}(\bar{\omega}'_m,\bar{k}'_\parallel)|^2 + 16\tilde{g}^2\tilde{\kappa}^2\bar{k}_\parallel'^4/\pi^2}\Psi(\bar{\omega}'_m,\bar{k}'_\parallel), \tag{F9}$$

where the rescaled self-energy is [38,57]

$$\bar{\Sigma}(\bar{\omega}_m,\bar{k}_\parallel) = \sqrt{|\bar{\omega}_m| + \bar{k}_\parallel^2} - |\bar{k}_\parallel|. \tag{F10}$$

We verified, using the same strategy as in our earlier work [61] on superconducting T_{SC} at $\tilde{\xi}^{-1} = 0$, that the leading contribution to the right-hand side of Eq. (F9) comes from the region where $\bar{\Sigma} > \bar{\omega}'_m$ and $\bar{k}_\parallel^2 > \bar{\omega}$. In this region, the momentum dependence of Ψ is more relevant than its frequency dependence. Keeping only the momentum dependence in Ψ and introducing $x = \bar{k}_\parallel^2$ and $y = \bar{k}$, we rewrite (F9) as

$$\Psi(y) = \frac{1}{2\pi}\int_{\bar{T}_{BO}}^{1}\frac{dx}{x+y}\ln\frac{x^2 + 64\tilde{g}^2\tilde{\kappa}^2x^3}{\bar{T}_{BO}^2 + 64\tilde{g}^2\tilde{\kappa}^2x^3}\Psi(x). \tag{F11}$$

For superconductivity, the same procedure yields

$$\Phi(y) = \frac{1}{\pi}\int_{\bar{T}_{SC}}^{1}\frac{dx}{x+y}\ln\frac{x}{\bar{T}_{SC}}\Phi(x). \tag{F12}$$

Comparing Eqs. (F11) and (F12), we find that extra terms in the logarithm in (F11) make it smaller than the logarithm in (F12), hence, in the presence of a FS curvature T_{BO} gets smaller than T_{SC}. Specifically, the curvature term couples to x^3 and provides a soft *upper* cutoff to the integral over x, at $x \sim 1/(\tilde{g}\tilde{\kappa})^2$. At the same time, T_{BO} remains finite, no matter how large κ is. Indeed, at large $\tilde{g}\tilde{\kappa}$ we have $T_{BO} \propto T_{SC}/(\tilde{g}\tilde{\kappa})^2 \ll 1$. In other words, at $\tilde{\xi}^{-1} = 0$, there is no threshold value of $\tilde{\kappa}$ above which BO would not develop.

To check our analytical reasoning, we solved Eqs. (F5) and (F6) numerically and obtained the same result, namely, T_{BO} decreases with increasing $\tilde{\kappa}$ but remains finite. We show the results in Fig. 24. We set $\tilde{g} = 0.1$, $\tilde{\xi} = \infty$, and varied $\tilde{\kappa}$.

2. T_{SC} and T_{BO} at a finite $\tilde{\xi}$

When the system moves away from the magnetic QCP, it eventually recovers a conventional FL behavior in the normal state. Indeed, as the correlation length $\tilde{\xi}$ decreases,

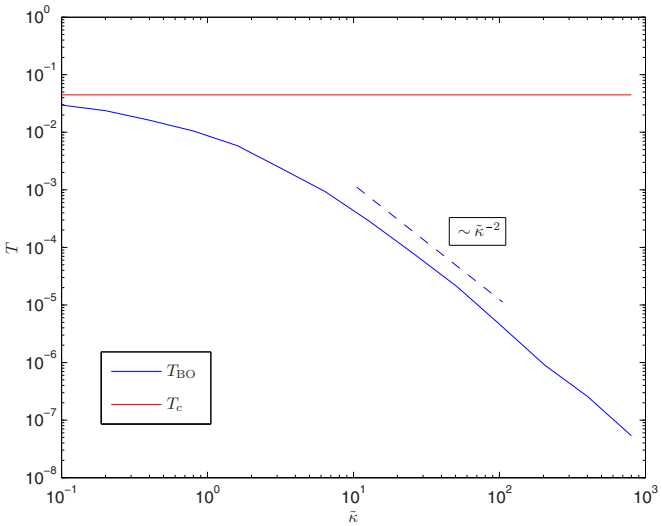

FIG. 24. (Color online) The onset temperatures for SC and BO $T_{\rm SC}$ and $T_{\rm BO}$, respectively, as functions of dimensionless FS curvature $\tilde{\kappa}$ at the onset of SDW order (magnetic $\xi^{-1}=0$). We set $\tilde{g}=0.1$. Superconducting $T_{\rm SC}$ is not affected by the curvature, while $T_{\rm BO}$ decreases but remains finite. In analytical consideration, $T_{\rm BO}/T_{\rm SC}$ was found to scale as $\tilde{\kappa}^{-2}$ at large enough curvature. We show this functional behavior by a dashed line.

$\omega_{\rm sf}=\tilde{\xi}^{-2}k_F^2/\gamma$ becomes the upper energy cutoff for the pairing [38,112]. Below this scale, the spin susceptibility can be treated as frequency independent and the fermionic self-energy is linear in frequency:

$$\begin{aligned}\Sigma(\omega_m,k_\parallel) &= \frac{3\tilde{g}k_F}{2\pi\sqrt{\gamma}}\Big(\sqrt{|\omega_m|+k_\parallel^2/\gamma+\omega_{\rm sf}}\\ &\quad -\sqrt{k_\parallel^2/\gamma+\omega_{\rm sf}}\Big)\mathrm{sgn}(\omega_m)\\ &\approx \frac{3\tilde{g}\tilde{\xi}\sqrt{\omega_{\rm sf}}}{2\pi}\frac{\omega_m}{2\sqrt{\omega_{\rm sf}}}\\ &= \lambda\omega_m. \end{aligned} \tag{F13}$$

In the last line, we have defined $\lambda=\frac{3\tilde{g}\tilde{\xi}}{4\pi}$. Plugging this into Eq. (F5) for superconducting $T_{\rm SC}$ and using the condition that typical $\omega,\omega_m',k_\parallel^2,k_\parallel'^2/\gamma$ are all small in this limit compared to $\omega_{\rm sf}$, we integrate over momentum $k_\parallel'$ and obtain

$$\Phi=\frac{\lambda}{1+\lambda}\ln\frac{\omega_{\rm sf}}{T_{\rm SC}}\Phi. \tag{F14}$$

For superconducting $T_{\rm SC}$ we then have a conventional BCS–McMillan result [113]

$$T_{\rm SC}\sim\omega_{\rm sf}\exp\left(-\frac{1+\lambda}{\lambda}\right). \tag{F15}$$

Hence, as the system moves away from the QCP, it crosses over to a BCS behavior, and $T_{\rm SC}$ gradually decreases as $\tilde{\xi}$ decreases and λ gets smaller.

For BO, the gap equation in the rescaled variables becomes, in this limit,

$$\Psi=\frac{1}{4\pi}\int_{\bar{T}_{\rm BO}}\frac{d\omega_m d\bar{k}_\parallel'}{\bar{k}_\parallel'^2+\tilde{\omega}_{\rm sf}}\frac{(1+\lambda)|\bar{\omega}_m'|}{(1+\lambda)^2|\bar{\omega}_m'|^2+16\tilde{g}^2\tilde{\kappa}^2\bar{k}_\parallel'^4/\pi^2}\Psi, \tag{F16}$$

where we defined

$$\tilde{\omega}_{\rm sf}\equiv\frac{\omega_{\rm sf}}{\omega_0}=(2\lambda)^{-2}. \tag{F17}$$

Typical $\bar{k}_\parallel'^2$ are of order $\tilde{\omega}_{\rm sf}$, and in the second term in the denominator we can safely replace $\bar{k}_\parallel'^4$ by $\tilde{\omega}_{\rm sf}^2$. We see that the curvature $\tilde{\kappa}$ now appears in a combination with a constant term and provides a *lower* cutoff for the BCS-type logarithmic behavior. This is qualitatively different from the behavior at the magnetic QCP, where the curvature was coupled to the running variable x^3. Because of the cutoff, the frequency integral in (F16) no longer diverges at $T=0$. Hence, at some critical $\tilde{\xi}$, the linearized gap equation for the BO vertex Ψ has a solution at $T=0$. Setting $T=0$ in (F16) and integrating over $\bar{k}_\parallel$, we obtain the condition when $T_{\rm BO}=0$:

$$\Psi=\frac{1}{2}\frac{\lambda\Psi}{1+\lambda}\int_{-\omega_{\rm sf}}^{\omega_{\rm sf}}\frac{d\omega|\omega|}{|\omega|^2+16\tilde{g}^2\tilde{\kappa}^2\omega_{\rm sf}^2/\pi^2}. \tag{F18}$$

Canceling out Ψ and integrating over frequency, we find

$$1=\frac{\lambda}{1+\lambda}\left(\ln\frac{\pi}{4\tilde{g}\tilde{\kappa}}\right). \tag{F19}$$

This defines a critical $\tilde{\xi}$ at which BO vanishes:

$$\tilde{\xi}_{\rm cr}^{-1}\sim\tilde{g}\ln\left(\frac{\pi}{4\tilde{g}\tilde{\kappa}}\right). \tag{F20}$$

At smaller $\tilde{\xi}<\tilde{\xi}_{\rm cr}$, the equation on Ψ only allows a trivial solution $\Psi=0$, hence, BO does not develop at any T. To verify this, we solved for $T_{\rm SC}$ and $T_{\rm BO}$ numerically. We set $\tilde{g}=0.1$ and $\tilde{\kappa}=0.14$ and varied $\tilde{\xi}$. We found that superconducting $T_{\rm SC}$ crosses over to BCS behavior at small enough $\tilde{\xi}$ and that for BO there exists a critical $\tilde{\xi}$ at which $T_{\rm BO}=0$. We show the results in Fig. 25.

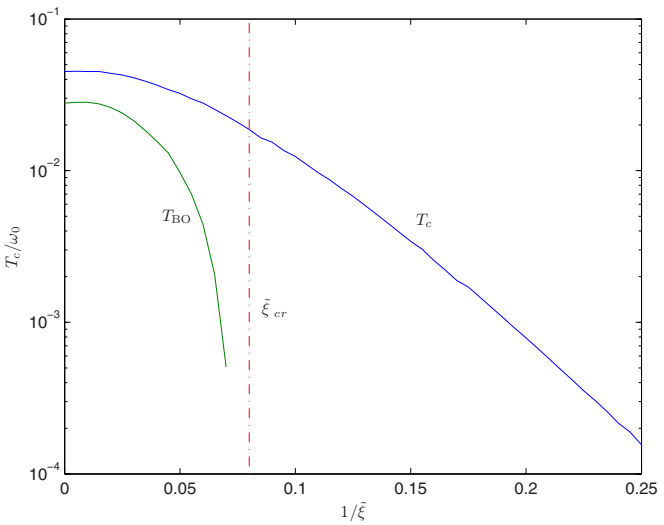

FIG. 25. (Color online) $T_{\rm SC}$ and the onset temperature $T_{\rm BO}$ for BO with diagonal $\mathbf{Q}$ as functions of the magnetic correlation length. We set $\tilde{\kappa}=0.14$ and $\tilde{g}=0.1$. The red dashed line is $\tilde{\xi}_{\rm cr}$, given by Eq. (F20).

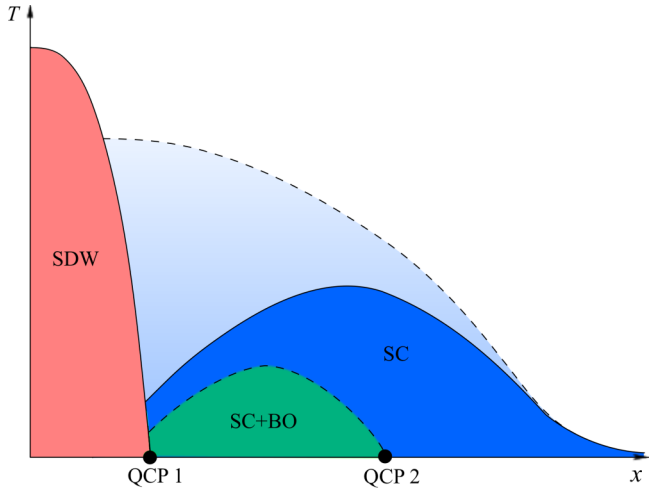

FIG. 26. (Color online) A schematic phase diagram for the (artificial) case when the only two competing states are SC and BO with a diagonal **Q**. The light blue region is the pseudogap phase, which combines SC fluctuations at large x (smaller ξ) and fluctuations between SC and BO at small x (large ξ).

Although the behavior of $T_{\rm BO}$ resembles that of $T_{\rm CDW}$ for CDW order with Q_x/Q_y, the physics behind the reduction of these temperatures with decreasing magnetic ξ is different. For BO with diagonal $\bar{Q} = (2Q, \pm 2Q)$, the reduction of $T_{\rm BO}$ compared to $T_{\rm SC}$ and its eventual vanishing is solely due to the FS curvature. If we set $\tilde{\kappa}$ to zero, $T_{\rm SC}$ and $T_{\rm BO}$ remain identical at any ξ. For CDW order with Q_x/Q_y, the reduction and eventual vanishing of $T_{\rm CDW}$ upon decreasing of $\tilde{\xi}$ are not related to curvature and hold even if we set the curvature to zero. At a small curvature then, $T_{\rm BO} > T_{\rm CDW}$, but which temperature is larger at $\tilde{\kappa} = O(1)$ depends on numbers. We emphasize again in this regard that for CDW with Q_x/Q_y the first instability upon lowering T is at $T > T_{\rm CDW}$, towards the state which breaks an Ising Z_2 symmetry. No such transition holds for BO with a diagonal **Q**.

3. Interplay between superconductivity and bond order

In Fig. 26, we present the phase diagram for the (artificial) case when the only two competing states are superconductivity and BO with a diagonal **Q**, i.e., when CDW order with Q_x/Q_y is just neglected. Because $T_{\rm SC}$ is larger than $T_{\rm BO}$, the leading instability upon lowering T is always into a superconducting state, BO may appear only at a lower T. At the same time, at large ξ, $T_{\rm SC}$ by itself is reduced because over some range of T the system fluctuates between superconductivity and BO [58,64] (a light blue region in Fig. 26). The phase diagram in Fig. 26 is similar to that in Ref. [58], but differs in that in our analysis BO only emerges at $\tilde{\xi} > \tilde{\xi}_{\rm cr}$, i.e., there exists a quantum-critical point towards BO ($\rm QCP_2$) at some distance away from a magnetic quantum-critical point $\rm QCP_1$.

[1] M. Hücker, M. v. Zimmermann, G. D. Gu, Z. J. Xu, J. S. Wen, Guangyong Xu, H. J. Kang, A. Zheludev, and J. M. Tranquada, Phys. Rev. B **83**, 104506 (2011).

[2] J. M. Tranquada, G. D. Gu, M. Hücker, Q. Jie, H.-J. Kang, R. Klingeler, Q. Li, N. Tristan, J. S. Wen, G. Y. Xu, Z. J. Xu, J. Zhou, and M. v. Zimmermann, Phys. Rev. B **78**, 174529 (2008).

[3] V. Hinkov, P. Bourges, S. Pailhès, Y. Sidis, A. Ivanov, C. D. Frost, T. G. Perring, C. T. Lin, D. P. Chen, and B. Keimer, Nat. Phys. **3**, 780 (2007).

[4] K. Fujita, A. R. Schmidt, E.-A. Kim, M. J. Lawler, D.-H. Lee, J. C. Davis, Hiroshi Eisaki, and S. Uchida, J. Phys. Soc. Jpn. **81**, 011005 (2012).

[5] K. Fujita, M. H. Hamidian, S. D. Edkins, C. K. Kim, Y. Kohsaka, M. Azuma, M. Takano, H. Takagi, H. Eisaki, S.-i. Uchida, A. Allais, M. J. Lawler, E.-A. Kim, S. Sachdev, and J. C. Séamus Davis, PNAS, doi:10.1073/pnas.1406297111.

[6] H. Karapetyan, M. Hücker, G. D. Gu, J. M. Tranquada, M. M. Fejer, Jing Xia, and A. Kapitulnik, Phys. Rev. Lett. **109**, 147001 (2012), and references therein; For the discussion on how Kerr effect can be understood without time-reversal symmetry breaking, see P. Hosur *et al.*, Phys. Rev. B **87**, 115116 (2013); J. Orenstein and J. E. Moore, *ibid.* **87**, 165110 (2013).

[7] For the latest review, see Y. Sidis and P. Bourges, arXiv:1306.5124.

[8] Yuan Li, V. Balédent, G. Yu, N. Barišić, K. Hradil, R. A. Mole, Y. Sidis, P. Steffens, X. Zhao, P. Bourges, and M. Greven, Nature (London) **468**, 283 (2010).

[9] Y. Lubashevsky, LiDong Pan, T. Kirzhner, G. Koren, and N. P. Armitage, Phys. Rev. Lett. **112**, 147001 (2014).

[10] G. Ghiringhelli, M. Le Tacon, M. Minola, S. Blanco-Canosa, C. Mazzoli, N. B. Brookes, G. M. De Luca, A. Frano, D. G. Hawthorn, F. He, T. Loew, M. Moretti Sala, D. C. Peets, M. Salluzzo, E. Schierle, R. Sutarto, G. A. Sawatzky, E. Weschke, B. Keimer, and L. Braicovich, Science **337**, 821 (2012).

[11] A. J. Achkar, R. Sutarto, X. Mao, F. He, A. Frano, S. Blanco-Canosa, M. Le Tacon, G. Ghiringhelli, L. Braicovich, M. Minola, M. Moretti Sala, C. Mazzoli, Ruixing Liang, D. A. Bonn, W. N. Hardy, B. Keimer, G. A. Sawatzky, and D. G. Hawthorn, Phys. Rev. Lett. **109**, 167001 (2012).

[12] R. Comin, A. Frano, M. M. Yee, Y. Yoshida, H. Eisaki, E. Schierle, E. Weschke, R. Sutarto, F. He, A. Soumyanarayanan, Y. He, M. Le Tacon, I. S. Elfimov, J. E. Hoffman, G. A. Sawatzky, B. Keimer, and A. Damascelli, Science **343**, 390 (2014).

[13] E. H. da Silva Neto, P. Aynajian, A. Frano, R. Comin, E. Schierle, E. Weschke, A. Gyenis, J. Wen, J. Schneeloch, Z. Xu, S. Ono, G. Gu, M. Le Tacon, and A. Yazdani, Science **343**, 393 (2014).

[14] T. Wu, H. Mayaffre, S. Krämer, M. Horvatić, C. Berthier, W. N. Hardy, R. Liang, D. A. Bonn, and M.-H. Julien, arXiv:1404.1617.

[15] L. Nie, G. Tarjus, and S. A. Kivelson, Proc. Natl. Acad. Sci. USA **111**, 7980 (2014).

[16] Tao Wu, Hadrien Mayaffre, Steffen Krämer, Mladen Horvatić, Claude Berthier, W. N. Hardy, Ruixing Liang, D. A. Bonn, and Marc-Henri Julien, Nature (London) **477**, 191 (2011).

[17] Tao Wu, Hadrien Mayaffre, Steffen Krämer, Mladen Horvatić, Claude Berthier, Philip L. Kuhns, Arneil P. Reyes, Ruixing Liang, W. N. Hardy, D. A. Bonn, and Marc-Henri Julien, Nat. Commun. **4**, 2113 (2013).

[18] David LeBoeuf, S. Krämer, W. N. Hardy, Ruixing Liang, D. A. Bonn, and Cyril Proust, Nat. Phys. **9**, 79 (2013).

[19] N. Harrison and S. E. Sebastian, Phys. Rev. Lett. **106**, 226402 (2011); S. E. Sebastian, N. Harrison, and G. G. Lonzarich, Rep. Prog. Phys. **75**, 102501 (2012).

[20] N. Doiron-Leyraud and L. Taillefer, Physica C (Amsterdam) **481**, 161 (2012).

[21] R.-H. He, M. Hashimoto, H. Karapetyan, J. D. Koralek, J. P. Hinton, J. P. Testaud, V. Nathan, Y. Yoshida, Hong Yao, K. Tanaka, W. Meevasana, R. G. Moore, D. H. Lu, S.-K. Mo, M. Ishikado, H. Eisaki, Z. Hussain, T. P. Devereaux, S. A. Kivelson, J. Orenstein, A. Kapitulnik, and Z.-X. Shen, Science **331**, 1579 (2011).

[22] I. M. Vishik, M. Hashimotoc, R.-H. He, W.-S. Lee, F. Schmitt, D. Lu, R. G. Moore, C. Zhang, W. Meevasan, T. Sasagawa, S. Uchida, Kazuhiro Fujita, S. Ishida, M. Ishikado, Y. Yoshida, H. Eisaki, Z. Hussain, T. P. Devereaux, and Z.-X. Shen, Proc. Natl. Acad. Sci. USA **110**, 17774 (2013).

[23] A. Kaminski, T. Kondo, T. Takeuchi, and G. Gu, arXiv:1403.0492, and references therein.

[24] D. N. Basov, R. D. Averitt, D. van der Marel, M. Dressel, and K. Haule, Rev. Mod. Phys. **83**, 471 (2011).

[25] H. Alloul, C. R. Phys., doi:10.1016/j.crhy.2014.02.007.

[26] C. Castellani, C. Di Castro, and M. Grilli, Phys. Rev. Lett. **75**, 4650 (1995); A. Perali, C. Castellani, C. Di Castro, and M. Grilli, Phys. Rev. B **54**, 16216 (1996).

[27] See S. Onari and H. Kontani, Phys. Rev. Lett. **109**, 137001 (2012), and references therein.

[28] See C. Castellani *et al.*, J. Phys. Chem. Solids **59**, 1694 (1998).

[29] S. Andergassen, S. Caprara, C. Di Castro, and M. Grilli, Phys. Rev. Lett. **87**, 056401 (2001).

[30] S. Caprara *et al.*, Phys. Rev. Lett. **95**, 117004 (2005); Phys. Rev. B **84**, 054508 (2011).

[31] G. Seibold, M. Grilli, and J. Lorenzana, Phys. Rev. Lett. **103**, 217005 (2009).

[32] G. Mazza, M. Grilli, C. Di Castro, and S. Caprara, Phys. Rev. B **87**, 014511 (2013).

[33] For a review, see G. Seibold *et al.*, Physica C (Amsterdam) **481**, 132 (2012), and references therein.

[34] A. Perali *et al.*, Phys. Rev. B **62**, R9295(R) (2000).

[35] D. J. Scalapino, Rev. Mod. Phys. **84**, 1383 (2012).

[36] P. Monthoux, D. Pines, and G. G. Lonzarich, Nature (London) **450**, 1177 (2007).

[37] Ar. Abanov, A. V. Chubukov, and M. A. Finkelstein, Europhys. Lett. **54**, 488 (2001).

[38] Ar. Abanov, A. V. Chubukov, and J. Schmalian, Adv. Phys. **52**, 119 (2003).

[39] S. A. Hartnoll, D. M. Hofman, M. A. Metlitski, and S. Sachdev, Phys. Rev. B **84**, 125115 (2011).

[40] A. V. Chubukov, D. L. Maslov, and V. I. Yudson, Phys. Rev. B **89**, 155126 (2014).

[41] D. B. Kyung, S. S. Kancharla, D. Sénéchal, A.-M. S. Tremblay, M. Civelli, and G. Kotliar, Phys. Rev. B **73**, 165114 (2006).

[42] J. Schmalian, D. Pines, and B. Stojkovich, Phys. Rev. Lett. **80**, 3839 (1998).

[43] T. A. Sedrakyan and A. V. Chubukov, Phys. Rev. B **81**, 174536 (2010).

[44] Y. Wang and A. V. Chubukov, Phys. Rev. B **88**, 024516 (2013).

[45] See, e.g., N. P. Armitage, P. Fournier, and R. L. Greene, Rev. Mod. Phys. **82**, 2421 (2010).

[46] C. M. Varma, Phys. Rev. B **55**, 14554 (1997).

[47] Z. Wang, G. Kotliar, and X.-F. Wang, Phys. Rev. B **42**, 8690 (1990).

[48] S. Chakravarty, R. B. Laughlin, D. K. Morr, and C. Nayak, Phys. Rev. B **63**, 094503 (2001).

[49] P. A. Lee, N. Nagaosa, and X.-G. Wen, Rev. Mod. Phys. **78**, 17 (2006).

[50] E. Gull, O. Parcollet, and A. J. Millis, Phys. Rev. Lett. **110**, 216405 (2013).

[51] A.-M. S. Tremblay, arXiv:1310.1481.

[52] T.-P. Choy and Ph. Phillips, Phys. Rev. Lett. **95**, 196405 (2005).

[53] T. M. Rice, K.-Y. Yang, and F. C. Zhang, Rep. Prog. Phys. **75**, 016502 (2012).

[54] V. J. Emery and S. A. Kivelson, Nature (London) **374**, 434 (1994).

[55] L. Benfatto, S. Caprara, C. Castellani, A. Paramekanti, and M. Randeria, Phys. Rev. B **63**, 174513 (2001).

[56] V. Mishra, U. Chatterjee, J. C. Campuzano, and M. R. Norman, Nat. Phys. **10**, 357 (2014).

[57] M. A. Metlitski and S. Sachdev, Phys. Rev. B **82**, 075128 (2010).

[58] K. B. Efetov, H. Meier, and C. Pépin, Nat. Phys. **9**, 442 (2013).

[59] L. E. Hayward, D. G. Hawthorn, R. G. Melko, and S. Sachdev, Science **343**, 1336 (2014).

[60] H. Meier, M. Einenkel, C. Pépin, and K. B. Efetov, Phys. Rev. B **88**, 020506(R) (2013).

[61] Y. Wang and A. V. Chubukov, Phys. Rev. Lett. **110**, 127001 (2013).

[62] R. Comin, R. Sutarto, F. He, E. da Silva Neto, L. Chauviere, A. Frano, R. Liang, W. N. Hardy, D. Bonn, Y. Yoshida, H. Eisaki, J. E. Hoffman, B. Keimer, G. A. Sawatzky, and A. Damascelli, arXiv:1402.5415.

[63] H. Meier, C. Pépin, M. Einenkel, and K. B. Efetov, Phys. Rev. B **89**, 195115 (2014).

[64] S. Sachdev and R. La Placa, Phys. Rev. Lett. **111**, 027202 (2013).

[65] J. D. Sau and S. Sachdev, Phys. Rev. B **89**, 075129 (2014).

[66] R. M. Fernandes, A. V. Chubukov, J. Knolle, I. Eremin, and J. Schmalian, Phys. Rev. B **85**, 024534 (2012).

[67] S. Lederer, Y. Schattner, E. Berg, and S. A. Kivelson, arXiv:1406.1193.

[68] A. M. Tsvelik, Phys. Rev. B **89**, 184515 (2014).

[69] C. Castellani, C. Di Castro, and W. Metzner, Phys. Rev. Lett. **72**, 316 (1994).

[70] C. M. Varma, Phys. Rev. B **73**, 155113 (2006).

[71] R. M. Fernandes, S. Maiti, P. Wölfle, and A. V. Chubukov, Phys. Rev. Lett. **111**, 057001 (2013).

[72] E. G. Moon and S. Sachdev, Phys. Rev. B **82**, 104516 (2010).

[73] B. A. Vorontsov, M. G. Vavilov, and A. V. Chubukov, Phys. Rev. B **81**, 174538 (2010).

[74] R. M. Fernandes and J. Schmalian, Phys. Rev. B **82**, 014521 (2010).

[75] E. Fradkin and S. A. Kivelson, Nat. Phys. **8**, 864 (2012).

[76] E. Berg, E. Fradkin, S. A. Kivelson, and J. Tranquada, New J. Phys. **11**, 115004 (2009).

[77] M. R. Norman, H. Ding, M. Randeria, J. C. Campuzano, T. Yokoya, T. Takeuchi, T. Takahashi, T. Mochiku, K. Kadowaki, P. Guptasarma, and D. G. Hinks, Nature (London) **392**, 157 (1998).
[78] A. V. Maharaj, P. Hosur, and S. Raghu, arXiv:1406.4154.
[79] Mark H. Fischer, Si Wu, Michael Lawler, Arun Paramekanti, and E.-A. Kim, arXiv:1406.2711.
[80] Ar. Abanov, A. V. Chubukov, and M. R. Norman, Phys. Rev. B **78**, 220507(R) (2008).
[81] E-G. Moon and A. V. Chubukov, J. Low Temp. Phys. **161**, 263 (2010).
[82] This result holds when fermionic self-energy $\Sigma(k,\Omega_m)$ is approximated by its value at hot spots. When the k dependence along the FS is included, the summation of the leading logarithms still does not lead to the instability [61], but the form of $\Delta_{SC}(\Omega_m)$ is more complex [57,61].
[83] A. J. Millis, S. Sachdev, and C. M. Varma, Phys. Rev. B **37**, 4975 (1988).
[84] D. F. Mross, J. McGreevy, H. Liu, and T. Senthil, Phys. Rev. B **82**, 045121 (2010).
[85] M. A. Metlitski, D. F. Mross, S. Sachdev, and T. Senthil, arXiv:1403.3694.
[86] W. A. Atkinson, A. P. Kampf, and S. Bulut, arXiv:1404.1335.
[87] D. T. Son, Phys. Rev. D **59**, 094019 (1999).
[88] K. B. Efetov (private communication).
[89] K. B. Efetov and C. Pépin (private communication).
[90] G.-W. Chern, R. M. Fernandes, R. Nandkishore, and A. V. Chubukov, Phys. Rev. B **86**, 115443 (2012).
[91] D. Chowdhury and S. Sachdev, arXiv:1404.6532.
[92] M. G. Vavilov, A. V. Chubukov, and A. B. Vorontsov, Supercond. Sci. Technol. **23**, 054011 (2010).
[93] S. Tewari, C. Zhang, V. M. Yakovenko, and S. Das Sarma, Phys. Rev. Lett. **100**, 217004 (2008).
[94] C.-H. Hsu, S. Raghu, and S. Chakravarty, Phys. Rev. B **84**, 155111 (2011).
[95] A. M. Polyakov, Phys. Lett. B **59**, 79 (1975).
[96] A. V. Chubukov and O. A. Starykh, Phys. Rev. Lett. **110**, 217210 (2013).
[97] A. Dhar *et al.*, Phys. Rev. A **85**, 041602 (2012).
[98] A. Dhar *et al.*, Phys. Rev. B **87**, 174501 (2013).
[99] S. Maiti and A. V. Chubukov, Phys. Rev. B **87**, 144511 (2013).
[100] M. Marciani, L. Fanfarillo, C. Castellani, and L. Benfatto, Phys. Rev. B **88**, 214508 (2013).
[101] A. Hinojosa, R. Fernades, and A. V. Chubukov, arXiv:1405.7077.
[102] R. Daou *et al.*, Nature (London) **463**, 519 (2010).
[103] A. A. Kordyuk, V. B. Zabolotnyy, D. V. Evtushinsky, D. S. Inosov, T. K. Kim, B. Büchner, and S.V. Borisenko, Eur. Phys. J. ST **188**, 153 (2010).
[104] T. Kondo *et al.*, Phys. Rev. Lett. **111**, 157003 (2013).
[105] U. Chatterjee *et al.*, Proc. Natl. Acad. Sci. USA **108**, 9346 (2011).
[106] H.-B. Yang *et al.*, Phys. Rev. Lett. **107**, 047003 (2011).
[107] A. V. Chubukov, M. R. Norman, A. J. Millis, and E. Abrahams, Phys. Rev. B **76**, 180501(R) (2007).
[108] N. Harrison and S. E. Sebastian, arXiv:1401.6590.
[109] A. Allais, D. Chowdhury, and S. Sachdev, arXiv:1406.0503.
[110] P. A. Lee, arXiv:1401.0519.
[111] D. Agterberg and M. Kashuap, arXiv:1406.4959.
[112] A. V. Chubukov and D. L. Maslov, Phys. Rev. B **86**, 155136 (2012); H. B. Rhee, F. Ronning, J.-X. Zhu, E. D. Bauer, J. N. Mitchell, P. H. Tobash, B. L. Scott, J. D. Thompson, Yu Jiang, C. H. Booth, and W. E. Pickett, *ibid.* **86**, 115137 (2012).
[113] W. L. McMillan, Phys. Rev. **167**, 331 (1968).